Understanding heat carrier effects in a laboratory-scale auger pyrolyzer

by

Tannon Jeffrey Daugaard

A dissertation submitted to the graduate faculty

in partial fulfillment of the requirements for the degree of

DOCTOR OF PHILOSOPHY

Co-majors: Mechanical Engineering; Biorenewable Resources and Technology

Program of Study Committee:
Mark Mba Wright, Major Professor
Robert C. Brown
Theodore J. Heindel
Brent H. Shanks
Jean-Philippe Tessonnier

The student author, whose presentation of the scholarship herein was approved by the program of study committee, is solely responsible for the content of this dissertation. The Graduate College will ensure this dissertation is globally accessible and will not permit alterations after a degree is conferred.

Iowa State University

Ames, Iowa

2018

DEDICATION

I would like to dedicate this work to my late uncle, Dan Lynn Daugaard. It was through idolizing him that I first became inspired to become an engineer.

I would also like to dedicate this work to my immediate family, close friends, and my little girl, Nala. I would not have gotten through the completion of this degree without them.

TABLE OF CONTENTS

NOMENCLATURE

AAEM – Alkali and Alkaline Earth Metals

BFB – Bubbling Fluidized Bed

BPDOE – Barrels per Day of Oil Equivalent

CBP – Consolidated Bioprocessing

EOS – Economies of Scale

EPA – Environmental Protection Agency

ESP – Electrostatic Precipitator

FCC – Fluid Catalytic Cracking

GC – Gas Chromatography

GGE – Gallons Gasoline Equivalent

GHG – Greenhouse Gas

HHV – Higher Heating Value

HPLC – High Performance Liquid Chromatography

IC – Ion Chromatography

NCG – Non-Condensable Gas

OPEC – Organization of Petroleum Exporting Countries

RFS – Renewable Fuels Standard

SF1 – Stage Fraction 1

SF2 – Stage Fraction 2

SLPM – Standard Liters Per Minute

WSS – Water Soluble Sugars

ACKNOWLEDGMENTS

I would like to express my appreciation to Dr. Mark Mba Wright for giving me the opportunity to pursue this degree. His guidance, financial support, mentorship, and expertise enabled me to have an excellent research experience and produce significant results.

I am also indebted to my committee members. I would like to thank Dr. Robert Brown for his continuous guidance, support and the opportunity to teach some classes. I would also like to thank Dr. Ted Heindel for his support and guidance throughout my research projects. I am very thankful to Dr. Brent Shanks and Dr. Jean-Philippe Tessonnier for their support and guidance on research as well as the opportunity to be a student in their class. I sincerely appreciate the valuable discussions and feedback provided by all during my presentations and examinations.

I am grateful to the Phillips 66 Company for their generous funding of my research projects. I appreciate their valuable discussions and feedback throughout these projects.

I would also like to express my extreme gratitude to the BioEconomy Institute staff. Specifically, I would like to thank Patrick Johnston, Marge Rover, and Ryan Smith. Their assistance with analytical work, laboratory care, and guidance helped me complete this work. I would also like to acknowledge Andy Suby, Jordan Funkhouser, Lysle Whitmer, and Andrew Friend from the BioCentury Research farm for their memories and friendships over the years.

I am extremely grateful for having the opportunity to not only work alongside some exceptional colleagues but to also make lifelong friends. I would specifically like to

thank Martin Haverly for his expertise, encouragement, memories, and brotherhood. I'd also like to thank Julie Haverly for her memories and welcoming me into the family. I would also like to acknowledge Dustin Dalluge and Erica Dalluge for their mentorship, memories, and friendship. Special thanks to both Wenqin Li and Kwang Ho Kim for being great teammates, great colleagues and even greater friends. I would also like to thank fellow colleagues Nate Hamlett, Yongsuk Choi, Mitchell Amundson, Juan Proano-Aviles, Arpa Ghosh, Fenglei Qi, Karl Broer, and Joe Polin.

I am grateful to have the assistance of numerous undergraduate research assistants throughout my degree. I would specifically like to thank Emily Hansen, Levi Naumann, and Ryan Spellerburg.

I would personally like to thank Laura J. Anderson for her guidance, wisdom, friendship, and endless support throughout my schooling and life. I would also like to extend the same thanks to Caleb Tollefson and wife, Emily, for their support, memories and friendship. Special acknowledgement to Kobe Bryant as I often draw inspiration from his work ethic, determination, and Mamba Mentality to overcome any challenge and obtain success. "Those times when you get up early and you work hard; those times when you stay up late and you work hard; those times when you don't feel like working, you're too tired, you don't want to push yourself but you do it anyway. That is actually the dream. That's the dream. It's not the destination, it's the journey. And if you guys understand that, what you'll see happen is that you won't accomplish your dreams. Your dreams won't come true. Something greater will."

Finally, I would like to express my deepest gratitude to my family for their unwavering support throughout my degree and more. I could not ask for better parents

than my mother, Jennifer, and my father, Darwin. Everything that I am and will become is because of their influence, support and love. I am forever indebted to them. I would also like to thank my sister, Tanisha, for her support and memories. Special thanks are also given to Daren and Tara Daugaard for their endless support and motivation throughout this degree.

Lastly, I would like to thank God. It is through Him that I was blessed with the opportunity and qualities to obtain this degree.

ABSTRACT

Pyrolysis of lignocellulosic biomass is a promising conversion pathway for the production of renewable fuels and chemicals. The vital component of the pyrolysis conversion process and biorefinery is the pyrolysis reactor. Auger pyrolysis reactors have been gaining recent research interest for their advantages over fluidized bed reactors. While auger pyrolysis research continues to grow, voids in literature exist and need to be addressed to minimize risk in scale-up to potential commercialization. Research in this dissertation addresses some of these voids, specifically, to develop a fundamental understanding of the phenomena that constraints heat transfer and heat recovery in directly-heated auger pyrolyzers.

A laboratory-scale, twin-screw auger pyrolyzer with heat carrier for the pyrolysis of red oak was of specific focus throughout this work. First, the effect of thermophysical properties of heat carriers on the performance of an auger reactor was investigated. Heat carriers with a wide range of thermal diffusivities were tested. This included stainless steel shot, fine sand, coarse sand and silicon carbide. It was found that the heat carriers exhibited similar organic yields and composition of bio-oil. However, significant differences of reaction water, char and non-condensable gas yields were observed. It was also found that residual carbon contributed to as high as 20 wt.% of total char yield for some heat carriers. Attrition of heat carrier as high as 7 wt.% was present after as little as 2 hours of operation. The results from this study suggest tradeoffs may exist between physical performance, material cost, and product yields when selecting heat carrier materials for pyrolysis of biomass in an auger reactor.

The second study investigated the effect of recycling sand heat carrier on the long-term performance of a laboratory-scale auger reactor. Sand heat carrier with a particle size range of 600-1000 µm was used in pyrolysis trials and was then subsequently regenerated and recycled at up to five times. Attrition as high as 8% on a mass basis and a decrease in mean particle size of the sand was evident after each recycle. This prompted further investigation into the effect of heat carrier particle size. A smaller fraction of sand (250-600 µm) was tested in comparison to the original. Significant differences in the yields of organic bio-oil, reaction water, char and non-condensable gases were observed between the two fractions of sand. The smaller sand fraction produced more char and reaction water at the expense of organic bio-oil and non-condensable gases. This study shows that heat carrier material selection and particle size plays an important role in the continuous operation of an auger pyrolyzer.

The third study investigated the effect of regeneration parameters on carbon burn-off times from biomass pyrolysis char. A laboratory-scale fluidized bed reactor was used to regenerate sand heat carrier and char from biomass pyrolysis. Regenerations were conducted with varying regenerator temperatures (450-750°C), varying superficial fluidization velocities (100-250% minimum fluidization), and varying oxygen sweep gas concentrations (13.6-28.5 vol.% O_2). Carbon burn-off times increased with increasing temperature at the same state of fluidization, suggesting superficial fluidization velocity plays an important role in carbon burn-off times at these temperatures. Increasing the superficial fluidization velocity and oxygen sweep gas concentration, both significantly decreased carbon burn-off times. Furthermore, increasing regeneration reaction temperatures was shown to promote carbon dioxide production. The results from this

study show the influence temperature, gas velocity, and oxygen concentration has on carbon burn-off times in biomass char regeneration unit.

Lastly, the potential impact of industry technology-learning rates was investigated on varying biorefinery capacities of advanced biofuel technologies. Predictions of learning-based economies of scale, S-Curve, and Stanford-B models were studied on the optimal plant capacities and production costs of biorefineries. Biofuel cost reductions of 55 to 73% compared to base case estimates were found using the Stanford-B model. The optimal capacities range from small-scale (grain ethanol and fast pyrolysis) producing 16 million gallons per year to large-scale production of 210 million gallons per year capacity for gasification facilities. Results from this study suggest there is an economic incentive to invest in strategies that increase the learning rates for advanced biofuel production, which could lead to the reduction of the optimal size and production costs of biorefineries.

CHAPTER 1. INTRODUCTION

Biomass as a Renewable Energy Source

Global energy consumption of fossil fuels continues to rise each year with increasing global population. In 2013, the world consumed 1.97 trillion gallons gasoline equivalent (GGE) of fossil fuels accounting for approximately 70% of the global final energy consumption [1]. Continued use and dependency on fossil fuels poses a risk of depleting fossil fuel reserves leading to a potential global energy crisis. The United States continually focuses on the production of renewable and sustainable energy making it a top priority in efforts to increase national and economic security, along with improving environmental quality. Of the renewable energy technologies, the conversion of biomass, specifically lignocellulosic biomass, to fuels and chemicals is currently the only technology with the ability to serve as a direct replacement to the products derived from petroleum. The importance of establishing a bioeconomy, where human societies obtain sustainable sources of energy and carbon from the biosphere [2], grows with time.

In 2005, approximately 60% of the United States annual consumption of oil came from net imports and only dropped to 45% in 2011 [3]. A large percentage of imports leaves the U.S. vulnerable to international oil suppliers such as the Organization of Petroleum Exporting Countries (OPEC), Russia, and other former Soviet republics. Some argue that the dependence on unstable and potentially hostile petroleum suppliers leaves the United States national security at risk [4]. In 2015, the United States imported 3.38 billion barrels of petroleum equaling a staggering total cost of $170.2 billion [5]. As the cost of petroleum is historically unstable and has been largely influenced by OPEC since

the 1970's [4], the U.S. economy becomes susceptible to international control when importing a large percentage of oil. Developing an established bioeconomy where domestic biorenewable resources would serve as a substitute to petroleum will decrease U.S. dependency on foreign oil and in turn increase both national and economic security.

The utilization of biorenewable resources for fuels and chemicals also has the potential to improve environmental quality. Greenhouse gas (GHG) emissions continue to rise to unprecedented levels and is in part due to the use of fossil fuels. In 2014, the GHG emissions in the U.S. was 6,870.5 million metric tons of carbon dioxide (CO_2) equivalent [6]. This equates to a 7.4 percent increase in total emissions since 1990 and an increase of 8.6% for CO_2 specifically. Approximately 76% of CO_2 emissions in the U.S. is attributed to fossil fuel combustion [6]. As biomass is grown, the plant absorbs CO_2 from the atmosphere, retains the carbon and releases the oxygen back to the atmosphere through photosynthesis. Using biomass as a fuel is often considered as a carbon-neutral process as carbon is harvested from the atmosphere during the plant's life and released back as CO_2 during combustion of the fuel in a continuously closed cycle. The potential sequestration of emissions from biomass fuels and the usage of biochar as a soil amendment can result in a carbon negative process [7, 8]. Using biorenewable resources for fuels will help mitigate fossil fuel emissions increasing the environmental quality at home and abroad.

The use of biomass as an energy source for replacement of fossil fuels is not farfetched from reality as it is both renewable and abundant in nature. Biomass, also known as biorenewable resources, can be defined as organic material of recent biological origin [2]. Types of biomass include dedicated energy crops, including both woody and

herbaceous, and waste materials such as agricultural residues, yard waste and municipal solid waste. The 2011 update to the *Billion Ton Study* estimates that the U.S. can sustainably produce up to 1.1 billion tons of biomass annually by the year 2030 [9]. Biomass does have disadvantages that must be overcome to establish a sustainable bioeconomy. Biomass has a relatively low bulk density which results in high transportation costs. Additionally, biomass has high oxygen content (typically 40-45 wt. %), in comparison to petroleum, resulting in a higher heating values of up to approximately 20 MJ/kg [2].

Biomass Structure

Biomass consists of three major structural components: hemicellulose, cellulose, and lignin. Variable amounts of these three components make up the three-dimensional polymeric plant structure referred to as lignocellulose [2]. Cellulose is a homopolysaccharide composed of repeating β-D-glucopyranose units linked together by (1-4)-glycosidic bonds. Cellulose, shown in Figure 1, is located predominately in the secondary wall accounting up to 45% of the dry weight in woody biomass [10]. Cellulose is moderately thermally stable and decomposes at 240-350°C.

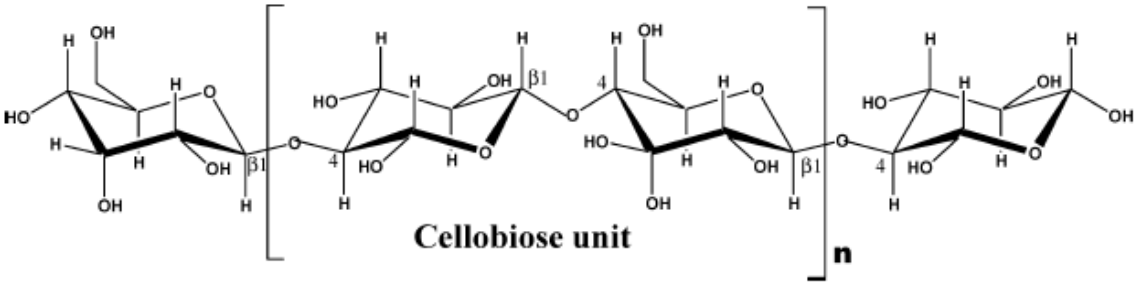

Figure 1: Chemical structure of cellulose. [11]

Hemicellulose is a heteropolysaccharide composed of a variety of monomeric components consisting of pentoses (D-arabinose, L-arabinose, and D-xylose) and hexoses

(D-mannose, D-galactose, and D-glucose). Most hemicelluloses have a degree of polymerization of approximately 150, compared to 5000-10000 for cellulose [11]. Hemicellulose accounts for 20-30 % of the dry weight in woody biomass and varies between softwoods and hardwoods [10]. The major hemicellulose component in softwoods is galactoglucomannan, shown in Figure 2, whereas hardwoods are rich in glucuronoxylan, commonly referred to as xylan as shown in Figure 3. Hemicellulose is less thermally stable than cellulose and decomposes at temperatures of 200-260°C.

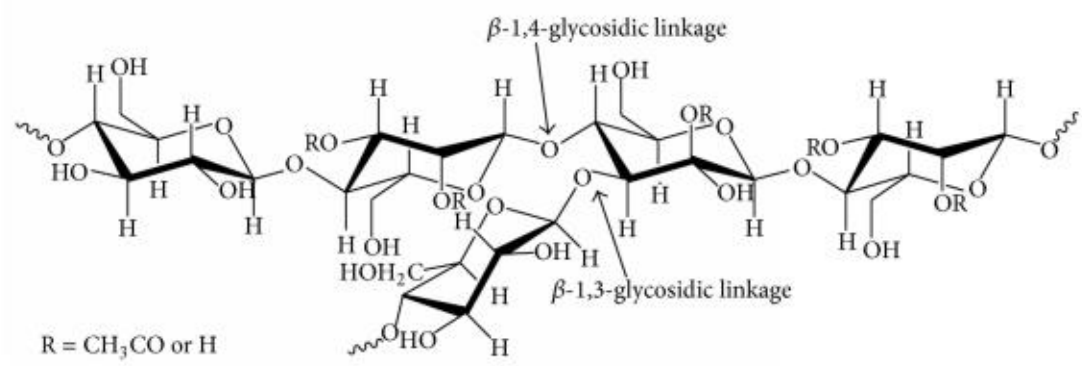

Figure 2: Chemical structure of glucomannan. [12]

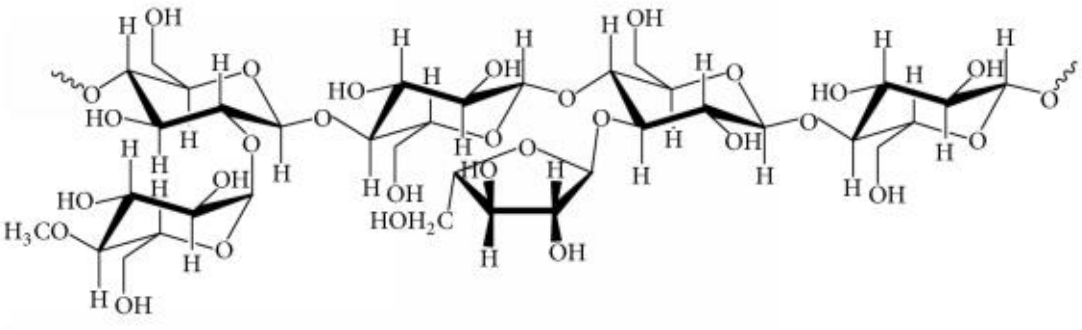

Figure 3: Chemical structure of Xylan. [12]

Lignin is a heterogeneous aromatic polymer and is the largest non-carbohydrate fraction of biomass. Lignins are composed of C_6C_3 units in various proportions according to botanical, physiological, and cytological criteria [13]. The type of lignin is often denoted by its phenylpropane building block: p-hydroxyphenyl (H), guiacyl (G), and

syringyl (S). The content of lignin varies with the type of biomass but hardwoods and softwoods have lignin compositions of 28 and 20 wt. %, respectively [13]. A general illustration of the structure of lignin is shown in Figure 4. Lignin is thermally stable over a wider temperature range, in comparison to cellulose and hemicellulose, and decomposes at 280-500°C. Biomass is a complex structure consisting of different compositions of cellulose, hemicellulose, and lignin across various feedstocks which contributes to its natural recalcitrance.

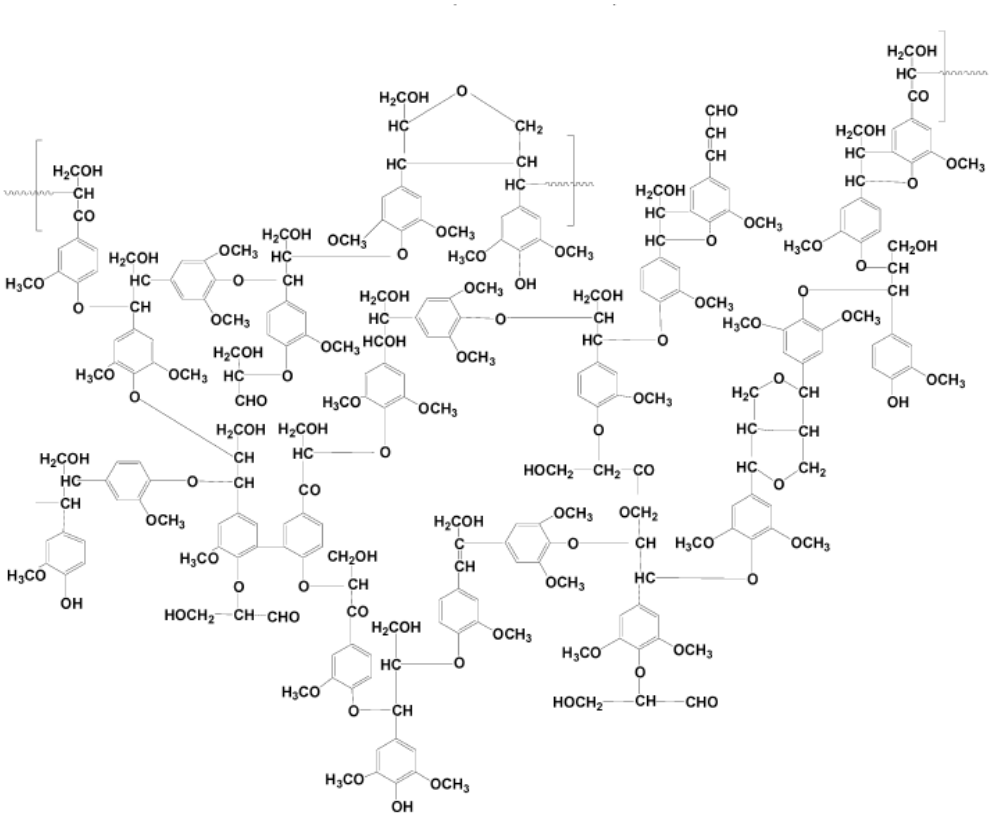

Figure 4: Partial chemical structure of lignin. [11]

Biomass Conversion Pathways

Two major pathways exist in biomass conversion: biochemical conversion and thermochemical conversion. Biochemical conversion is conversion of biomass into value added products through the use of enzymes and microorganisms [2]. Biochemical

conversion processes include fermentation of sugars, enzymatic or acid hydrolysis followed by fermentation to sugars, and consolidated bioprocessing. Typical reaction times take place on the order of hours to weeks. Liquid products include mainly ethanol, other alcohol fuels such as butanol, and organic chemicals such as acetic acid and acetone [2]. The use of lignocellulosic biomass in biochemical processes, specifically fermentation steps, is proven difficult due to the recalcitrance of the biomass constituents. Specifically, lignin cannot be used in fermentation processes and must be removed prior to hydrolysis [14]. Pretreatment processes such as steam explosion and the use of lignin degrading enzymes are used to remove the lignin and separate hexoses and pentoses in the biomass. However, fermentation inhibitors such as aldehydes, aromatic acids, and phenols may be released during the pretreatment processes [14]. Additionally, pretreatment processes are costly and can account for up to 33% of the processing costs in the conversion of lignocellulose to sugars [2].

Enzymatic hydrolysis uses different enzymes to break down the cellulose and hemicellulose into fermentable sugars. A two-step pretreatment process is used to first solubilize the hemicellulose followed by subsequent enzymatic hydrolysis of the cellulose. Low conversion rates and susceptibility to inhibitors are problems associated with enzymatic hydrolysis [2]. Acid hydrolysis of sugars from lignocellulose can be done by using either concentrated acid hydrolysis or dilute acid hydrolysis. Concentrated acid hydrolysis uses large amounts of sulfuric acid (up to 77 wt. %) mixed with water and is heated to release the sugars used for fermentation [14]. Whereas, dilute acid hydrolysis uses sulfuric acid (less than 4% concentration) in higher temperatures and at longer exposure times to produce the monosaccharides for fermentation [14]. Consolidated

bioprocessing (CBP) combines cellulase production, cellulose hydrolysis, and fermentation into a single step. The reduction in number of processing steps, reactors, and cost of chemicals makes CBP an attractive technology to biochemical processing [2].

Thermochemical processing of biorenewable resources uses heat to convert plant polymers into fuels, chemicals, or electric power [15]. Figure 5 shows the pathway from some thermochemical conversion processes to final products. The reaction residence times in thermochemical processing range from seconds to minutes, which offers an advantage over biochemical processing. Additional benefits include the ability to process recalcitrant materials and the ability to produce a range of products as a result of different processing temperatures and conditions. Biomass can be converted to heat, power, and gaseous products at moderate to high temperature conditions through direct combustion and gasification. Alternatively, biomass can be converted into fuels and chemicals via fast pyrolysis and solvolysis.

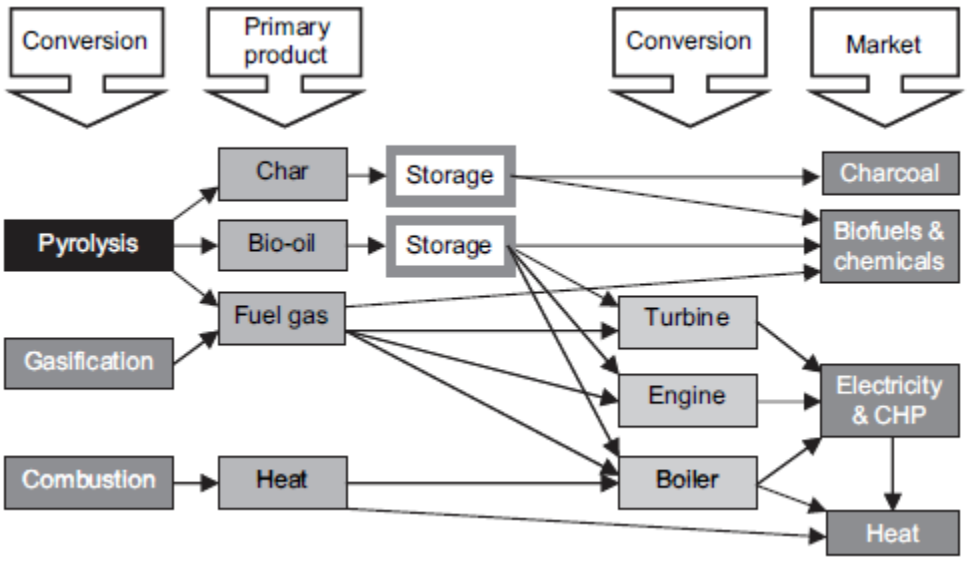

Figure 5: Products from thermochemical conversion of biomass. [16]

Direct combustion is the rapid oxidation of biomass to produce thermal energy and flue gas, mainly carbon dioxide and water [15]. Combustion temperatures can reach as high as 2000°C. Several disadvantages limit the use of biomass as a fuel for combustion. High moisture content and the presence of alkali compounds in the biomass lead to operation penalties, agglomeration, and ash fouling of the combustors. To overcome these issues and use current combustion infrastructure, biomass can be burned together with coal in a process called cofiring [2]. Cofiring offers advantages to coal combustion in increased boiler efficiencies, reduced fuel costs, and emissions of NO_x and SO_x [17]. Issues of ash fouling and agglomeration still arise in cofiring which typically limits the percentage of biomass cofired with coal to only 5-20% [18].

Gasification is the conversion of solid, carbon-rich materials under oxygen-starved conditions and elevated temperatures into a producer gas [2]. Temperatures for gasification fall in the range of 750-1500°C and are dependent on the method of heating (air-blown, steam/oxygen-blown or indirectly heated) [15]. The producer gas is sometimes referred to as syngas and contains a mixture of carbon dioxide, carbon monoxide (CO), hydrogen (H_2), methane (CH_4), small amounts of additional hydrocarbons and inorganic contaminants. Byproducts include both char and tar with their yields dependent upon reaction temperature, equivalence ratio and bed material, such as calcined dolomite [15]. In addition to thermal energy, gasification also offers flexibility for the production of gaseous products, such as hydrogen or a natural gas substitute, or synthesis to fuels and chemicals. Products of the latter include gasoline and diesel from Fischer-Tropsch Synthesis, methanol, mixed alcohols, and olefins [15].

Fast pyrolysis is the rapid thermal decomposition of organic compounds in the absence of oxygen to produce liquids, gases, and char [2]. Operating conditions of fast pyrolysis include moderate temperatures (400-600°C), short residence times (0.5-2s), and rapid quenching of the pyrolysis vapors [15]. Liquid bio-oil is the main product and can be obtained in yields up to around 80% on a weight basis of dry feed [19]. The byproducts of fast pyrolysis include biochar and noncondensable gases (NCG), primarily consisting of CO_2 and CO. Biochar can be directly combusted for process heat or alternatively used as a soil amendment due to its ability to absorb nutrients and retain water [7]. The bio-oil produced from fast pyrolysis is a complex mixture of highly oxygenated compounds including alcohols, aldehydes, carboxylic acids, saccharides, and phenolic compounds attributing to shortcomings such as instability and corrosiveness [20, 21]. Upgrading of bio-oil is required to remove undesirable characteristics and properties for the production of upgrading is required to produce chemicals and fuels.

Solvolysis is the interaction of a solvent with a solid or liquid reactant to produce chemical products and is considered pyrolysis in the presence of a solvent [2]. Solvents used can be both polar and nonpolar and act as a catalyst to increase selectivity of desired products. Solvolysis of biomass with a hydrocarbon solvent is commonly referred to as direct liquefaction and occurs at elevated pressures (7-50 MPa) and moderate temperatures (230-450C°) [2]. Hydrothermal processing is solvolysis with the use of water as the solvent. Although solvolysis produces a higher quality bio-oil than pyrolysis, the continuous feeding of biomass into high pressure reactors results in a major technology barrier to commercialization.

Commercialization of biomass conversion technologies, whether biochemical or thermochemical, is dependent on competition with fossil fuel resources and the ability to overcome biomass utilization barriers. Processing of biomass for drying and size reduction is energy intensive and thus costly. Additionally, low bulk density content of biomass results in significant transportation costs over long distances. One study suggests that baled herbaceous feedstocks become more economical to transport by locomotive rail instead of truck after about 60 miles [22]. These processing barriers may lead to biorefineries smaller than that of large, centralized refineries used in the petroleum industry.

The optimal size of biorefineries have been studied by Wright et al. [23] and You et al. [24]. Distributed biorefineries offer the ability to build smaller plants and transport product intermediates to larger upgrading facilities. Dahlgren et al. [25] discusses the benefits of building smaller, modular plants or reactors to increase learning from mass production which results in reductions of plant capital costs. Daugaard et al. [26] studied the effect of these learning rates on the optimal size of biorefineries suggesting significant reduction in optimal plant sizes and production costs. Many studies have been conducted comparing the type technologies used in biorefineries by evaluating their economic potential in commercialization [27-32]. Although barriers to commercialization of biomass conversion technologies exist, analyses suggest that some biomass derived products are economically competitive to petroleum alternatives.

Fast Pyrolysis

Pyrolysis is defined as thermal decomposition of organic material in the absence of oxygen. It is the first step in combustion and gasification processes followed by partial

or full oxidation of the products [33]. Generally, pyrolysis processes are referred to as either slow pyrolysis or fast pyrolysis. Slow pyrolysis is geared for the production of char with reaction temperatures up to around 500°C and long vapor residence times of 5-30 minutes [11]. Heating rates of slow pyrolysis are lower than that of fast pyrolysis. Williams et al. [34] tested the influence of temperature and heating rates (5-80 K/min) on slow pyrolysis and found that lower temperatures had a greater effect on the production of char. When looking at the profitability of slow pyrolysis versus fast pyrolysis, Brown et al. [35] concluded that even with higher char yields and carbon credits, fast pyrolysis had higher rates of return due to the ability to refine gasoline from its bio-oil.

Fast pyrolysis employs high heating rates of up to 1000°C/s at temperatures of up to 650°C [11]. The process conditions for fast pyrolysis are geared for the optimal production of bio-oil. In addition to high heat heating rates, some generally accepted rules of thumb of fast pyrolysis include short vapor residence times and rapid quenching of the pyrolysis smoke [11, 15, 16, 36]. The objective is to minimize the exposure time primary pyrolysis decomposition products have in contact with char in order to collect a higher quality product. Primary pyrolysis vapors in contact with char can: 1) thermally crack into light oxygenates and non-condensable gasses and 2) repolymerize into char. Thus, for optimal bio-oil yield it is essential to prevent these phenomena and reduce vapor residence times.

The optimal bio-oil yield also depends on the composition of the biomass, specifically its composition cellulose, hemicellulose, and lignin. Additionally, the presence ash or alkali and alkaline earth metals inherent in the biomass are known to act as a catalyst to promote the production of char and noncondensable gases. Typical fast

pyrolysis bio-oil yields fall in the range of 60-70 wt. %. Biomass rich in cellulose composition can produce bio-oil yields over 70 wt. % [15], while biomass with high lignin content and high ash can result with yields below 50 wt.% [37]. Although from a conversion standpoint high bio-oil yields are desired, tradeoffs may exist with the desired quality of the bio-oil.

The bio-oil from fast pyrolysis is high in oxygen content (typically 40-50 wt. %) [11, 33] and is a mixture of over 300 compounds [38]. Bio-oil has both an organic phase (water insoluble) and an aqueous phase (water soluble). The organic phase contains mostly phenolic oligomers and is often referred to as pyrolytic lignin. Highly desired phenolic monomers are also present in the organic phase. The aqueous phase consists water, alcohols, aldehydes, carboxylic acids, esters, furans, pyrans, ketones, monosaccharides, and anhydrosugars. The high oxygen content and acidity makes the bio-oil chemically and thermally unstable resulting in issues for handling and storage [11, 20, 39]. The aging of bio-oil requires the bio-oil to be processed quickly or upgraded. The complex mixture of bio-oil limits its commercial applications available without further upgrading. Upgrading can be done through processes such as pretreatment of the biomass and bio-oil catalytic treatment.

Biomass pretreatments can be used to improve the quality of pyrolysis products. Torrefaction is a thermal conversion process that takes place in the absence of oxygen at low temperatures of 200-300°C. It is considered as a biomass pretreatment process due to its ability to increase the energy density of the biomass thus making it more attractive for biomass transportation. Several reviews on the torrefaction of biomass for biofuel production have been completed [40, 41]. Torrefaction removes moisture from the

biomass and begins hemicellulose decomposition with the removal of some organic acids. Several studies have been conducted to test the effect of torrefaction on the quality of bio-oil from fast pyrolysis [42-44]. While the quality of bio-oil from pyrolysis of torrefied biomass did improve, it either did so marginally or came at a significant sacrifice to the total yield. This suggests that the torrefaction of biomass is more likely to serve as a biomass pretreatment to reduce transportation and grinding costs.

Another form of biomass pretreatment is the acid infusion of biomass. Specifically used to passivate the alkali and alkaline earth metals (AAEM), the acid infusion of biomass is also referred to as AAEM passivation. Alkali and alkaline earth metals catalyze primary pyrolysis vapors decreasing the yield of anhydrosugars for the production of noncondensables and light oxygenates [45, 46]. Thus acid infusion, typically done with sulfuric or phosphate acid, will produce thermally stable salts from the inherent AAEM cations in biomass. The effect of acid infusion on cellulose and lignocellulosic biomass using benchtop reactors has been studied [47, 48]. Although when scaled up to laboratory reactors, the acid infused biomass resulted in operation issues due to agglomerations [49]. Dalluge et al. [50] was able to increase bio-oil quality using AAEM passivated biomass in a continuous auger reactor. They increased total sugars yield from red oak and switchgrass pyrolysis by 105 and 259 wt. %, respectively.

Improving the quality of bio-oil from fast pyrolysis can also be done by modifying operating conditions such as the type of sweep gas. Typically, nitrogen is used as a sweep due to its inertness, abundance and cost. However, it is thought that the addition of oxygen to the sweep gas can further devolatilize the lignin fraction and provide autothermal operation. Kwang et al. [51] tested a range of oxygen concentrations

(0-8.4 %, v/v) in sweep gas for a lab-scale fluidized bed pyrolysis. They found that trace amounts of oxygen {0.525-1.05 %, v/v) in the sweep gas improved the quality of bio-oil by increasing the total hydrolysable sugars and phenolic monomers. Furthermore, they extended the study and tested the effect of oxidative pyrolysis on acid infused red oak [49]. Here it was found that oxygen present in the sweep gas reduced agglomerations of the bed by approximately 90%, allowing for continuous operation of the pyrolysis of acid pretreated biomass in a fluidized bed. Additionally, the total hydrolysable sugar production increased to as high as 67 wt. % of the bio-oil yield.

In addition to studying oxygen in the pyrolysis sweep gas, studies have also been conducted recycling the noncondensable gasses. Mullen et al. [52] pyrolyzed a variety of biomass feedstocks using recycling of the product gas in a lab-scale fluidized bed. They were able to produce a deoxygenated oil richer in aromatic hydrocarbons and nonmethoxylated phenolics. Tarves et al. [53] investigated the effects of various reactive gas atmospheres in microwave pyrolysis. They found that using H_2, CH_4, or PyGas produced a more deoxygenated bio-oil as compared to pyrolysis in the presence of CO or N_2. The use of pure hydrogen at elevated pressures to improve the quality of bio-oil is called hydropyrolysis. Dayton et al. [54] tested the effect of temperature and pressures in hydropyrolysis and Marker at al. [55] converted cellulosic biomass directly into hydrocarbon fuels using an integrated hydropyrolysis system.

Catalytic pyrolysis is pyrolysis in the presence of a promoter to accelerate desired chemical reactions for the production of upgraded bio-oil, fuels or chemicals [56-62]. Goals of catalytic pyrolysis include deoxygenation of pyrolysis vapors through decarbonylation, decarboxylation and dehydration, as well as stabilizing the phenolic

monomers and dimers released during pyrolysis [2]. Common pyrolysis catalysts include metal oxides, zeolites, aluminas, silicas, molecular sieves and soluble inorganics [63]. Heterogeneous catalysts, specifically zeolites such as HZSM-5, are the most commonly used in biomass catalytic pyrolysis. Asadieraghi et al. [64] reviewed the different heterogeneous catalysts for upgrading of vapors from catalytic pyrolysis. Red mud, a by-product of the Bayer process for the production of alumina, has also been recently investigated as a catalyst for biomass pyrolysis [65, 66]. These catalysts can be used in two forms during pyrolysis: either *in-situ* or *ex-situ*.

In-situ catalytic pyrolysis employs direct contact between the biomass and catalysts within the pyrolysis reactor, whereas *ex-situ* catalytic pyrolysis only allows the pyrolysis products to come into contact with the catalyst downstream from the reactor. Advantages of *in-situ* catalytic pyrolysis include the ability to influence primary reactions and the use of a single reactor which reduces capital costs. However, the poising of the catalyst during reactions due minerals and salts inherent to the biomass comes as a disadvantage for *in-situ* catalytic pyrolysis. *Ex-situ* avoids poisoning by separating solid-phase and vapor-phase reactions, but it has its own disadvantage in the potential fouling of the catalyst due to the formation of oligomers from pyrolysis. Several recent studies have offered a comparison of *in-situ* and *ex-situ* catalytic pyrolysis of biomass [67-69].

Pyrolysis Reactor Technologies

The most crucial piece of equipment in a biorefinery is the pyrolysis reactor itself. Multiple reactor technologies exist for the fast pyrolysis of biomass and have previously been extensively reviewed [11, 16, 70, 71]. The reactors are designed to operate with high heating rates and low vapor residence times required for the optimal production of

bio-oil from fast pyrolysis. The main reactor types reviewed in this work include fluidized beds, free fall, and auger reactors.

The most widely used pyrolysis reactor is the bubbling fluidized bed (BFB) due to its well developed technology and ability to achieve high liquid yields [72-74]. The BFB uses a sweep gas to fluidize a bed with heat carrier material in order to create a homogeneous environment. The sweep gas is pre-heated in the plenum and flowed through the bed at high rates resulting in short vapor residence times and high heating rates from convection [75]. Bubbling fluidized beds are used in many industrial applications and thus are readily scaled-up. Disadvantages to the BFB reactor include sensitive hydrodynamic conditions and large quantities of inert gas at commercial scales. Large flowrates of sweep gas result in significant energy input and cost to operate at desired pyrolysis temperatures. Additionally, the bed is sensitive to biomass feedstocks that can cause agglomeration resulting in a halt of operation.

Another pyrolysis reactor technology of recent interest is the free fall or drop-tube reactor [76-79]. Drop-tube reactors are simple in design as they employ no moving parts. The biomass is fed from the top of the reactor and falls through the reactor, which is heated up by external sources such as heaters. Drop-tube reactors offer advantages compared to fluidized beds in the extremely low requirements of an inert gas and the lack of dependence on a heat carrier bed. Drop-tube reactor use gravity, rather than entrainment, to transport the devolatilizing biomass thus limiting the need for a sweep gas. Disadvantages to the drop-tube pyrolysis reactor include lower heating rates than that of a BFB reactor and a requirement for a relatively small biomass particle sizes.

The auger reactor is another promising pyrolysis reactor technology with increasing interest [11, 50, 80-83]. Auger reactors pyrolyze biomass through means of mechanical mixing with a heat carrier. Advantages of the auger pyrolyzers include minimal sweep gas rates, ability to convey robust materials, and ability to achieve similar heat transfer rates to the BFB reactor. The minimal requirement of sweep gas also make the auger reactor attractive for portable or mobile pyrolysis technologies. Additionally, auger pyrolyzers can employ different modes of heat transfer such as indirect or direct heating via heat carrier materials to provide higher heat transfer rates. The use of a heat carrier allows flexibility in the selection of reaction media with different thermophysical properties. The auger pyrolysis reactor has not been demonstrated at commercial scales resulting in a disadvantage in terms of scale-up uncertainty.

Research still needs to be completed at the lab-scale and pilot scale levels to answer questions of uncertainty for auger pyrolyzers. This includes the effect that the use of heat carrier and its flexibility of different materials have on pyrolysis product yields. The ability to recycle the heat carrier is essential for commercial operation. Thus, investigations into the recyclability of the heat carrier and its effect on pyrolysis products are required.

Current State of Auger Pyrolyzers with Heat Carrier

As previously mentioned, auger pyrolyzers (screw pyrolyzers) are a promising technology due to their minimal dependence on inert gas while still achieving comparable product yields to fluidized bed reactors. Additionally, auger pyrolyzers can be operated in either slow pyrolysis or fast pyrolysis conditions. Compared to BFBs, auger pyrolyzers

operate with lower heating rates and typically longer solid residence times. Bio-oil yields upwards of 65 wt. % have been obtained [80].

There are two fundamental different heating methods used for biomass pyrolysis with auger reactors. These will be referred to as indirect heating and direct heating. Indirect heating, shown in Figure 6, refers to heating reactor walls externally to induce pyrolysis reactions within the reactor. External heaters are typically used in lab-scale set-ups. In comparison, direct heating involves mixing a preheated heat transfer media with the biomass.

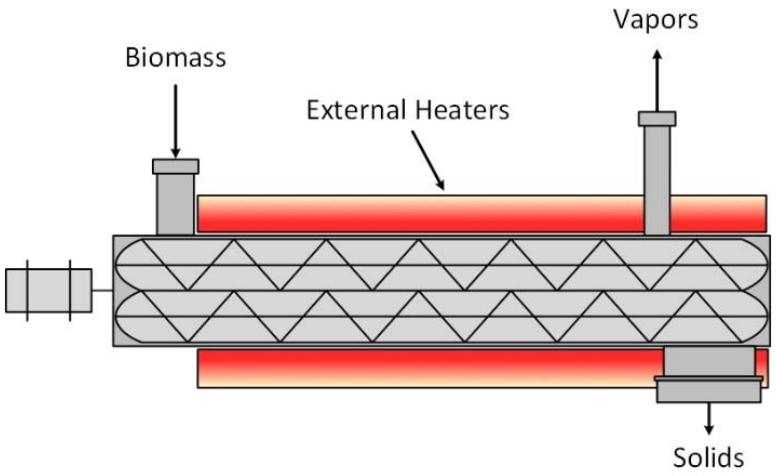

Figure 6: Schematic of an indirectly heated auger pyrolyzer.

Indirectly heated auger pyrolyzers

Auger pyrolyzers using indirect heating can be dated back to 1969 when Lakshmanan et al. [84] pyrolyzed carbohydrates using a manually operated continuous screw pyrolyzer. Ingram et al. [85] used an auger pyrolyzer indirectly heated with band heaters and at a total solids residence times of about 50 seconds. They concluded that with slower heating rates than BFB and longer residence times, a similar quality of bio-oil could be produced. More recent studies have tested the effects of operation parameters

such as temperature, residence times, and biomass flow rates in indirectly heated auger pyrolyzers [83, 86]. Thangalazhy-Gopakumar et al. [86] studied the properties of bio-oil produced from pine wood pyrolysis over a temperature range of 425-500°C. A maximum bio-oil yield of 50 wt. % was achieved at a pyrolysis temperature of 450°C, however they declared 475°C to be the optimal temperature due to the increased quality of bio-oil. Puy et al. [83] tested the pyrolysis of pine at a higher temperature range of 500-800°C. They concluded that the optimal pyrolysis temperature was 500°C due to the maximum bio-oil yield (58.7 wt. %) and composition. Additionally, they tested solid residences times of 1.5-5.0 min concluding that a time of 2 minutes was required for complete conversion. Both studies confirmed that biomass pyrolysis in an indirectly heated auger reactor offered high liquid yields comparable to conventional BFB pyrolysis systems.

Recent studies have also been conducted to further increase the quality of bio-oil produced from indirectly heaty auger pyrolyzers through means of acid or thermal pretreatment [82, 87-89]. Pittman Jr. et al. [82] acid pretreated corn stalk biomass with sulfuric acid and increased total levoglucosan and other anhydrosugar bio-oil concentrations from 16.4 to 32.2 wt. % for untreated and acid treated stalks, respectively. Zhou et al. [89] showed similar increased bio-oil quality with the sulfuric acid pretreatment of Douglas fir. Additionally, they compared the results from both an auger reactor and a fluidized bed reactor, concluding that similar product concentrations were achieved in both reactor technologies. Liaw et al. [88] and de Wild et al. [87] both studied the thermal pretreatment of biomass through torrefaction followed by subsequent pyrolysis. Bosong et al. [90] demonstrated pine catalytic pyrolysis using an auger pyrolyzer followed by *ex-situ* catalytic upgrading with a fixed bed. They showed

increased phenol, aromatic, and hydrocarbon production of 6% (peak area) to 41% from non-catalytic and catalytic pyrolysis, respectively. Even at lower heating rates, indirectly heated auger pyrolyzers offer comparable yields to fluidized bed pyrolyzers. However, limited studies exist for auger pyrolyzers with direct heating which provide higher heating rates than indirectly heated auger reactors.

Directly heated auger pyrolyzers via heat carrier

Auger pyrolysis with direct heating employs different heat transfer media, also known as heat carrier, as the heat source for pyrolysis reactions from mechanically mixing with biomass particles. A schematic of an auger pyrolyzer with direct heating via heat carrier is shown in Figure 7. In this technology, heat carriers are preheated to a desired temperature and dropped in with the biomass to begin pyrolysis reactions. Mixing is done through mechanical conveying down the length of the reactor. A heat source, such as an external heater, around the reactor may be used to prevent heat loss from the reactor to the surroundings. The use of heat carriers offers advantages over traditional indirect heated augers such as: higher heating rates, the ability to heat larger biomass particles and the flexibility of heat transfer media with desired physical or chemical characteristics. Although the use of heat carrier has advantageous heat transfer properties, it may also result in mass transfer limitations. There is limited published work on the optimization of using heat carrier in auger pyrolyzers and even less on the phenomena associated with its properties.

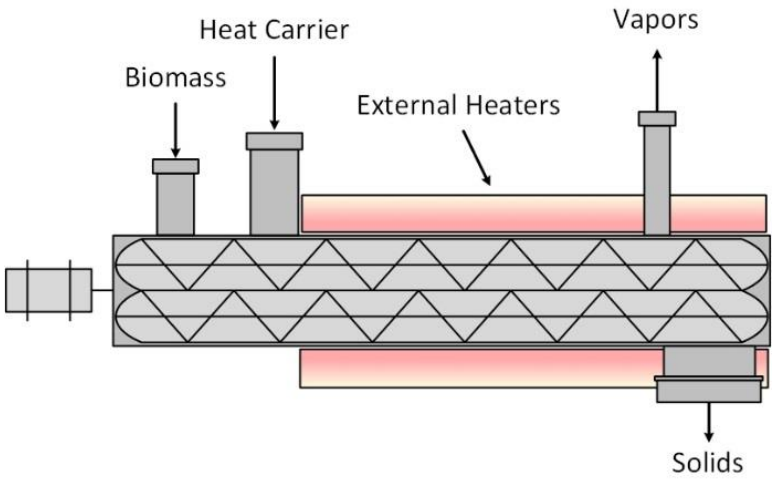

Figure 7: Schematic of auger reactor with direct heating via heat carrier.

Previous work at Iowa State University included the development of a twin-screw auger reactor with heat carrier for lab-scale pyrolysis experiments [80]. Furthermore, Brown et al. [91] tested different heat carrier temperatures, mass flow ratios, auger speeds, and sweep gas rates in said reactor. Although this is the only known study for optimization of heat carrier in an auger reactor, only one heat carrier (stainless steel) was used and the effect of its thermophysical properties were not investigated. Some work has been done to understand the mixing properties between biomass and heat carrier in twin screw mixers [92, 93]. Kingston et al. [93] built a transparent plastic model identical to the screw pyrolyzer Brown et al. [91] used. Kingston et al. optimized the mixing effectiveness via operating parameters such as screw pitch, screw rotation speed and screw rotation configurations. Although this study provides insight into the mixing effectiveness, a lack of knowledge still exists with varying heat carrier physical and thermophysical properties in a heated screw mixer.

Dalluge et al. [50] used the same twin-screw reactor developed by Brown [80] to test the feasibility of the continuous production of sugars from acid-infused biomass.

Previous work has also been done with acid-infused biomass in an auger pyrolyzer [89]. However, it was done using indirect heating and on the gram-scale. Dalluge et al. was able to increase the total sugar production by 105% using acid-infused red oak. Additionally, they were able to decrease the production of lignin oligomers and light oxygenates by 49 and 46%, respectively. Similar trends were also achieved with acid-infused switchgrass. The ability to continuously pyrolyze acid-infused biomass using an auger reactor with heat carrier was successfully demonstrated, whereas the same cannot be said about using a fluidized bed under inert conditions [49].

Additional recent work using directly heated auger pyrolyzers have tested the effect of using catalysts [69, 94]. Veses et al. [94] used the same reactor from Puy et al. [83] with modifications by mixing sand and catalyst with biomass for *in-situ* catalytic pyrolysis. Yildiz et al. [69] compared three auger pyrolysis scenarios: a control (sand), *ex-situ* catalytic pyrolysis (sand + separate catalyst reactor) and *in-situ* catalytic pyrolysis (sand mixed with catalyst). Whereas both studies used sand, there is a void in literature on the effect of sand particle size and properties in the performance of auger pyrolyzers. This can also be said about all heat transfer media used in auger pyrolyzers. Henrich et al. [95] built and operated a 10 kg/h twin-screw pyrolyzer with heat carrier. They used stainless steel balls and quartz (SiC sand) with heat carrier mass flow ratios of 30-100 and 5-20, respectively. It is of increasingly importance to understand the effects of using heat carriers with different properties and their ability to be recycled in order to minimize the operability risk when building larger auger pyrolyzers at pilot and demonstration scales.

Although Brown [80] tested a range of heat carriers (steel, sand, silicon carbide) in an auger pyrolyzer, no study has directly compared the heat transfer materials used in pyrolysis. Specifically, the effect of their heat transfer properties, such as thermal conductivity and heat capacity, are not well understood. The same can be said for physical properties such as particle size, shape and porosity. As high heating rates are desirable for fast pyrolysis [36], a heat carrier with high thermal conductivity and specific heat capacity may be advantageous. It is known that heat transfer properties of biomass, such as thermal conductivity, have an influence on its conversion time [96], and therefore a similar conclusion can be drawn for the properties of heat carriers. Thus, a study comparing different heat carriers with varying thermophysical properties in an auger pyrolyzer would fill a void in auger pyrolysis literature.

Additionally, a gap exists in the literature on the continuous use and recyclability of heat carriers used in auger pyrolyzers. In order for a biorefinery using an auger pyrolyzer to be sustainably operated, the heat carrier must be recycled through the reactor to cut down on operating costs. No study currently exists testing the recyclability of heat carrier in an auger pyrolyzer. Heat carrier attrition and compositional changes may affect the performance and cost of the biomass pyrolysis system. Henrich et al. [95] operated a 10 kg/h auger pyrolyzer with a heat carrier recycle loop for continuous operation, however the effects of recycling this heat carrier was not tested. Thus, a study looking at the effects of recycling heat carrier is needed.

Along with recyclability, the heat carrier will likely need to be regenerated. Yildiz et al. [69] reported evidence of char and coked mixed with catalyst and sand mixture. Additionally, Dalluge et al. [50] reported significant char and heat carrier

agglomeration. Heat carriers used in auger pyrolysis can also expect to accumulate carbon loading over time. Thus, regeneration of the heat carrier is needed in order to prevent the char from undesirably cracking pyrolysis vapors during the recycle. The regeneration of heat carrier and/or char could provide significant heat recovery back to the process. This is especially important for economic operation at commercial scales. A comparison could be made to fluid catalytic cracking (FCC) regeneration in the petroleum industry. As the catalyst builds up coke during the cracking process, it is regenerated via combustion. The combustion process is exothermic offering a significant amount of heat to be used back in the catalyst riser. A similar concept may be applied to the heat carrier from auger pyrolysis, however this understanding of heat carrier regeneration specific to auger pyrolyzers and its ability to provide heat recovery is not well understood. Thus, a study into the potential heat recovery of regenerated heat carriers would also fill a void in literature for auger pyrolysis.

Dissertation Organization

As discussed throughout *Chapter 1*, pyrolysis of biomass is a promising avenue to produce renewable fuels and chemicals. Specifically, auger pyrolysis reactors have been getting an increasing amount of interest as an alternative reactor to conventional fluidized bed pyrolyzers. When compared to fluidized beds and indirectly heated auger pyrolyzers, auger pyrolyzers with direct heating via a heat carrier offer advantages such as low sweep gas velocities, high heat transfer rates, and flexibility of reaction media. While auger pyrolyzers have become an increasingly promising technology, a lack of fundamental studies at the lab-scale exist and need to be realized to mitigate risk in transition to commercialization. The purpose of this work is to address some of the gaps in auger

pyrolysis literature, specifically related to continuous operation of directly heated auger pyrolyzers with heat carrier.

The work in this dissertation in summarized into four chapters, not including the introduction and conclusions. *Chapter 2* investigates the effect of heat carrier selection on the yields and composition of pyrolysis products in a laboratory-scale auger pyrolyzer. Heat carriers of interest included stainless steel shot, sand, and silicon carbide due to their varying degrees of thermophysical properties. Differences in product yields and attrition between heat carriers raised question about the long-term performance and recyclability of the heat carriers which led to the focus of *Chapters 3* and *4*.

Chapter 3 studies the effect of recycling regenerated heat carrier in a laboratory-scale auger pyrolysis reactor. Multiple recycles following regeneration with the same batch of sand heat carrier were performed. Additionally, attrition and decreasing mean particle size of the sand led to an additional investigation regarding the effect of sand particle size. *Chapter 4* investigates the regeneration conditions of heat carrier and char produced from auger pyrolysis. This study uses a fluidized bed regenerator to explore the effect of regeneration temperature, superficial fluidization velocity, and oxygen sweep concentration on carbon burn-off times.

As auger pyrolyzers offer the unique opportunity to be built at smaller capacities than commercial fluidized beds pyrolyzers, *Chapter 5* investigates the effect learning rates have on the implementation biorefineries. This study quantifies the impact learning rates through the determination of optimal biorefinery sizes and productions costs of different advanced biofuel technologies.

Chapter 6 provides a summary of the general conclusions and key findings from the preceding chapters. Also provided are some recommendations for future work on directly heated auger pyrolyzers. Lastly, the *Appendix* provides a heat transfer analysis of auger pyrolyzers with heat carriers. The rate of heat transfer between the tested heat carrier materials from *Chapter 2* was of specific focus.

CHAPTER 2. EFFECT OF THERMOPHYSICAL PROPERTIES OF HEAT CARRIERS ON PERFORMANCE OF A LABORATORY-SCALE AUGER PYROLYZER

Modified from a paper published in *Fuel Processing Technology.*

Tannon J. Daugaard[a], Dustin L. Dalluge[a], Robert C. Brown[ab], Mark Mba Wright[abc]

Abstract

This study evaluated the effect of thermophysical properties of heat carriers on the performance of a laboratory-scale auger reactor. Heat carriers tested included stainless steel shot, fine sand, coarse sand and silicon carbide. The results showed similar organic yield and composition of bio-oil among the heat carriers when pyrolyzing red oak. Significant differences in yields of reaction water, char and non-condensable gases were observed. It was also found that residual carbon contributed to as high as 20 wt.% of total char yield and attrition of heat carrier as high as 7% on a mass basis were present after as little as 2 hours of operation. Tradeoffs between physical performance, material cost, and product yields may exist when selecting heat carrier materials for pyrolysis of biomass in an auger reactor.

Introduction

Fast pyrolysis is a promising pathway to convert biomass into fuels and value added products [15]. Bio-oil is the primary product of fast pyrolysis and resembles that of

[a] Department of Mechanical Engineering, Iowa State University, Ames, Iowa 50011, United States
[b] Bioeconomy Institute, Iowa State University, Ames, IA 50011, United States
[c] Corresponding author at: 2025 Black Engineering, Iowa State University, Ames, IA 50011, United States
Email address: markmw@iastate.edu (M.M. Wright)

petroleum but is approximately half the energy density and is compositionally very different [11]. As a result, much of pyrolysis research is focused on producing a higher quality bio-oil through techniques such as biomass pretreatments [42, 49, 50, 89, 97], both *in-situ* and *ex-situ* catalytic pyrolysis [66, 69, 98, 99], and the addition of reactive gases to the inert pyrolysis atmosphere [49, 51-55].

Bubbling fluidized bed reactors are widely employed in pyrolysis applications due to their technological maturity and ability to achieve high liquid yields [11, 16, 72, 74]. Fluidized bed pyrolyzers use a pre-heated sweep gas to fluidize a bed of heat carrier material creating a homogenous environment with short vapor residence times and high heating rates from convection [75]. However, fluidized bed reactors have various disadvantages at commercial scales. Sensitive hydrodynamic conditions prevent both the use of feedstocks that cause bed agglomeration [49] and the use of bed material with high densities requiring high fluidization velocities [100]. Additionally, the use of fluidization sweep gas leads to increased energy input and cost. These disadvantages have led to research in alternative pyrolysis reactors such as the auger reactor.

Auger reactor pyrolyzers offer advantages over traditional fluidized bed pyrolyzers while achieving similar product yields [85, 91]. Advantages include minimal requirements of sweep gas, the ability to convey robust materials, and reduced solid particle entrainment in the primary product effluent stream. Several studies using indirectly heated auger pyrolyzers have been conducted to test the effect of temperature and solid residence times [81, 85, 101, 102]. Puy, Murillo [101] concluded that bio-oil yield reached a maximum at 500°C although a solids residence time of at least 2 minutes was required for complete feedstock conversion. Other researchers have proved the

viability of using indirectly heated auger reactors for the pyrolysis of both acid and thermal pretreated biomass [82, 87-89].

Direct heat transfer through the use of heat carriers in auger pyrolyzers offers higher biomass heating rates than indirect heating of the reactors. Additionally, heat carriers allow for flexibility in selecting materials with different thermophysical properties. Sand and steel shot are often employed [50, 62, 91, 95, 103]. These studies focused on the effect of biomass pretreatment [50], catalytic pyrolysis [62, 95, 103], and optimization of operating conditions [91]. Brown [80] tested multiple heat carriers and optimized pyrolysis conditions with steel shot [91]. However, to our knowledge no study has systematically compared different kinds of heat carriers in auger pyrolyzers.

One of the essential features of a fast pyrolysis process is very high heating and heat transfer rates [104]. Rapid heating combined with small biomass particle sizes (typically < 2 mm) are required to achieve high liquid yields. To achieve this rapid heating, the biomass is heated either by gas-solid heat transfer through convection, or solid-solid heat transfer driven by conduction [75]. The relative contribution from different modes of heat transfer in a pyrolysis reactor vary depending on reactor configuration. Heat transfer in fluidized beds are thought to be dominated by conduction at 90% with a small contribution of convection at up 10% [75]. Circulating fluid beds and transport reactors will have a higher contribution of heat transfer due to convection (up to 20%) [75]. Conversely, auger reactors utilize very little carrier gas, thus the primary modes of heat transfer in auger reactors will be conduction and radiation. Directly heated auger reactors with heat carrier materials will have primarily solid-solid heat transfer from conduction with additional contribution from radiation. Therefore, to achieve high

heat transfer rates, it is desirable to select a heat carrier material with advantageous thermal properties.

The objective of the present study is to determine the effect of thermophysical properties of heat carriers on the performance of an auger pyrolyzer. For solid heat carriers with no internal heat generation, we hypothesize that only the thermophysical properties influence temperature changes in the heat carrier. This study investigates the effect of three thermophysical properties (thermal conductivity, heat capacity, density) covering a wide range of a heat carrier thermal diffusivities. The larger the thermal diffusivity the faster temperature changes will propagate through the heat carrier. Therefore, it is theorized that heat carriers with large thermal diffusivities will provide higher heat transfer rates to the biomass resulting in improved product yields and composition. Four different heat carriers (stainless steel shot, fine sand, coarse sand, silicon carbide) were selected for comparison in pyrolysis trials of red oak using a laboratory-scale, twin screw reactor.

Materials and Methods

Feedstock preparation

Northern red oak (*Quercus rubra*) obtained from Wood Residuals Solutions (Montello, WI) was used as feedstock for all trials in this study. The as-received feedstock was dried to moisture content of 7.3 $\pm$ 0.1 wt.% and ground using a Schutte-Buffalo Hammermill® Model 18-7-300 pilot-scale Circ-U-Flow Hammer Mill with a 1/8” screen. Additional size reduction was completed using a Retsch® Type SM2000 Heavy-Duty Cutting Mill with a 750 μm screen. The feedstock was then sieved to a final

particle size range of 300-710 µm using a W.S. Tyler Ro-Tap® sieve shaker. Proximate and ultimate analysis of the red oak feedstock used in this study is reported in Table 1.

Table 1: Proximate and ultimate analysis of Northern Red Oak (*Quercus rubra*).

Proximate analysis	**wt.%**
Moisture content	7.3
Volatiles	78.8
Fixed carbon	13.2
Ash	0.7
Ultimate analysis	**wt.% dry, ash-free**
Carbon	50.4
Hydrogen	5.9
Nitrogen	0.1
Oxygen[a]	43.6
Higher heating value (HHV)[b]	**MJ/kg**
HHV	18.5

[a]determined by difference.

[b]determined by theoretical calculation. [105]

Heat carrier preparation

Three different heat carriers with a wide range of thermophysical properties were obtained and tested in this study. Stainless steel cut-wire shot (Type 316) and silicon carbide were obtained from Pellets LLC. (North Tonawanda, New York) and sieved to particle size ranges of 710-1000 µm and 710-1180 µm, respectively. Quikrete® All-purpose Sand No. 1152 was obtained from Lowe's (Ames, Iowa) and sieved into two size fractions: 250-600 µm denoted as fine sand and 600-1000 µm denoted as coarse sand for this work. All heat carriers were sieved using a W.S. Tyler Ro-Tap® sieve shaker.

Copper cut-wire shot was also obtained from Pellets LLC., but was abandoned during trials due to reactor operational difficulties caused by the hot copper shot becoming soft. The thermophysical properties and characteristics of the heat carriers tested in this study are shown in Table 2.

Table 2: Normalized operating conditions and thermophysical properties for stainless steel, fine sand, coarse sand, and silicon carbide.

	Operating Conditions		Thermophysical Properties at 300 K			
	Mass Flow Rate[a] (kg/h)	**Inlet Temperature (°C)**	**Bulk Density[b] (kg L^{-1})**	**Heat Capacity[c] (J kg^{-1} K^{-1})**	**Thermal Conductivity[c] (W m^{-1} K^{-1})**	**Thermal Diffusivity[c] (mm^2 s^{-1})**
Stainless steel (710-1000 µm)	15.0	575	4.6	468	13.4	3.48
Fine sand (250-600 µm)	5.1	610	1.6	800	0.27	0.22
Coarse sand (600-1000 µm)	5.0	613	1.5	800	0.27	0.22
Silicon Carbide (710-1180 µm)	4.9	623	1.6	675	490	230

[a]biomass mass flow rate = 1 kg/h

[b]measured by volumetric beaker.

[c]property from Fundamentals of Heat and Mass Transfer, 6th Edition. [106]

All heat carriers were aged prior to pyrolysis trials by to clean and remove any impurities. The aging procedure was as follows: as-received heat carrier was sieved to desired particle size (e.g. 600-1000 µm). The heat carrier was then cycled through the reactor system at specific operating conditions in the absence of biomass. After cool down, the heat carrier was re-sieved to its original particle size range (e.g. 600-1000 µm)

with any particle fines (e.g. <600 µm) discarded. The remaining heat carrier was then used for experimental trials.

Pyrolysis experiments

A laboratory-scale auger reactor first described by Brown and Brown [91] and later by Dalluge, Daugaard [50] was used in this study. A schematic of the modified reactor set-up is shown in Figure 8. The reactor is equipped with 1" OD (2.54 cm) twin-screws which co-rotate to effectively mix the heat carrier and biomass. The red oak was calibrated and fed into the reactor at 1 kg/h for all trials using a Tecweigh® Flex-Feed® Volumetric Feeder Model No. CR5. Nitrogen was used as an inert sweep gas controlled by an Alicat® mass flow controller and purged at a rate of 2.5 standard liters per minute (SLPM) for all trials. The heat carrier was preheated to a desired temperature and fed at a calibrated mass flow rate into the reactor via the heat carrier preheat system. During pyrolysis, heat carrier and reacting biomass were concurrently conveyed through the reactor at an auger speed of 54 rpm and dropped into a solids catch. This correlates to an approximate solids residence time of 12 seconds. The pyrolysis vapors (pyrolysate) and sweep gas were directed out of the reactor through the first vapor port located 10.8 cm axially down the length of the reactor from the heat carrier inlet.

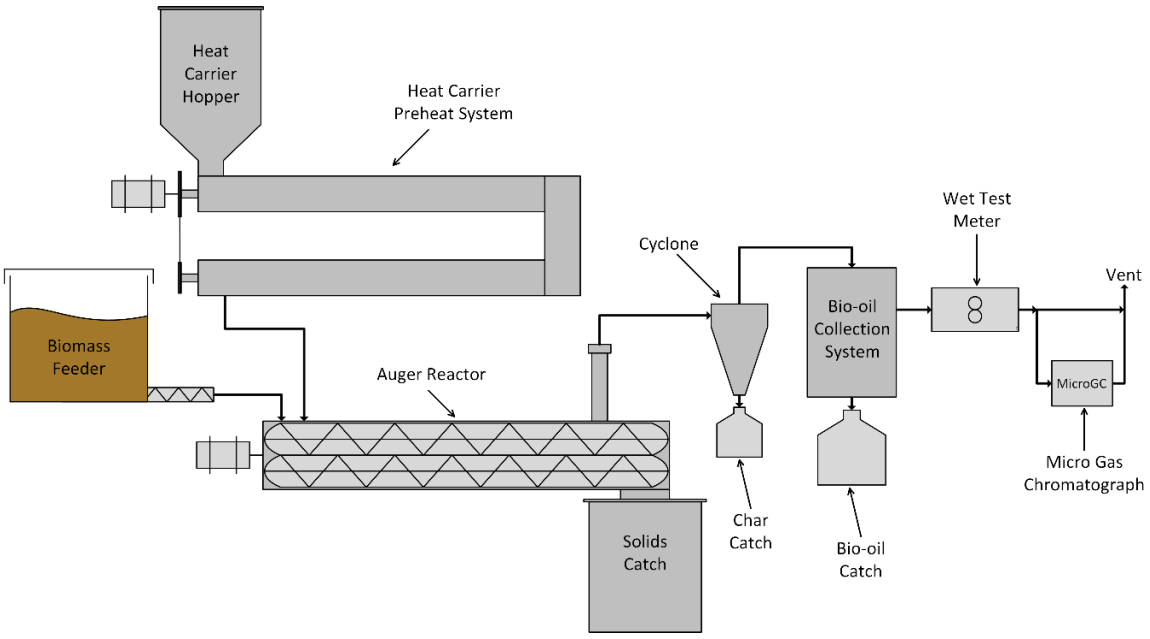

Figure 8: Schematic of auger reactor system with heat carrier preheat, solids catch, bio-oil collection, and micro gas chromatograph.

The pyrolysate and sweep gas entered a cyclone to remove entrained solids followed by a bio-oil collection unit that condensed pyrolysis liquids. The vapors were then quenched using a cold gas quench system first described by Dalluge, Daugaard [50]. Liquid nitrogen was used to quench the exiting pyrolysis stream from approximately 515°C to 110°C. An electrostatic precipitator (ESP) was then used to collect this first stage fraction (SF1), also known as heavy ends. A shell and tube heat exchanger was used to collect the remaining condensable vapors at a wall temperature of -5°C. This second stage fraction (SF2) is known as light ends. The non-condensable gases (NCGs) then passed through a Ritter® TG5/4-ER1 bar drum type gas meter to determine the total gas flow rate before being vented.

Baseline heat carrier trials were conducted with the stainless steel shot at optimized operating conditions for this reactor as determined by Brown and Brown [91]. A stainless steel shot mass flow rate of 15 kg/h was used, correlating to an approximate

heat carrier volumetric flow rate of 0.0033 m^3/h. The stainless steel shot was preheated and fed into the reactor at a temperature of 575°C. After mixing with biomass, a pyrolysis reaction temperature of approximately 515°C was measured via an internal thermocouple located 5.4 cm axially from the heat carrier inlet port.

In order to provide an accurate comparison across all heat carriers, the total volumetric flow rate and pyrolysis reaction temperature were held constant. The heat carrier mass flow rate was adjusted to maintain a constant volumetric flow rate of 0.0033 m^3/h. The required mass flow rate was calculated based on the heat carrier's bulk density. This resulted in a constant solids residence time and volumetric fill ratio across all varying heat carrier trials. The heat carrier inlet temperature was adjusted to maintain a constant pyrolysis reaction temperature of 515°C. The required inlet temperature was calculated based on the required mass flow rate and the heat carrier's heat capacity. The heat carrier mass flow rates and inlet temperatures employed for each heat carrier are found in Table 2. All experiments were conducted in duplicate. Following the completion of trials from each respective heat carrier, the reactor and heat carrier preheat system was cleaned thoroughly to prevent any contamination between heat carrier trials.

Mass balances

Mass balances were completed on the bio-oil, char, and non-condensable gases for each trail. To assure accurate mass balances, each component of the product collection system was weighed before and after an experiment. The NCGs were quantified via measuring the concentration of gases exiting the product collection system and the total volumetric flow rate of these gases. A Varian® CP-4900 micro-Gas Chromatograph (micro-GC) was used for measuring concentrations by taking a slip

stream of the exiting vapors prior to the wet test meter. The micro-GC was calibrated for gas species of acetylene, carbon dioxide, carbon monoxide, ethane, ethylene, hydrogen, methane and oxygen.

At the completion of a test, the solids catch was sieved to separate char from the heat carrier. In some trials, larger char particle sizes intermixed with heat carrier even after sieving. In this case, the burn-off procedure described by Dalluge, Daugaard [50] was used to account for this char. The contents from the solids catch were loaded into a fixed bed reactor that was then heated to 750°C by Watlow® ceramic heaters. Air was admitted at 4.0 SLPM to combust the char. The oxidized carbon in the form of carbon monoxide and carbon dioxide was measured with a Varian® CP-4900 micro-GC. Burn-off was considered complete when the composition of carbon monoxide and carbon dioxide approached zero percent in the exhaust stream. The total mass of carbon in the heat carrier was calculated from the composition and the volumetric flow of the exhaust stream measured by a Ritter® TG5/4-ER1 bar drum type gas meter during the burn-off procedure. This mass was then normalized to the percentage of carbon in a sieved char sample. The total char yield from an experimental trial includes the mass of sieved char and the mass of char from the burn-off procedure.

Bio-oil characterization

Several analytical methods were used to characterize the bio-oil due to its complex chemical composition. The methods of quantification in this study were adapted from Choi, Johnston [107]. Karl Fischer titration was used to measure water content. Water soluble sugars were quantified using High Performance Liquid Chromatography (HPLC), while organic acids were quantified using Ion Chromatography (IC). Gas

chromatography (GC) was used to identify and quantify remaining volatile compounds. Each of the two bio-oil stage fractions were analyzed individually with the results combined and reported as whole bio-oil.

Moisture analysis

A Karl Fischer MKS-500® moisture titrator with Hydranal Composite 5K® titrant was used to measure the water content in the bio-oil. The solvent used was Hydranal Working Medium K®. The titrator was calibrated using deionized water before bio-oil analysis.

Water Soluble Sugars (WSS)

High Performance Liquid Chromatography (HPLC) was used to quantify cellobiosan, galactose, levoglucosan, maltose and xylosan through a water wash method described in detail by Choi, Johnston [107]. Approximately 500 mg of a bio-oil sample was dissolved in 5 mL of distilled water and homogenously mixed using a vortex mixer. The sample was then centrifuged at 3500 rpm for 15 minutes. The supernatant was decanted and filtered using a Whatman® 0.45 µm glass microfiber filter. 25 µL of the filtered solution was injected on the HPLC for analysis.

Ion Chromatography (IC Acids)

Ion chromatography, described in detail by Choi, Johnston [107], was used to analyze organic acids including acetic acid, formic acid, glycolic acid and propanoic acid. A sample of approximately 100 mg of bio-oil was dissolved in 1.5 mL of methanol and 6 mL of distilled water. The mixture was well mixed using a vortex mixer followed by filtration through a Whatman® 0.45 µm glass microfiber filter before injection into the

IC. Samples found to have concentration of organic acids higher than the calibrated concentration range were re-run with a dilution of up to 45 mL of distilled water, opposed to the original 6 mL.

Gas Chromatography-Flame Ionization Detection (GC/FID)

Gas chromatography following the method of Choi, Johnston [107] was used for identification and quantification of volatile compounds in the bio-oil. Major compounds were first identified using an Agilent® 5977A GC/MSD coupled with an Agilent® 7890B GC. The mass spectrometer operated with electron impact ionization at a source temperature of 280˚C. The mass-to-charge ratio values (m/z) were recorded over a range of 35-650 m/z at a rate of 2 seconds per scan. A 2008 NIST library was used to identify the recorded peaks which were confirmed through GC injection of commercially available pure compounds. Quantification was done using a Bruker® 430-GC equipped with a Varian® CP-8400 liquid autosampler and Galaxy® interface software. The capillary column used was a 60 m Phenomenex ZB-1701® with an inner diameter of 0.25 mm and a film thickness of 0.25 μm. The stationary phase was 14% cyanopropylphenyl and 86% dimethylpolysiloxane. The GC injector operated isothermally at 280°C with a split ratio of 20. Ultra-high purity helium was used as the carrier gas at a constant flow rate of 2 mL/min. The oven temperature was programmed to hold at 35°C for 3 minutes, followed by ramping at 5°C/min to 300°C and held there for 3 minutes.

A four-point calibration of each identified compound was completed prior to quantification using pure compound diluted with methanol. An internal standard of Phenanthrene was added to the calibration standards. The calibration curves were

produced using the relative areas from the integration of each identified compound and Phenanthrene peaks. Correlations having R^2 values of $\geq$ 0.98 were obtained for all calibrated pure compounds. The FID relative response factor method was used to quantify commercially unavailable compounds. Each bio-oil sample was quantified by mixing at approximately 15 wt.% in a solution of methanol and Phenanthrene. One μL of each diluted sample was injected on the GC following filtration through a Whatman® 0.45 micron glass microfiber filter.

Results and Discussion

Experimental trials were conducted in duplicate. Their respective average yields are reported in this study with error bars representing the standard error of the mean for each heat carrier. The effect of thermophysical properties of different heat carriers on pyrolysis product distribution and composition was evaluated by analysis of variance (ANOVA). The ANOVA test was conducted by using SAS Institute's SAS 9.4 statistical software. Parameters with *p-values* less than 0.10 and 0.05 were considered significant with 90% and 95% confidence, respectively.

Product distribution

The mass yield of the organic bio-oil, reaction water, char and non-condensable gases from the different heat carriers are shown in Figure 9(a). The yields are reported on a mass percentage of dry feedstock with mass closures >93% for all trials. The total liquid product yield (organic bio-oil + reaction water) for stainless steel shot is comparable to previous work on the same reactor system [50, 91]. In this study, the average organic bio-oil yield was as low as 47.8 wt.%, dry basis for stainless steel and fine sand and as high as 49.9 wt.%, dry basis for silicon carbide heat carrier. The

differences in the mean organic bio-oil yields across all heat carriers were statistically insignificant. However, a comparison of the mean reaction water yields proved to be statistically significant at the 95% confidence level. Reaction water was determined in this study by calculating the total water in the bio-oil and subtracting the carried water from the feedstock moisture. As shown in Figure 9(a), stainless steel produced the lowest average yield of reaction water at 12.3 wt.% dry feedstock basis, while fine sand heat carrier produced considerably more at 15.9 wt.% dry feedstock basis.

Significant differences across the tested heat carriers were also found for both char and non-condensable gas yields. The average char yield for stainless steel heat carrier was 16.1 wt.%, dry basis and varied for all other heat carriers, reaching as high as 21.7 wt.%, dry basis for coarse sand. The differences in mean char yield across all heat carriers proved to be statistically significant at the 95% confidence level. Similarly, a comparison of the difference in the mean non-condensable gas yields for all heat carriers was statistically significant at the 90% confidence level. As shown in Figure 9(a), stainless steel shot produced the most NCGs at an average yield of 16.7 wt.%, dry basis. The NCG yield then varied for all other heat carriers to as low as 13.9 wt.%, dry basis for silicon carbide.

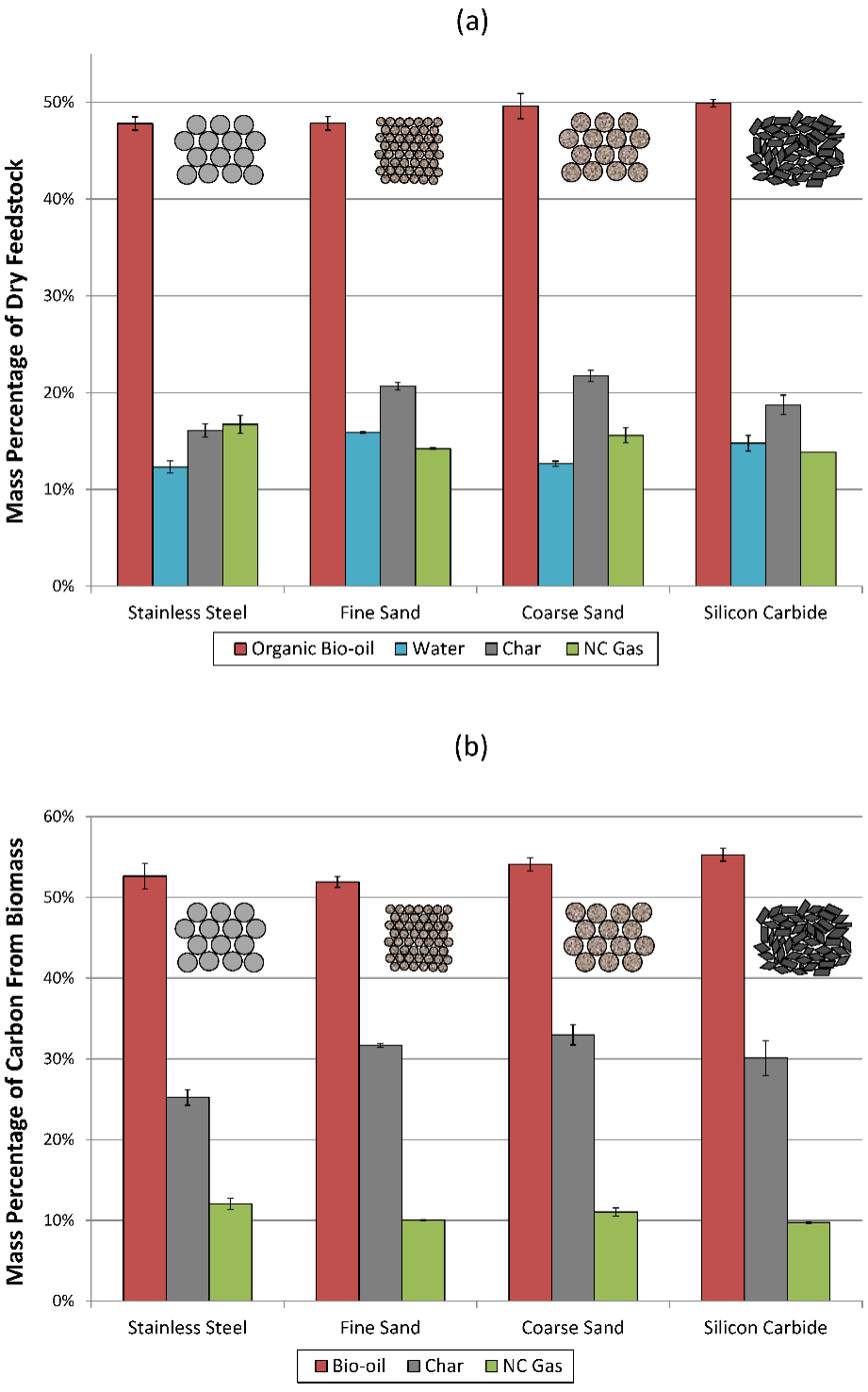

Figure 9: (a) Mass balance of pyrolysis products from different heat carriers; (b) carbon balance of pyrolysis products from different heat carriers.

A carbon mass balance for each of the heat carrier trials is shown in Figure 9(b). Carbon mass closures for all trials fell in the range of 90-98 wt.%. Silicon carbide proved to be the most successful at converting carbon from the feedstock to bio-oil with an average bio-oil carbon content of 55.3 wt.%, whereas fine sand had the lowest conversion to bio-oil at 51.9 wt.%. However, the difference in the average bio-oil carbon yield from biomass was observed to be statistically insignificant across all heat carriers. On the other hand, the difference in the average carbon yield from biomass distribution for both the char and non-condensable gases was statistically significant across all heat carriers at the 90% confidence level. As shown in Figure 9(b), stainless steel heat carrier produced the lowest char carbon conversion and highest NCG carbon conversion from biomass at 25.2 wt.% and 12.1 wt.%, respectively. The carbon yield from biomass to char was significantly larger for the other three heat carriers reaching as high as 33.0 wt.% for coarse sand. These results align with the total product yields shown in Figure 9(a).

When comparing the stainless steel shot to the other heat carriers, an increase in char and reaction water yields were present at the expense of non-condensable gases. The increase in both char and water is possible evidence of enhanced carbonization reactions [108]. This is further supported by the significantly larger carbon yields associated with char. Another possible explanation for the increase in reaction water and char is the polymerization of carbohydrate and phenolic oligomers. The restriction of carbohydrate and phenolic oligomers from leaving the reactor would lead to polymerization and charring with increased dehydration reactions [50]. Mass transfer limitations associated with low sweep gas rates and varying heat carrier size and shapes (e.g. fine sand) may be the responsible for the secondary reactions. Additionally, the sand and silicon carbide

heat carriers have a higher heat capacity and thus ability to retain the high heat carrier temperatures through to the solids catch.

Bio-oil composition and properties

The two fractions of bio-oil (heavy ends and light ends) collected in this study were distinct in appearance. The heavy ends were viscous and dark in color, while the light ends exhibited a consistency similar to water with a light reddish tint. Mass yield of both bio-oil fractions for each heat carrier is shown in Table 3. The ratio of heavy ends to light ends varied from 0.79 to 0.85 across the heat carriers but was statistically insignificant.

Table 3: Mass yield, water content, elemental composition, and heating value of whole and fractionated bio-oil (SF1 and SF2).

		Stainless steel	Fine sand	Coarse sand	Silicon carbide
Bio-oil Yield	SF1	27.7	28.4	27.4	28.7
(wt. %, dry feedstock)	SF2	32.4	35.3	34.8	36.0
Water content	SF1	7.6	7.1	6.9	9.0
(wt.%)	SF2	48.6	54.3	47.0	49.1
	Whole[a]	29.7	33.2	29.3	31.2
Elemental composition	SF1				
(wt.%)	C	56.7	56.3	57.5	56.7
	H	6.2	6.3	5.4	6.3
	N	0.1	0.1	0.1	0.1
	O[b]	37.0	37.2	36.9	36.9
	SF2				
	C	23.4	20.2	23.7	23.4
	H	7.8	7.1	7.5	6.8

Table 3. (continued)

	N	0.3	0.1	0.1	0.1
	O[b]	68.5	73.9	68.8	69.7
Higher heating value[c] (MJ/kg)	SF1	22.1	22.1	21.3	22.3
	SF2	8.4	5.5	8.0	6.8

[a]whole indicates combining SF1 and SF2 based on their respective yields.

[b]determined by difference.

[c]determined by theoretical calculation.[105]

Each bio-oil fraction (SF1 and SF2) was analyzed individually and the results where combined and reported as whole bio-oil when determining composition. The water content, elemental composition and heating value for both bio-oil fractions are reported in Table 3. Fine sand heat carrier produced bio-oil with the highest water content, whereas coarse sand produced the lowest. Looking at the elemental composition of the bio-oil fractions, the difference in the average carbon content of the heavy ends (SF1) statistically insignificant. The average carbon content of light ends (SF2) was considerably lower proved to be statistically significant at the 90% confidence level. The difference in the average oxygen yield for both the heavy ends and light ends was statistically insignificant across all heat carriers. The heating value of the heavy end bio-oil was as high as 22.3 MJ/kg for the silicon carbide. Furthermore, the heating value of the light end bio-oil was considerably less at a high calorific value of only 8.4 MJ/kg for the stainless steel.

The chemistry of bio-oil is very complex as bio-oil contains over 300 compounds, most of which are oxygenated [11]. This work identified and quantified 50 compounds

from both the carbohydrate and lignin fractions of the biomass, which is summarized in Figure 10. The total quantification of identified compounds in bio-oil, including water content, ranged from 56.9 to 60.3 wt.% for stainless steel and fine sand, respectively. The remaining unidentified portion of the bio-oil consists of non-volatiles and unidentifiable GC detectables. The results from this work, specifically from stainless steel shot heat carrier, are in close agreement with previous work conducted in the same auger system [50].

The average quantified carbohydrate fraction (anhydrosugars, carbohydrate dehydration products and light oxygenates) of the whole bio-oil ranged from 22.9 to 23.9 wt.% across heat carriers. Carboxylic acids, specifically acetic acid, accounted for the highest percentage of the carbohydrate fraction as shown in Figure 10(b). Acetic acid was as low as 4.8 wt.% for fine sand and as high as 5.3 wt.% for stainless steel. Anhydrosugars, shown in Figure 10(a) were also one of the highest carbohydrate fractions quantified ranging from 5.9 to 6.7 wt.% for stainless steel and silicon carbide, respectively. Levoglucosan yield was as high as 3.6 wt.% for fine sand and as low as 3.3 wt.% for stainless steel. A comparison of the difference in the total carbohydrate fraction, acetic acid, and levoglucosan yields were all statistically insignificant across the tested heat carriers.

The total average quantified lignin fraction of the whole bio-oil ranged from 2.9 to 3.0 wt.% for all heat carriers and is shown in Figure 10(c). Syringols, specifically 2,6-dimethoxyphenol and 4-methyl-2,6-dimethoxyphenol, accounted for the largest lignin fraction at around 1.5 wt.% for all heat carriers. Accounting for the rest of the lignin fraction was total guaiacols and total phenols each ranging from 1.2 to 1.4 wt.% and 0.1

to 0.2 wt.%, respectively, of the whole bio-oil. The difference in the total quantified lignin fraction proved to be statistically insignificant.

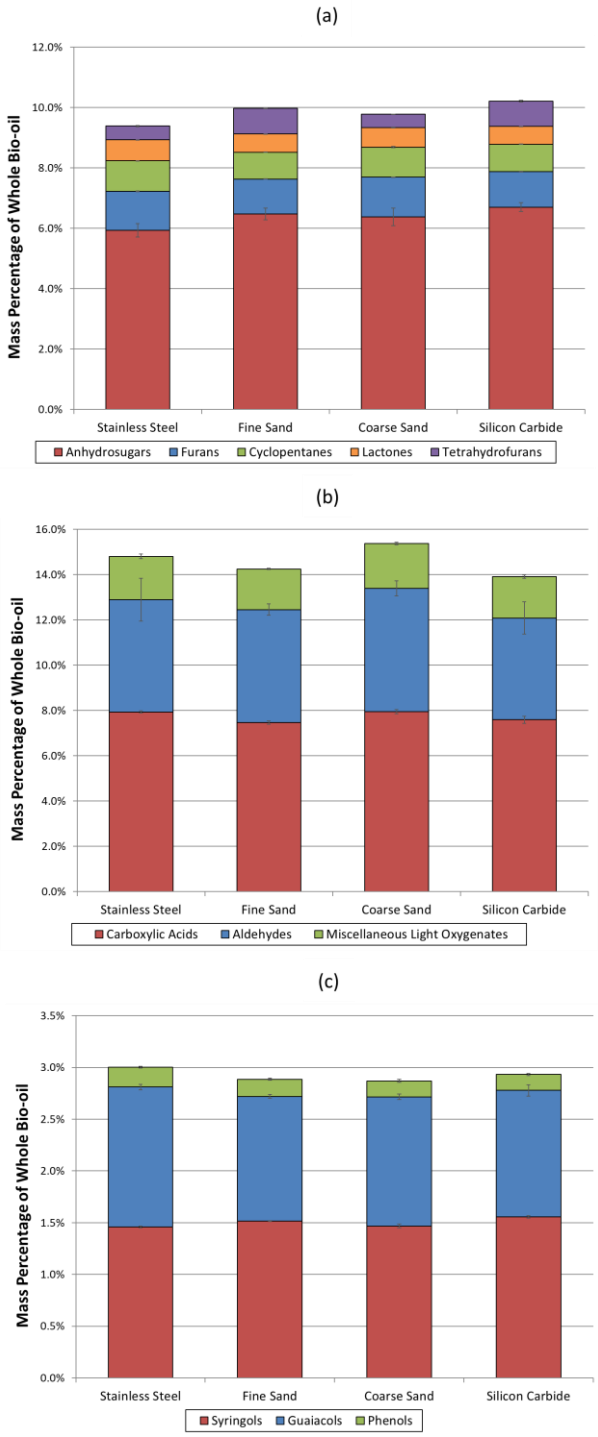

Figure 10: (a) Average yields of anhydrosugars and carbohydrate dehydration products in whole bio-oil; (b) Average yields of light oxygenates in whole bio-oil; (c) Average yields of lignin derivatives in whole bio-oil.

The lack of statistical significance in comparing the difference of organic bio-oil composition across the heat carriers was a bit surprising. It was originally theorized that the heat carriers with larger thermal diffusivities and suspected heating rates will produce increased desired primary pyrolysis products; however, this was not the case. Silicon carbide, having a significantly larger thermal diffusivity, did produce the most anhydrosugars on average but was statistically insignificant and thus comparable to fine sand with a much lower thermal diffusivity. Furthermore, stainless steel shot produced more light oxygenates and acetic acid than the fine sand. These results along with the previously discussed product yields might suggest that the rate limiting stage in the process is the heat transfer into the biomass particles rather than the heat transfer provided by the heat carriers.

Heat carrier and char characterization

During pyrolysis trials the heat carrier and reacting biomass/char are conveyed down the length of the reactor and drop into a solids catch, which is removed following a cool down of the system. The solids material consisted of both char and clean heat carrier, which was conveyed through the system to reach steady state prior to biomass feeding. Interestingly, the solids material also contained heat carrier that appeared to be coated in carbon in varying degrees. This carbon is hereinafter referred to as residual carbon. The residual carbon could not be separated from the heat carrier by physical means such as sieving or washing. Instead the residual carbon had to be combusted off and quantified to maximize carbon and mass balance closures. This carbon burn-off procedure was described previously and was conducted on the heat carrier for all trials.

Sieving was used to recover the majority of char particles prior to carbon burn-off for stainless steel (710-1000 µm) and silicon carbide (710-1180 µm) trials. This is because char particles were expected to fall below the maximum biomass particle size (310-710 µm) and the minimum size of heat carrier particles. The burn-off process allowed the mass of residual carbon on the heat carrier to be determined. This residual carbon mass is added to the mass of the sieved char to give the total char yield. Figure 11 shows the distribution of the total char yield with respect to the sieved char mass and the mass recovered from carbon loading for both the stainless steel and silicon carbide heat carrier. Both fine sand (250-600 µm) and coarse sand (600-1000 µm) had particles that overlapped the size distribution of biomass particles, making recovery of char by sieving difficult. In these cases, the carbon mass determined by burn-off was assumed to be equal to the total char yield.

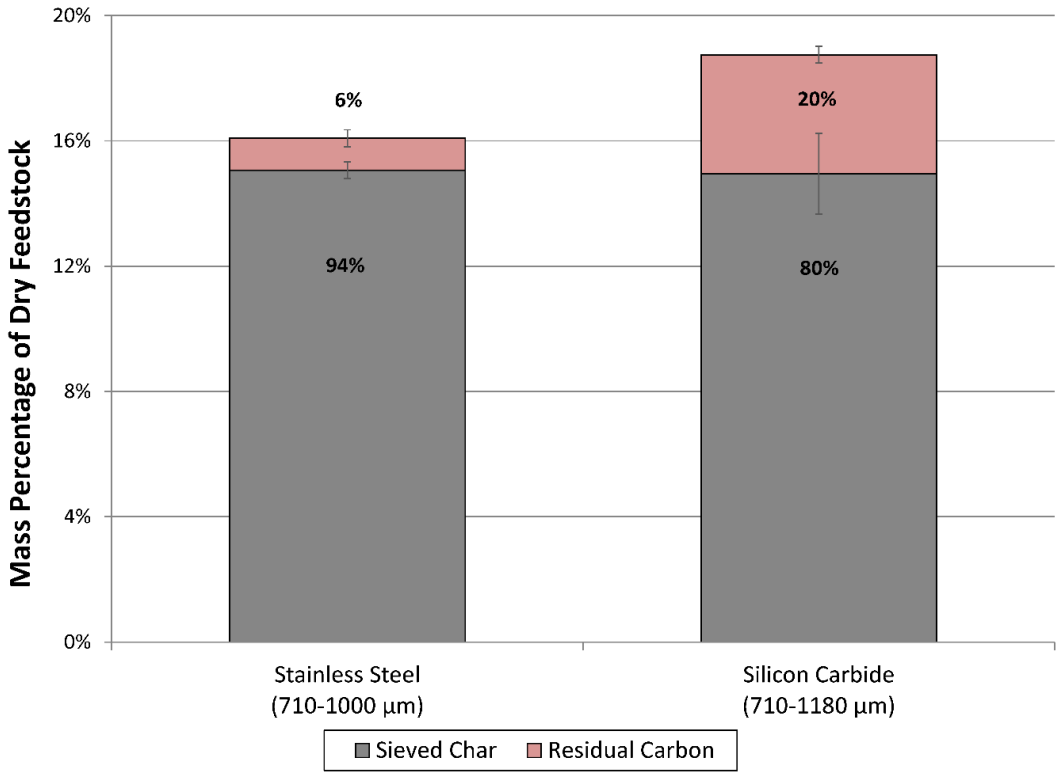

Figure 11: Char yield distribution from stainless steel and silicon carbide heat carrier.

As shown in Figure 11, sieved char particles accounted for 94 wt.% of the total char yield for stainless steel heat carrier with the remaining 6 wt.% attributed to residual carbon on the heat carrier. This distribution was similar to findings by Dalluge, Daugaard [50] using the same stainless steel heat carrier. The extent of the residual carbon for silicon carbide heat carrier, however, was significantly higher at 20 wt.%. of total char. The large difference in total char yield between stainless steel and silicon carbide is primarily due to residual char attached to heat carrier particles. One possible reason for this difference may be due differences in the shapes of heat carrier particles. The as-received stainless steel shot was smooth and spherical, where-as the silicon carbide was more shard-like with a wider range of particle sizes and sphericity. Additionally, the silicon carbide appeared to be more porous suggesting more surface area for the carbon to adhere to.

Elemental analysis and heating value for char from each trial is shown in Table 4. Silicon carbide produced the highest quality char in terms of both carbon content and heating value at 80.3 wt.%, carbon on a dry basis and 27.5 MJ/kg, respectively. Conversely, coarse sand produced char with the lowest average carbon content at 76.0 wt.%, carbon on a dry basis. Furthermore, the difference in the mean carbon content of char is statistically significant across all heat carriers at the 90% confidence level. The heating value of char produced from coarse sand was 1.4 MJ/kg lower than char from silicon carbide, however, the difference in the average heating values was statistically insignificant across all heat carriers.

Table 4: Char elemental composition and heating value.

Elemental Composition (wt.%, dry basis)	Stainless Steel	Fine Sand	Coarse Sand	Silicon Carbide
Carbon	78.5	76.7	76.0	80.3
Hydrogen	3.4	3.3	3.5	3.2
Nitrogen	0.2	0.2	0.2	0.2
Oxygen[a]	17.9	19.7	20.3	16.2
HHV (MJ/kg)[b]	27.0	26.2	26.1	27.5

[a]determined by difference.

[b]determined by theoretical calculation. [105]

During the sieving process to recover char, a considerable amount of heat carrier particles was observed in screen sizes below the initial heat carrier operating size. To determine the extent of particle breakdown, each heat carrier was cycled through the pyrolysis system at experimental operating conditions in the absence of biomass. After cool down, the cycled heat carrier was sieved to its original particle size and the fines massed. The attrition of each heat carrier was calculated and is reported in Table 5. Coarse sand produced the highest attrition at 6.6% on a mass basis, while the stainless steel shot did not show evidence of breakdown during these experiments. Interestingly, the fine sand exhibited a much lower rate of attrition (0.8% on a mass basis) than coarse sand, which were derived from the same lot of sand.

Table 5: Attrition of heat carrier.

	Initial Particle Size	Total Mass of Heat Carrier Fed (kg)	Attrition (wt.% of fines[a])
Stainless steel	710-1000 µm	30.0	Not detectable
Fine sand	250-600 µm	13.2	0.8%
Coarse sand	600-1000 µm	13.5	6.6%
Silicon carbide	710-1180 µm	11.2	3.1%

[a]fines denote the amount of heat carrier below its respective starting size range.

The extent of attrition may be attributed to system design parameters, such as the clearance between the augers and the reactor walls. Smaller heat carrier particles may easily flow through this void space whereas larger particles could catch and be mechanically ground. Support for this theory was found in abrasion and boring of surfaces in the pre-heat system after tests with larger particles. This was particularly evident for silicon carbide, which has a Mohs hardness (9.3 compared to only 5.5-6.3 for stainless steel [109]. Sand has a Mohs hardness intermediate to these two (approximately 7.0).

Non-condensable gas composition

The composition of non-condensable gases produced in the auger pyrolyzer is shown in Figure 12. As expected, carbon dioxide and carbon monoxide accounted for most the non-condensable gas yield. Small amounts of ethane, ethylene, hydrogen, and methane were also produced and grouped into light hydrocarbons shown in the figure. While the difference in the average yield of carbon dioxide was insignificant for the different heat carriers, the difference in carbon monoxide yield across all heat carriers was statistically significant at the 95% confidence level. Furthermore, the difference in

the average ratio of carbon dioxide to carbon monoxide was significant and ranged from 1.37 to 1.59 for stainless steel and silicon carbide, respectively.

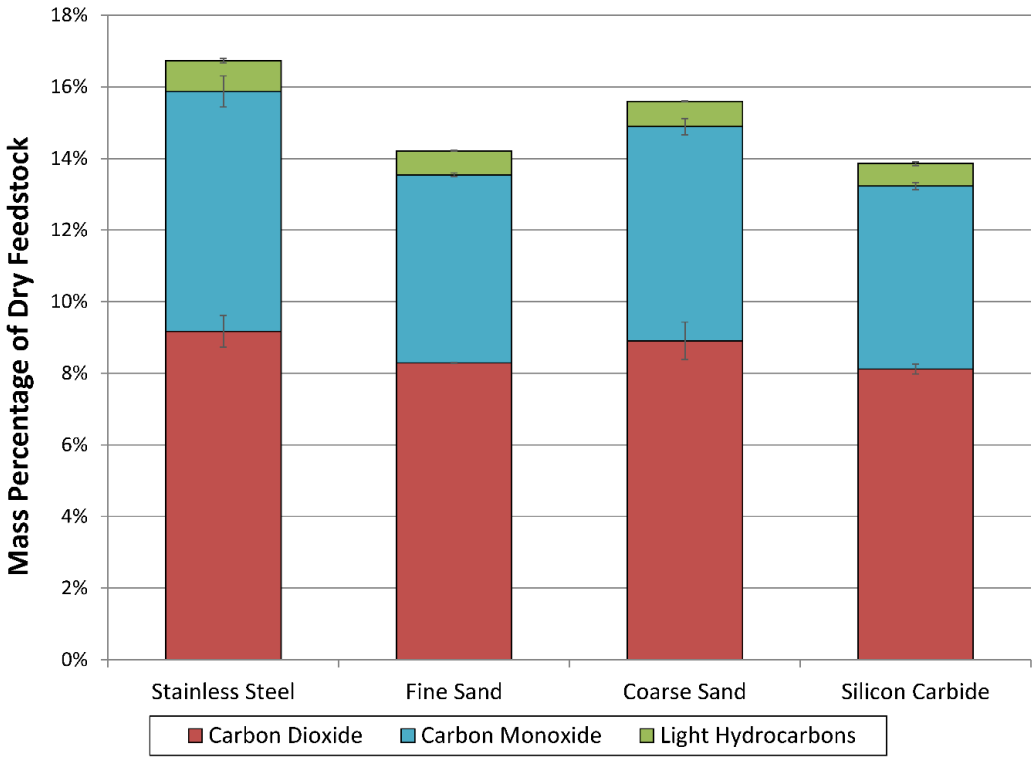

Figure 12: Composition of non-condensable gases from different heat carriers.

Conclusions

This study shows that careful consideration should be made when selecting heat carrier materials for auger pyrolyzers. Heat carriers with varying degrees of thermal diffusivities exhibited no differences in the yield of organic fraction and composition of the bio-oil. However, significant differences were observed in reaction water, char and non-condensable gas yields. Furthermore, significant residual carbon and attrition were evident for some materials after only a single pyrolysis trial. Tradeoffs may exist between the cost, physical performance, and yields between heat carrier materials.

Given the limited number of trials for each heat carrier in this work, stainless steel shot appeared to have superior performance in both low attrition and low residual carbon

yield. The low residual carbon yield of the stainless steel heat carrier allows for recovery of char particles which may be used as a soil amendment. The material cost of stainless steel shot, however, is significantly more expensive than sand heat carrier. The coarse sand heat carrier produced the highest overall char yields. The high char yields and higher heat capacity of sand suggests an ideal heat carrier for optimal performance in a continuous process with power generation from the solids material. However, the coarse sand suffered high attrition after only a single trial. High attrition leads to increased material costs over time during continuous operation and potential particle entrainment issues. Future studies are needed to understand the long-term performance and continuous operability of the heat carriers.

Acknowledgments

The authors gratefully acknowledge funding from Phillips 66. We would like to thank Patrick Johnston for assistance and guidance in analysis of pyrolysis products. The authors also thank Kwang Ho Kim and Juan Proano-Aviles for valuable discussion and analytical assistance. The authors also acknowledge the assistance of Nate Hamlett, Emily Hansen, Mitch Amundson and Levi Nauman in running pyrolysis experiments and sample preparation.

CHAPTER 3. EFFECTS OF RECYCLING REGNERATED HEAT CARRIER ON THE PERFORMANCE OF A LABORATORY-SCALE AUGER PYROLYZER

A working paper to be submitted to *Fuel Processing Technology*.

Tannon J. Daugaard[a], Theodore J. Heindel[a], Mark Mba Wright[a]

Abstract

This study investigated the effect of recycling sand heat carrier on the long-term performance of a laboratory-scale auger reactor. Similar results of bio-oil yield and composition were observed for up to five recycles of coarse sand heat carrier when pyrolyzing red oak. Attrition as high as 8% on a mass basis and a decrease in mean particle size of the heat carrier was evident after each recycle. This prompted further investigation into the effect of heat carrier particle size. Significant differences in the yields of organic bio-oil, reaction water, char and non-condensable gases were all observed when comparing coarse sand and fine sand. The smaller sand fraction produced more char and reaction water at the expense of organic bio-oil and non-condensable gases. This study shows that particle size and material selection play an important role when recycling heat carrier for continuous operation of biomass pyrolysis in an auger reactor.

Introduction

In 2007, the United States enacted the Energy Independence and Security Act with a goal to increase energy independence and security while producing clean

[a] Department of Mechanical Engineering, Iowa State University, Ames, Iowa 50011, United States

renewable fuels [110]. A provision was made to the Renewable Fuels Standard (RFS2) within the bill requiring the production of 16 billion gallons of transportation fuels from lignocellulosic biomass by 2022 in addition to conventional ethanol production. Thermochemical conversion technologies, specifically fast pyrolysis, rapidly convert biomass into a predominantly liquid product, commonly referred to as bio-oil. [15] Bio-oil can be used directly as an energy source, such as a substitute for fuel oil, or it can be further upgraded into drop-in fuels and chemicals. The recalcitrance of biomass and the low value of the intermediate bio-oil has motivated current research towards pyrolysis upgrading technologies. Examples include biomass pretreatments [42, 49, 50, 89, 97], both *in-situ* and *ex-situ* catalytic pyrolysis [66, 98, 99], and the addition of reactive gas to the inert pyrolysis atmosphere[49, 51-55].

The fast pyrolysis of biomass to bio-oil has traditionally been conducted using bubbling fluidized bed pyrolyzers due to their high heating rates and ability to achieve high liquid yields[11, 16, 72, 74]. However, disadvantages, such as sensitive hydrodynamic conditions, high fluidization velocities, and the energy required to operate at commercial scale pyrolysis temperatures, have led to increasing research in alternative pyrolysis reactor technologies. The auger reactor is one of promising interest due to its minimal dependence on a sweep gas, ability to convey robust materials, and ability to achieve similar product yields of fluidized bed pyrolyzers. Auger pyrolysis reactors in literature typically use one of two forms of heating: indirect heating with the use of external heaters or direct heating via the use of a heat transfer material. Indirectly heated auger pyrolyzers have been used to investigate the effect of temperature, solid residence times, and the pretreatment of biomass [81, 82, 85, 87-89, 101, 102]. However, direct

heating employing the use of a heat carrier offers unique advantages over indirect heating.

The use of heat carrier in auger pyrolyzers offer higher heating rates over indirect heating and allows the use of reaction media with different thermophysical properties. While much of literature uses sand or steel shot heat carrier [50, 62, 91, 95, 103], our previous work investigated the effect of other heat carrier materials with varying degrees of thermal conductivity and heat capacity[111]. We found that there was no difference in liquid product yields, but some materials had superior performance in terms of char production and physical operability. After only a single use, some heat carriers exhibited carbon loadings as high as 20% of their overall char yield. Additionally, attrition of select heat carrier materials was found to be as high as 6 wt.%. For auger reactors to run continuously at commercial scales, the heat carrier materials will need to be regenerated and recycled to minimize operating costs and maintain high process efficiencies. The effect of recycling regenerated heat carrier materials and attrition is not well understood on the long-term performance of an auger reactor.

It is well known that char, and alkali and alkaline earth metals' exposure to primary pyrolysis vapors lead to secondary reactions decreasing the yields of desired pyrolysis products such as anhydrosugars [11, 47]. Several studies using heat carrier materials in auger pyrolyzers have reported carbon loadings/coking and heat carrier agglomerations [50, 69]. Yildiz et al. [69] showed evidence of char and coked catalyst in a sand mixture of in-situ catalytic auger pyrolysis. Additionally, Dalluge et al. [50] reported significant evidence of char and heat carrier agglomerations in the same system used in this work. Regeneration of these heat carriers is required to prevent the re-

introduction of the char and coke to the pyrolysis system inhibiting primary reaction products under continuous operation. Furthermore, there is limited work utilizing recycled heat carrier materials in auger pyrolyzers. Henrich et al. [95] designed and operated a pilot-scale auger pyrolyzer utilizing a heat carrier recycle loop for continuous operation, however they did not test the effects of recycling said heat carrier. To our knowledge, no study has systematically investigated the effects of recycling regenerated heat carrier materials in auger pyrolyzers.

The objective of the present study was to determine the effect of heat carrier regeneration on the long-term performance of an auger pyrolysis reactor. A better understanding on the effect of heat carrier recycling will help to mitigate unnecessary risk in the scale-up of continuously operated auger pyrolyzers. In this study, the effect of recycling regenerated heat carriers was examined by recycling sand at up to five recycles for the pyrolysis of red oak in a lab-scale twin screw auger reactor. Additional trials were conducted to test the effect of heat carrier particle size and heat carrier to biomass mass flow ratios.

Materials and Methods

Feedstock preparation

The feedstock used in this work is northern red oak (Quercas rubra) and was obtained from Wood Residuals Solutions (Montello, WI). The as-received red oak was dried to a moisture content of <10 wt.% and milled through a 1/8" screen using a Schutte-Buffalo® Model 18-7-300 Hammermill to reduce the size of the particles. The 1/8" minus particles were then sieved using a W.S. Tyler Ro-Tap® sieve shaker using screens to a desired particle size range of 300-710 μm. The feedstock was then calibrated in the

biomass feeder for the desired operating mass flow rates. Proximate and ultimate analysis of the feedstock used in this study is reported in Table 6.

Table 6: Proximate and ultimate analysis of Northern Red Oak (*Quercus rubra*).

Proximate analysis	**wt. %**
Moisture content	7.3 ± 0.1
Volatiles	78.8 ± 0.2
Fixed carbon	13.2 ± 0.2
Ash	0.7 ± 0.1
Ultimate analysis	**wt. % dry, ash-free**
Carbon	50.4 ± 0.1
Hydrogen	5.9 ± 0.1
Nitrogen	0.1 ± 0.1
Oxygen[a]	43.6 ± 0.1
Higher heating value (HHV)[b]	**MJ/kg**
HHV	18.5 ± 0.1

[a]determined by difference.

[b]determined by theoretical calculation.[105]

Pyrolysis experiments

The chosen heat carrier of interest for this study was sand with a particle size range of 600-1000 μm, which was previously denoted as coarse sand [111]. The sand is washed Quikrete® All-Purpose Sand (No. 1152) purchased from Lowes (Ames, IA) and meets ASTM C 33 specifications. Upon arrival, the sand was sieved to its desired particle size using a W.S. Tyler Ro-Tap® sieve shaker. The sand was then aged prior to pyrolysis trials to clean and remove any impurities acquired during the shipment process. The

aging procedure was as follows: as-received sand was sieved to its desired particle size (600-1000 μm). The sand was then cycled through the reactor system at pyrolysis operating conditions in the absence of biomass. After cool-down, the sand was re-sieved to its original particle size range (600-1000 μm), and any particle fines (<600 μm) were massed and discarded. The remaining sand was then used for experimental trials.

The reactor used in this study is a laboratory-scale, twin screw auger pyrolyzer first described in studies by Brown [80, 91], Dalluge et al. [50] and more recently by Daugaard et al. [111]. A schematic of the reactor system was provided previously [111] and a brief description is provided as follows. The reactor is equipped with 1" OD (2.54 cm) twin-screws which co-rotates to effectively mix the heat carrier and biomass. A Tecweigh® Flex-Feed® Volumetric Feeder Model No. CR5 was used to calibrate and feed the red oak at 0.5 kg/h for all recycled trials. Nitrogen was used as an inert sweep gas controlled by an Alicat® mass flow controller and purged at a rate of 2.5 standard liters per minute (SLPM). The sand heat carrier was preheated to a desired temperature and fed at a calibrated mass flow rate into the reactor via a heat carrier preheat system. During pyrolysis, the solids, consisting of heat carrier and reacting biomass, were conveyed down the length of the reactor into a solids catch at an auger speed of 54 rpm. This correlates to an approximate solids residence time of 12 seconds. The pyrolysis vapors and sweep gas were directed out of the reactor through the first vapor port located 10.8 cm axially down the length of the reactor from the heat carrier inlet.

The exiting pyrolysis vapors and sweep gas then entered a product collection system consisting first of a cyclone to remove any entrained solids. The pyrolysate was then quenched using a two-staged, cold gas quench system first described by Dalluge et

al. [50]. Liquid nitrogen was used to quench the exiting pyrolysis stream from approximately 515°C to 110°C. An electrostatic precipitator (ESP) was then used to collect this first stage fraction (SF1) and will be referred to as heavy ends. A shell and tube heat exchanger was used to collect the remaining condensable vapors at a wall temperature of -5°C. This second stage fraction (SF2) will be referred to as light ends. The non-condensable gases (NCGs) then passed through a Ritter® TG5/4-ER1 bar drum type gas meter to determine the total gas flow rate and a Varian® CP-4900 micro-Gas Chromatograph (microGC) to determine gas composition before being vented.

To test the effect of recycling the sand, heat carrier was regenerated and recycled a total number of five times throughout the system at the same operating conditions. The sand was fed at 5 kg/h yielding a 10:1 kg/kg heat carrier to biomass mass flow ratio. A pyrolysis reaction temperature of approximately 515°C was maintained for all trials. Following each pyrolysis trial, the solids catch consisting of sand and char was regenerated via carbon burn-off. The regenerated sand was then sieved to its original particle size (600-1000 μm) with the fines (<600 μm) massed and discarded. The sand was then used for the next pyrolysis trial, also known as the next recycled trial. This process was repeated for a total of five recycled trials.

The regeneration process consisted of loading the solids catch into a fixed bed, carbon burn-off reactor, as described in previous work [111]. The reactor was heated to a desired temperature by Watlow® ceramic heaters in the presence of nitrogen sweep gas. Once the reactor reached steady state temperature, air was switched for the sweep gas to initiate the combustion of char and thus the regeneration process. The oxidized carbon was then measured on a Varian® CP-4900 micro-GC for quantities of carbon monoxide

and carbon dioxide. The burn-off was considered complete when the composition of carbon monoxide and carbon dioxide was below detection levels in the exhaust stream. The total mass of carbon in the sand was calculated from the composition and the volumetric flow of the exhaust stream measured by a Ritter® TG5/4-ER1 bar drum type gas meter during the burn-off procedure. This mass was then normalized to the percentage of carbon in a sieved char sample. The total char yield from an experimental trial includes the mass of sieved char and the mass of char from the burn-off procedure.

Mass balances

Mass balances were completed on the bio-oil, char, and NCGs for each trail. To accurately account for all the mass attributed to bio-oil, each component of the product collection system was weighed before and after each experiment. The NCGs were quantified via measuring the concentration of gases exiting the product collection system and the total volumetric flow rate of these gases. A Varian® CP-4900 micro-Gas Chromatograph (micro-GC) was used for measuring concentrations by taking a slip stream of the exiting vapors prior to the wet test meter. The micro-GC was calibrated for gas species of acetylene, carbon dioxide, carbon monoxide, ethane, ethylene, hydrogen, methane and oxygen. The total char yield from an experimental trial includes the mass of sieved char and the mass of char from the regeneration procedure described previously.

Bio-oil characterization

The bio-oil was characterized using several analytical methods. The methods of quantification in this study follows previous work [111] which was adapted from Choi et al. [107]. Karl Fischer titration was used to measure water content. Gas chromatography (GC) was used to identify and quantify volatile compounds. Each of the two bio-oil stage

fractions were analyzed individually with the results combined and reported as whole bio-oil.

Moisture analysis

A Karl Fischer MKS-500® moisture titrator with Hydranal Composite 5K® titrant was used to measure the water content in the bio-oil. The solvent used was Hydranal Working Medium K®. The titrator was calibrated using deionized water before bio-oil analysis.

Gas Chromatography-Flame Ionization Detection (GC/FID)

Gas chromatography adapted from Choi et al. [107] was used for the identification and quantification of volatile compounds in the bio-oil. Major compounds were first identified using an Agilent® 5977A GC/MSD coupled with an Agilent® 7890B GC. The mass spectrometer operated with electron impact ionization at a source temperature of 280˚C. The mass-to-charge ratio values (m/z) were recorded over a range of 35-650 m/z at a rate of 2 seconds per scan. A 2008 NIST library was used to identify the recorded peaks which were confirmed through GC injection of commercially available pure compounds. Quantification was done using a Bruker® 430-GC equipped with a Varian® CP-8400 liquid autosampler and Galaxy® interface software. The capillary column used was a 60 m Phenomenex ZB-1701® with an inner diameter of 0.25 mm and a film thickness of 0.25 μm. The column is coated with 14% cyanopropylphenyl and 86% dimethylpolysiloxane. The GC injector operated isothermally at 280°C with a split ratio of 20. Ultra-high purity helium was used as the carrier gas at a constant flow rate of 2 mL/min. The oven temperature was programmed

to hold at 35°C for 3 minutes, followed by ramping at 5°C/min to 300°C and held there for 3 minutes.

A four-point calibration of each identified compound was completed prior to quantification using pure compound diluted with methanol. An internal standard of Phenanthrene was added to the calibration standards. The calibration curves were produced using the relative areas from the integration of each identified compound and Phenanthrene peaks. Correlations having R2 values of > 0.98 were obtained for all calibrated pure compounds. The FID relative response factor method was used to quantify commercially unavailable compounds. Each bio-oil sample was quantified by mixing at approximately 15 wt.% in a solution of methanol and Phenanthrene. One μL of each diluted sample was injected on the GC following filtration through a Whatman® 0.45 micron glass microfiber filter.

Results and Discussion

All recycled trials were conducted in duplicate. The average yields for each condition were reported in this study with error bars representing the standard error of the mean for each trial. The effect of recycling regenerated heat carrier on pyrolysis product distribution and composition was evaluated by analysis of variance (ANOVA). The ANOVA test was conducted by using SAS Institute's SAS 9.4 statistical software. Parameters with p-values < 0.10 were considered significant with 90% confidence, while p-values <0.05 were considered significant with 95% confidence.

Product distribution

The mass yields of the organic bio-oil, reaction water, char and non-condensable gases from the recycled trials are shown in Figure 13. The yields are reported on a mass

percentage of dry feedstock with mass closures for all trials > 90 wt.% excluding RT4. The trial denoted as RT0 reports the yield of the coarse sand with no regeneration. This was completed from the previous work [111] and was conducted with a mass flow ratio of 5:1 kilograms of sand to kilograms of biomass. The batches of sand from RT0 were then regenerated and used as the heat carrier for the first recycled trial (RT1) at the operating parameters described previously with a mass flow ratio of 10:1 kilograms of sand to kilograms of biomass. The spent heat carrier was then regenerated, and the process was repeated for the second recycled trial (RT2) through a fifth recycled trial (RT5). It is important to note that both duplicate trials of RT4 had low mass closures (~80%) due to downstream reactor inconsistency and thus resulted in lower char yields. The char yield for RT4 shown in Figure 13 was calculated by statistical inference from the other recycled trials. The average organic bio-oil yield ranged from 41.8 to as high as 46.3 wt.%, dry basis for all five recycled trials. However, a comparison of the mean organic bio-oil yield for these trials proved to be statistically insignificant.

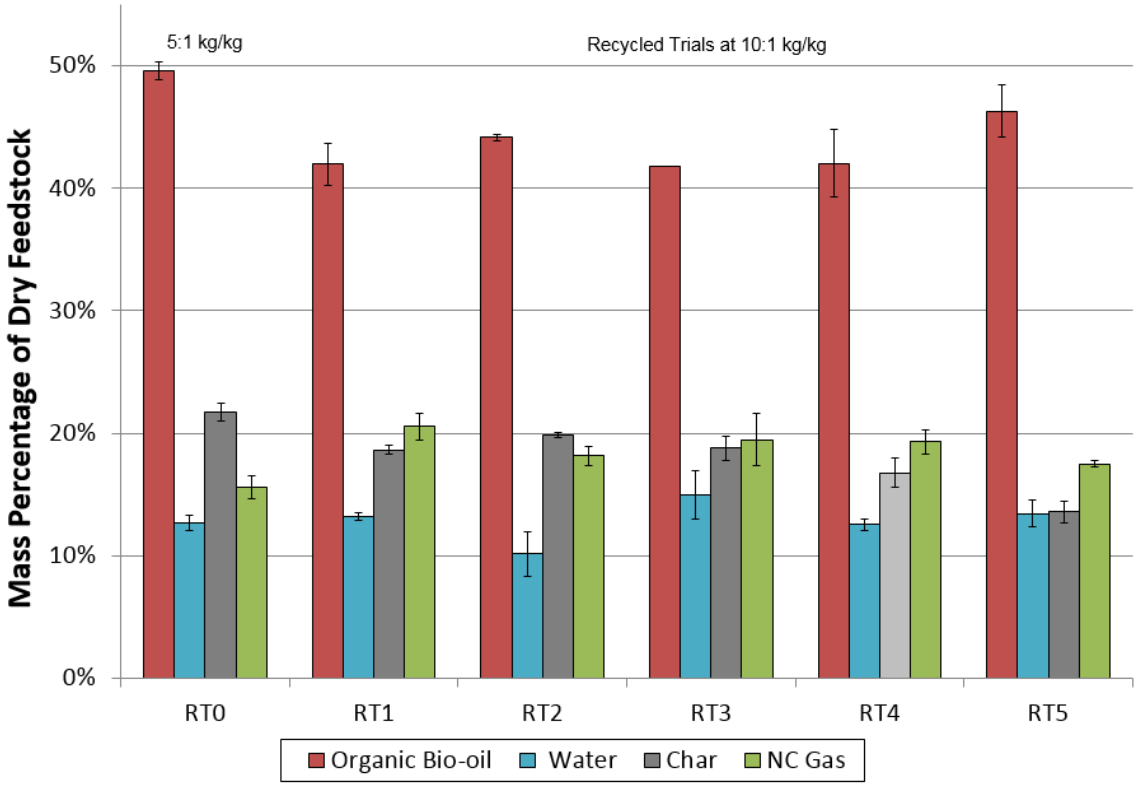

Figure 13: Mass balance of pyrolysis products from recycled coarse sand.

Reaction water, which is the difference of the carried water attributed to the feedstock moisture from the total water in the bio-oil, ranged from 10.2 to 15.0 wt.%, dry basis across the recycled trials. The difference in the average char yields between the recycled trials proved to be statistically significant. The lowest average char yield was 13.6 wt.%, dry basis for the fifth recycled trial (RT5) while RT2 produced the most char of the recycled trials at 19.8 wt.%, dry basis. The differences in the mean non-condensable gas yields was statistically insignificant across all recycled trials. The average NCG yields varied from 17.5 wt.%, dry basis for RT5 to 20.5 wt.%, dry basis for RT1.

A total carbon mass balance for each of the recycled trials was also calculated and is shown in Figure 14. Carbon mass closures for all trials were >86 wt.% for all trials.

When comparing the bio-oil carbon yields from biomass across the recycled trials, it was found that the difference in the mean yields was statistically insignificant. The fifth recycled trial produced the highest carbon content bio-oil at 52.3 wt.%, whereas the first recycled trial had the lowest yield at 48.6 wt.%. Furthermore, the differences in the average carbon yield from biomass for the non-condensable gases was also insignificant. Trials RT2 and RT5 produced the lowest conversion of carbon to NCGs at <13.0 wt.%. The difference in the mean carbon yield from biomass distribution for char however proved to be statistically significant. The third recycled trial produced the highest carbon conversion to char at 30.2 wt.%, whereas RT5 produced the lowest at 21.0 wt.%.

When comparing the number of heat carrier recycles from 1 to 5, the average organic bio-oil, reaction water and NCG yields varied but were insignificant. However, the difference in the average char yield was statistically significant. There is no evident trend in the difference of the char yields across the number of recycles. The lowest char yield was from the fifth recycled trial (RT5) which also had the lowest average mass closure at around 91 wt.% where the other recycled trials had mass closures around 95 wt.%. This difference in mass closure may be one explanation for the lower char yield where all other product yields for RT5 were within statistical insignificance of the other recycled trials. This also supports the low carbon conversion to char for RT5 shown in Figure 14.

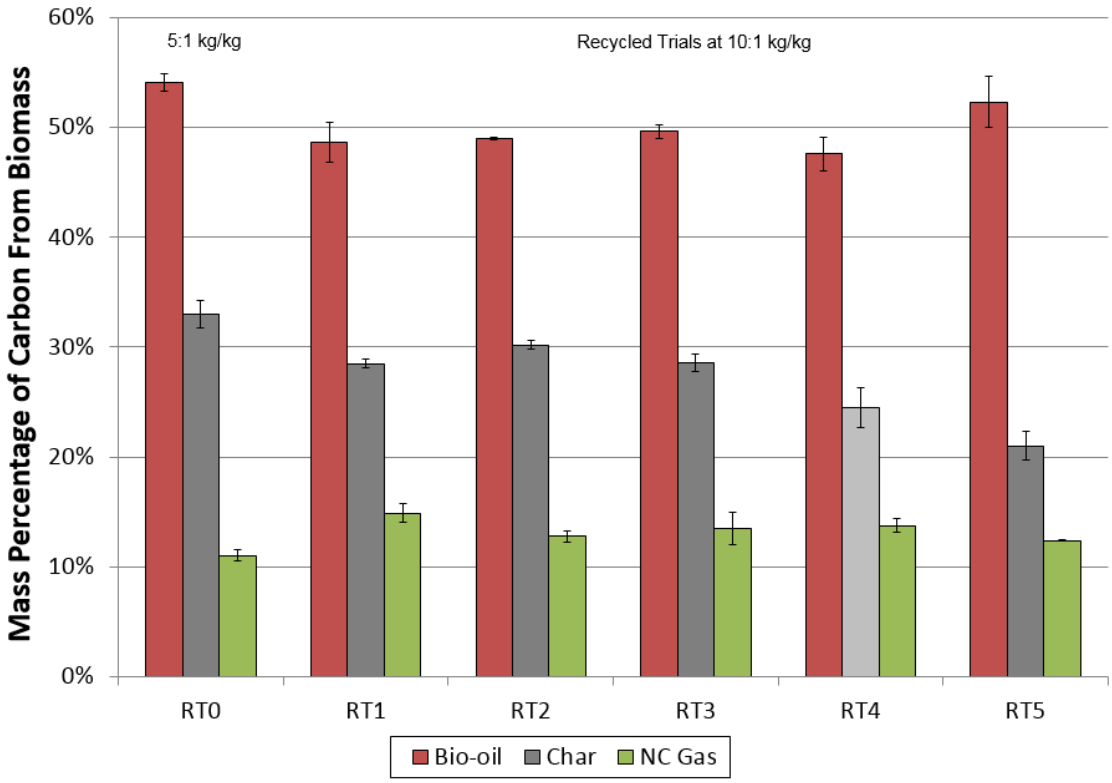

Figure 14: Carbon balance of pyrolysis products from recycled coarse sand.

Bio-oil composition and properties

Two separate fractions of bio-oil were collected for each trial in this study. The first fraction, noted as heavy ends or SF1, is dark in color and viscous. The second fraction is more aqueous with a light reddish tint and is referred to as light ends or SF2. The distribution of each fraction for the recycled trials is shown in Table 7. Also provided is the moisture content of each fraction and the whole bio-oil, the elemental composition, and the calculated heating value.

Table 7: Mass yield, water content, elemental composition, and heating value of bio-oils from recycled coarse sand trials.

		RT1	RT2	RT3	RT4	RT5
Bio-oil Yield (wt. %, dry feedstock)	SF1	25.6	26.0	26.5	25.3	29.8
	SF2	29.5	28.3	30.3	29.2	30.0
Water content (wt.%)	SF1	9.4	7.1	10.6	6.6	6.7
	SF2	54.1	49.0	56.9	55.6	56.3
	Whole[a]	33.4	29.0	35.3	32.7	31.6
Elemental composition (wt.%)	SF1					
	C	57.0	56.6	57.4	57.8	57.3
	H	5.2	5.3	5.2	5.2	5.2
	N	0.1	0.1	0.1	0.1	0.1
	O[b]	37.7	38.0	37.3	36.9	37.4
	SF2					
	C	22.8	23.8	21.9	21.2	20.3
	H	7.4	7.5	7.8	7.7	7.5
	N	0.7	0.6	0.2	0.1	0.1
	O[b]	69.2	68.1	70.1	70.9	72.1
Higher heating value[c] (MJ/kg)	SF1	20.7	20.6	20.8	21.0	20.8
	SF2	7.4	8.1	7.6	7.1	6.3

[a]whole indicates combining SF1 and SF2 based on their respective yields.

[b]determined by difference.

[c]determined by theoretical calculation.[105]

The ratio of heavy ends to light ends ranged from 0.87 to 1.00 for all recycled trials but a comparison of the difference in the means proved to be statistically insignificant. Furthermore, the difference in the average moisture content of the whole

bio-oil between recycled trials was also statistically insignificant. Whole bio-oil moisture contents of 29.0 to 35.3 wt.% were observed. Carbon content of the heavy end bio-oils ranged from 56.6 to 57.8 wt.%, while the light end bio-oil had a much lower carbon content of 20.3 to 23.8 wt.%. The heating value of the bio-oils reached as high as 21.0 and 8.1 MJ/kg for the heavy ends and light ends, respectively. These results were consistent with findings from un-recycled sand heat carrier trials shown in previous work [111].

Char and non-condensable gas composition

Table 8 shows the elemental analysis and calculated heating value of the char from each recycled trial. The average carbon content of the char ranged from 76.3 wt.%, dry basis for RT2 and RT3 to as high as 77.7 wt.%, dry basis for RT4. However, the difference in the average means of the carbon content was statistically insignificant across all recycled trials. This also held true for the calculated average higher heating values of the char from each recycled trial. Heating values varied from 24.8 to 25.9 MJ/kg for trials RT2 and RT5, respectively. The elemental composition and heating value of the char from the recycled trials were consistent with that of previous work using the same type of heat carrier [111].

Table 8: Char elemental composition and heating value from recycled trials.

Elemental Composition (wt.%, dry basis)	RT1	RT2	RT3	RT4	RT5
Carbon	76.7	76.3	76.3	77.7	77.5
Hydrogen	2.6	2.7	2.7	2.7	2.9
Nitrogen	0.3	0.3	0.3	0.3	0.3
Oxygen[a]	20.4	20.8	20.8	19.3	19.3
HHV (MJ/kg)[b]	24.9	24.8	24.9	25.5	25.9

[a]determined by difference.

[b]determined by theoretical calculation. [105]

The composition of the NCGs for each recycled trial is shown in Figure 15. Carbon dioxide and carbon monoxide account for over 80% of the volumetric gases from each trial. The remainder consists of a mixture of ethane, ethylene, hydrogen, and methane which was grouped together and denoted as light hydrocarbons. The mean difference in the respective yields for carbon dioxide, carbon monoxide, and light hydrocarbons were statistically insignificant over the recycled trials. Carbon dioxide yields varied from 36.7 to 41.8 vol.% of NCGs while carbon monoxide ranged from 42.4 to 44.9 vol.%. The yield for the remaining light hydrocarbons varied from 15.4 to 18.5 vol.% of the non-condensable gas stream.

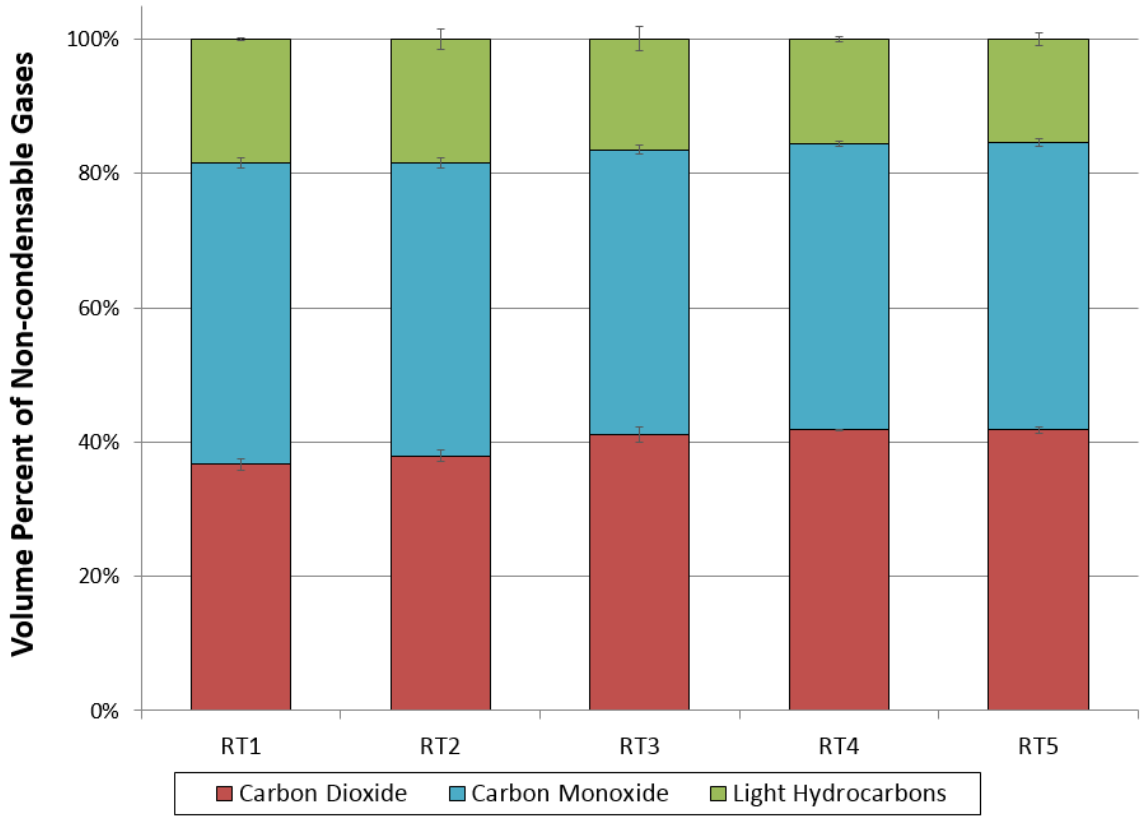

Figure 15: Composition of non-condensable gases from recycled coarse sand.

Heat carrier characterization

In our previous work, it was discovered that coarse sand (600-1000 µm) had significant attrition rates at up to 6 wt.% [111] after a single pyrolysis trial. Thus, the attrition after each recycle was quantified in this work. Following each regeneration of the solids catch from the respective pyrolysis trial, the coarse sand was sieved to the original heat carrier particle size of 600-1000 µm. The percent of fines (< 600 µm) on a weight basis was calculated to determine the attrition after each recycled trial. It is also worth noting that the recycled sand physically appeared not to be as robust in comparison to the first trial with the as-received sand (RT0). That is, there was more evidence of heat carrier dust throughout the system due to the breakdown of the regenerated and recycled heat carrier. The measured attrition is shown in Table 9.

Table 9: Attrition of Coarse Sand after Recycled Trial.

	Percent below 600 µm
RT 0 (after first sand use)	7.6 + 1.4%
RT 1 (after first recycle)	6.5 + 1.7 %
RT 2 (after second recycle)	4.6 + 1.9 %
RT 3 (after third recycle)	4.7 + 1.8 %
RT 4 (after fourth recycle)	6.0 + 1.0 %
RT 5 (after fifth recycle)	4.3 + 1.3 %

As shown in Table 9, the sand attrition was evident in all recycled trials and ranged from approximately 4 to 8% on a mass basis. However, there was no apparent correlation between the specific recycled number and the extent of attrition as the average varied across all recycled trials. Furthermore, to quantify the weakening robustness of the sand, a size distribution of the sand was conducted after the 5th recycled trial (RT5). This distribution is compared to the batch of as-received sand and is shown in Figure 16. It is clear that after only five recycled trials, the mean particle diameter of the recycled heat carrier drastically decreases. A decreasing mean particle size of heat carrier in a continuous system may have implications on product yields, so it was also decided to test the effect of heat carrier particle size in this work.

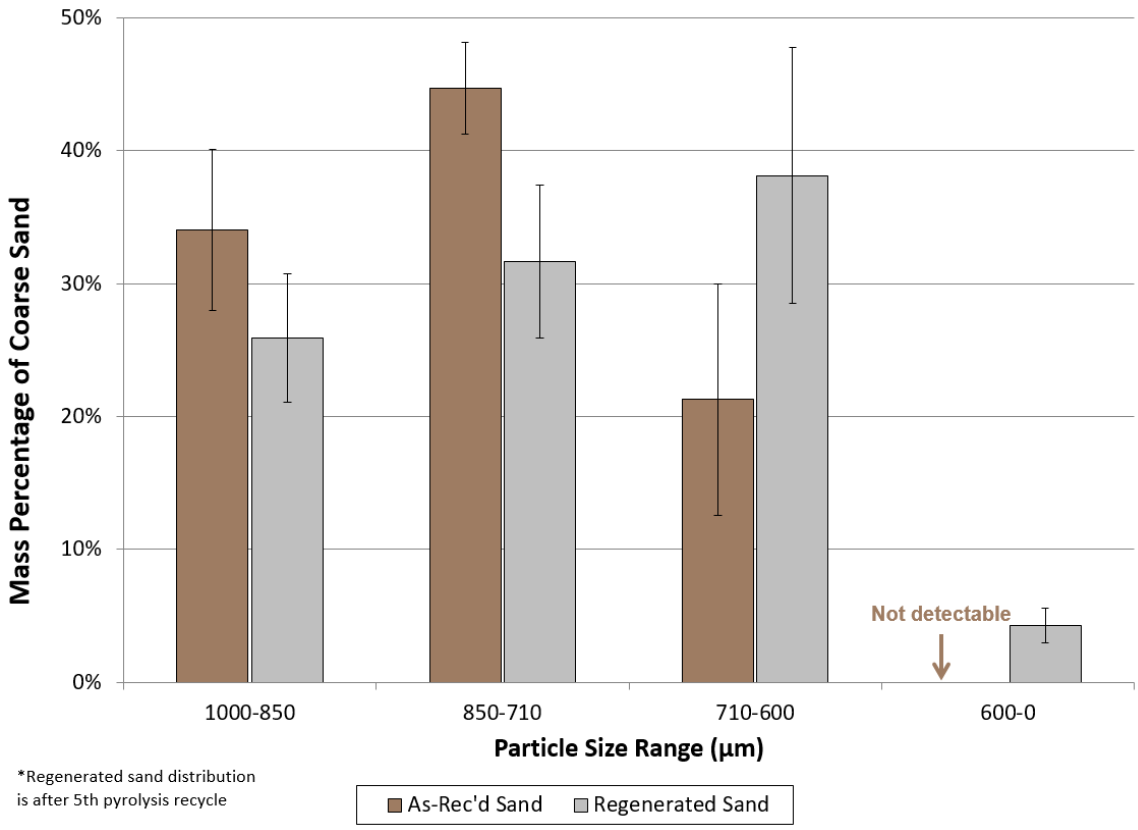

Figure 16: Coarse sand particle size distribution of as-received and recycled heat carrier.

Effect of heat carrier particle size

It was found that after only a limited number of recycled trials, the recycled heat carrier was decreasing in particle size. This raised the question as to the impact of heat carrier particle size on the pyrolysis product yields from auger pyrolyzers. Therefore, to test the impact of heat carrier particle size, trials of a smaller fraction of sand denoted as fine sand (250-600 µm) were conducted and compared to the previously tested coarse sand (600-1000 µm) in this work. Duplicate trials of each heat carrier were conducted at the same reaction conditions for adequate comparison. Additionally, the procurement and aging of the fine sand was conducted in the same fashion as the coarse sand which was described previously. The same reaction temperature of approximately 515 °C and the same heat carrier to biomass mass flow ratio of 10:1 was used to compare the coarse and

fine sand. Following the pyrolysis trials, the solids catch was regenerated via carbon burn-off to determine the carbon mass of the char for a complete mass balance for each sand fraction. Figure 17 contains a comparison of the mass balance between the different particle sizes of coarse sand and fine sand operated at the same pyrolysis conditions. The average mass closures for each heat carrier was >94 wt.%.

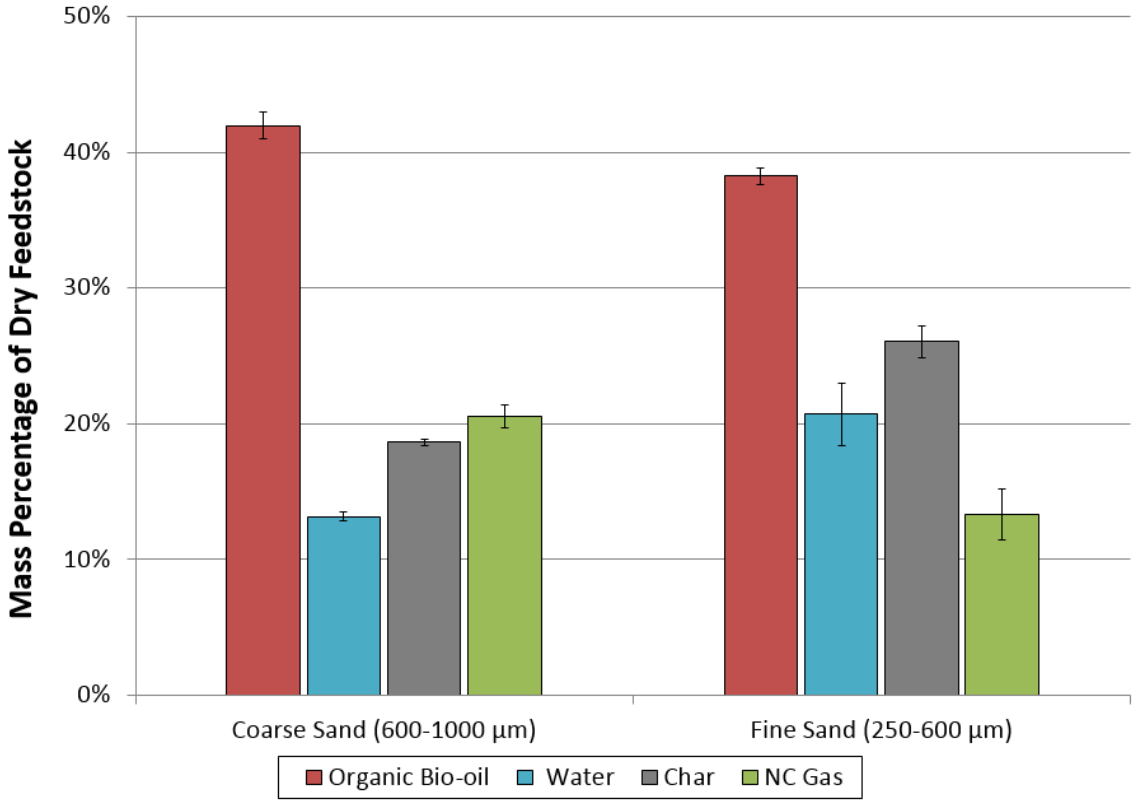

Figure 17: Mass balance of pyrolysis products from coarse and fine sand.

Interestingly, the difference in the means of each respective product yields between the coarse sand and the fine sand proved to be statistically significant. As the sand particle size decreased, the average organic bio-oil yield decreased from 42.0 to 38.2 wt.%, dry basis for coarse sand and fine sand, respectively. The average non-condensable gas yield also decreased with decreasing sand particle size. Coarse sand had an average NCG yield of 20.5 wt.%, dry basis whereas fine sand yielded only 13.3 wt.%, dry basis of

NCGs. On the other hand, both reaction water and char yields increased with decreasing sand particle size. The average reaction water yield for coarse sand was 13.2 wt.%, dry basis where a significantly higher yield of 20.7 wt.%, dry basis was produced for fine sand. Similarly, fine sand produced 7.4 wt.%, dry basis more char than coarse sand at yields of 26.0 and 18.6 wt.%, dry basis, respectively. A carbon balance comparison of the different sand particle sizes was also completed and is shown in Figure 18.

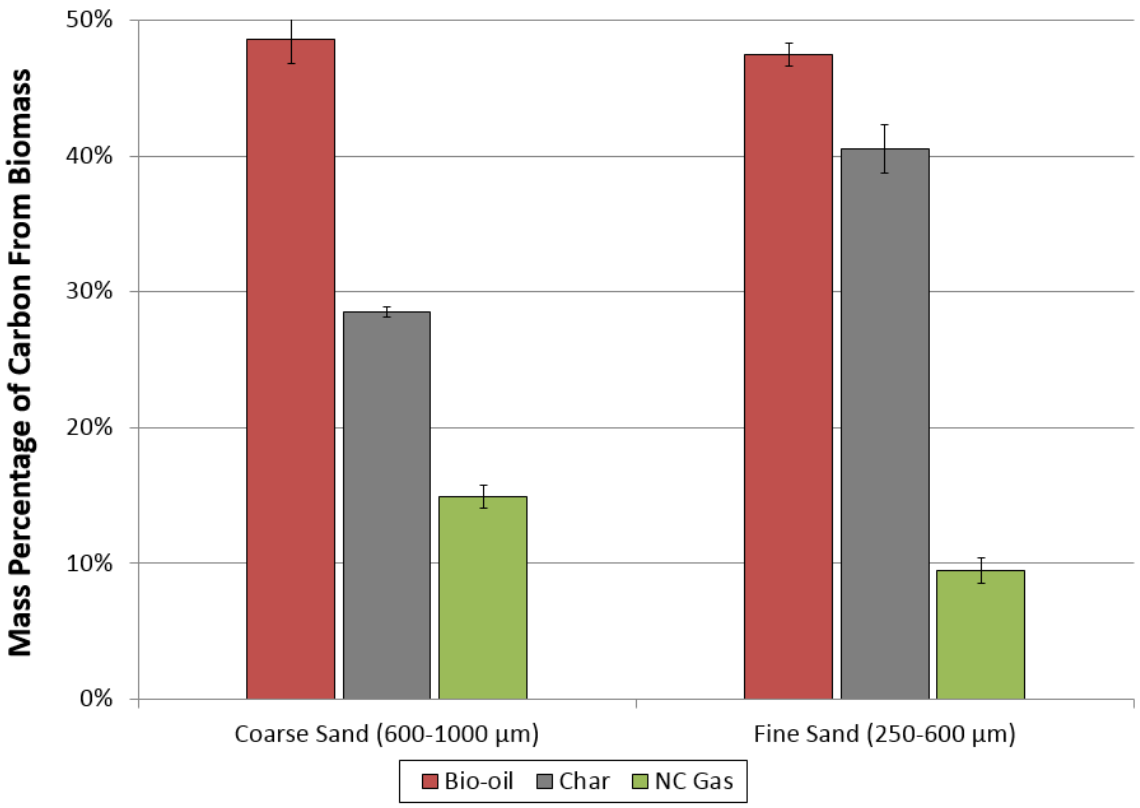

Figure 18: Carbon balance of pyrolysis products from coarse and fine sand.

Both fractions of sand converted carbon from the feedstock to bio-oil at a carbon yield of around 48 wt.% with the difference in the average mean proving to be statistically insignificant. However, the difference in the average carbon yield distribution for both char and to NCGs was statistically significant between the coarse sand and fine sand. Fine sand had the highest carbon conversion to char at 40.5 wt.% and the lowest

conversion to NCG at 9.5 wt.%. Whereas, coarse sand's char carbon conversion was considerably lower at 28.5 wt.% with a higher NCG carbon yield at 14.9 wt.%. Carbon mass closures of all coarse and find trials were between 92-97 wt.%.

Significant differences were observed when comparing the coarse and fine sand trials despite having the same heat carrier composition. The fine sand (250-600 μm) heat carrier produced significantly more reaction water and char than the larger coarse sand (600-1000 μm) particles. This came at the expense of both the organic bio-oil and NCG yields. The likelihood of secondary reactions as the result of mass transfer limitations is one theory for the significant difference. The smaller particle size of fine sand, and thus reduced void space between the heat carrier and reacting biomass particles, may restrict the vapors from leaving the reactor system. Polymerization and charring with increased dehydration reactions would be evident with the restriction of said vapors (e.g. carbohydrates and phenolic oligomers) [50] and lead to the increased reaction water and char yields for fine sand trials. Additionally, carbonization reactions would also contribute to the increased char yields [108]. Increased carbon conversion from biomass to char for fine sand as shown in Figure 18 supports this. Additionally, the carbon content of the char for the fine sand trials was significantly higher than the coarse sand at 77.9 and 76.7 wt.%, dry basis. The heating value of the fine sand char (26.6 MJ/kg) was also significantly higher than the coarse sand char (24.9 MJ/kg). These results suggest that heat carrier particle size plays an important role in the distribution and composition of pyrolysis products.

Conclusions

The results from this study suggest that heat carrier selection may have important implications for continuous auger pyrolysis operation with recycled heat carrier. There was no significant difference between the product yields of organic bio-oil, reaction water and non-condensable gases given the limited number of recycled trials. However, significant amounts of attrition were evident after each recycle of the coarse sand. Attrition as high as 8 wt.% for each recycle was observed which would lead to increased material costs during continuous operation and potential particle entrainment issues affecting the downstream product quality. Furthermore, the heat carrier mean particle size decreased with each recycle.

A comparison of two size fractions of sand heat carrier yielded significant results despite the same material composition. The fine sand fraction produced significantly higher char yields and lower NCG yields than the coarse sand. However, this came at the expense of the organic bio-oil yield and also resulted in an increase in reaction water. This study shows that heat carrier particle size has an effect on pyrolysis product yields in auger pyrolysis. Furthermore, as heat carrier is being recycled in continuous operation, the particle size is shown to decrease with high attrition suggesting pyrolysis product yields will change over time. Future studies looking at recycling of a more robust heat carrier as well as optimization of the regeneration process to understand the its effect on heat carrier properties are needed.

Acknowledgments

The authors would like to acknowledge Phillips 66 for funding. The authors would also like to thank Patrick Johnston for assistance and guidance in some of the

analytical work. We also would like to acknowledge Nate Hamlett, Levi Nauman, Ryan Spellerburg, Eric McPeak, and Catherine Le-Denmat in running pyrolysis experiments and sample preparation.

CHAPTER 4. REGENERATION OF PYROLYSIS CHAR AND HEAT CARRIER IN A FLUIDIZED BED COMBUSTOR

A working paper to be submitted to *Fuel Processing Technology*.

Tannon J. Daugaard[a], Dane Erickson[a], Theodore J. Heindel[a], Mark Mba Wright[a]

Abstract

This study investigated the effect of regeneration operating parameters on the carbon burn-off times of a laboratory-scale fluidized bed reactor. Regenerations of sand heat carrier and char from biomass pyrolysis were conducted at varying reactor temperatures, superficial fluidization velocities, and oxygen sweep gas concentration. When raising regenerator temperatures up to 750°C at the same state of fluidization, the carbon burn-off times increased due to the increase of superficial fluidization velocity. This was further investigated, and results show that with superficial fluidization velocities ranging from 100% to 250% minimum fluidization, the carbon burn-off time significantly decreases. Increasing oxygen sweep gas concentration also significantly decreases carbon burn-off times. Furthermore, increasing regeneration reaction temperatures was shown to promote carbon dioxide production. This study shows temperature, fluidization velocity and oxygen concentration play an important role in the total carbon burn-off time during the regeneration of biomass pyrolysis char.

[a] Department of Mechanical Engineering, Iowa State University, Ames, Iowa 50011, United States

Introduction

In a commercialized pyrolysis process utilizing heat transfer media, such as heat carrier in directly heated auger pyrolyzers, it may be required to regenerate the heat transfer media due to char agglomerates [50] or residual carbon [111]. The regenerations allow for complete carbon recovery from the char and prevent the re-introduction of char and ash to the pyrolysis system, which is known to promote undesirable secondary reactions. The process would also have to be continuous with recycling of the heat transfer media following regeneration, as shown in the Chapter 3. The regeneration reactor has potential in being the limiting stage of a continuous biorefinery operation. Therefore, understanding the effect regeneration conditions have on carbon burn-off times is important in designing a combustion regeneration unit for sufficient char residence times and to maximize heat recovery.

Carbon burning rates have been of interest in literature with specific focus on coal combustion. Coal char combustion has resulted in the development of many char combustion models and kinetic studies found in literature. Several studies for coal combustion investigated coal char burning rates at high temperatures, in oxygen-rich conditions and particle characteristics [112-117]. Additionally, several kinetic studies have been conducted in fluidized beds to determine coal char burning rates [118-121]. Combustion and char burnings rates for lignocellulosic biomass have only recently started to be investigated [122-124].

While coal char combustion models have evolved in the literature over the past several decades, coal combustion kinetic parameters may not be well suited to model char combustion from pyrolysis. The composition and structure of biomass char is quite

different than coal char and will impact burning rates. The porosity of biochar contributes to a higher surface area, which should result in higher reaction rates. Additionally, the high ash content in some biomass feedstocks is carried over to the char. These higher concentrations of inorganics could catalyze reactions and thus further increase reaction rates for biochar. Furthermore, it may be desired to operate regenerations of pyrolysis char and heat carrier at lower temperatures than that of combustion. Thus, improving the accuracy of char combustion reaction models from lignocellulosic biomass is needed in current combustion literature. These impacts could significantly influence the design and operation of a combustion/regeneration unit for biomass pyrolysis.

Using global reactions with the assumption of a sufficient supply of oxygen, one expression for carbon burn-off rate can be simplified to:

$$\frac{dm_{char}}{dt} = -\frac{12}{16} A_p k_e \rho_{O_2} \qquad \text{(Eq. 1)}$$

where A_p is the external particle surface area, k_e is the effective rate constant, and ρ_{O2} is the oxygen density at the surface [125]. It is clear from this equation that both temperature and oxygen concentration will influence the burning rate of carbon or char. An investigation into the effects of these conditions served as the foundation of this work.

The objective of this study is to determine the effect regeneration operating parameters have on the carbon burn-off times and heat availability from biomass char. The impact of regeneration temperature, superficial fluidization velocity, and oxygen sweep gas concentration is of specific focus. Furthermore, understanding the optimal operating conditions will be impactful on the design and implementation of a regeneration unit for continuous biomass pyrolysis. Regenerations of pyrolysis char and

sand heat carrier at these varying operating parameters were carried out in a laboratory-scale fluidized bed reactor.

Materials and Methods

Regenerator feedstock

Char produced from the pyrolysis of northern red oak was used as regenerator feedstock for all trials in this study. The pyrolysis was conducted using Iowa State University's pilot-scale, fluidized bed reactor with a pyrolysis reaction temperature of approximately 500°C. Following the pyrolysis trials, the char was sieved using a 250 µm screen with the fines discarded resulting in a final particle size range of approximately 250-1600 µm. Proximate and ultimate analysis of a sample of the char used in this study is reported in Table 10. Proximate analysis was conducted using a Mettler Toledo® Thermogravimetric Analyzer Model TGA/DSC1, while a LECO TruSpec® CHNS analyzer was used for ultimate analysis.

Table 10: Proximate and ultimate analysis of char from pyrolysis of red oak.

Proximate analysis	**wt. %**
Moisture content	1.3 ± 0.1
Volatiles	22.6 ± 0.5
Fixed carbon	74.0 ± 0.3
Ash	2.1 ± 0.2
Ultimate analysis	**wt. % dry, ash-free**
Carbon	80.1 ± 0.5
Hydrogen	3.5 ± 0.1
Nitrogen	0.2 ± 0.1
Oxygen[a]	16.4 ± 0.5

Table 10. (continued)

Higher heating value (HHV)[b]	**MJ/kg**
HHV	29.3 ± 0.1

[a]determined by difference.

[b]determined by theoretical calculation.[105]

The fluidizing and heat transfer media used in this work was silica sand, specifically, Badger® Hydraulic Fracturing Sand from Badger Mining Corporation (BMC). Badger® T30/50F sand was obtained and sieved using a W.S. Tyler Ro-Tap® sieve shaker to a tighter size range of 425-500 µm. The true density was then measured using a Quantachrome Instruments Pentapyc 5200e Gas Pycnometer. This measured density of 2660 kg/m^3 and particle size of the sand was used to calculate the sweep gas velocities to reach minimum fluidization in the regeneration unit.

Experimental set-up and procedure

The regeneration unit used in this study was first described by Dalluge et al. [50] and later by Daugaard et al. [111] but was modified for this work to operate as a fluidized bed reactor. Further description is as follows. The regeneration unit has a diameter and volume of approximately 0.108 m and 0.011 m^3, respectively. The regenerator is heated with Watlow® ceramic heaters and equipped with several internal thermocouples to measure reaction temperatures. A schematic of the regenerator is shown in Figure 19.

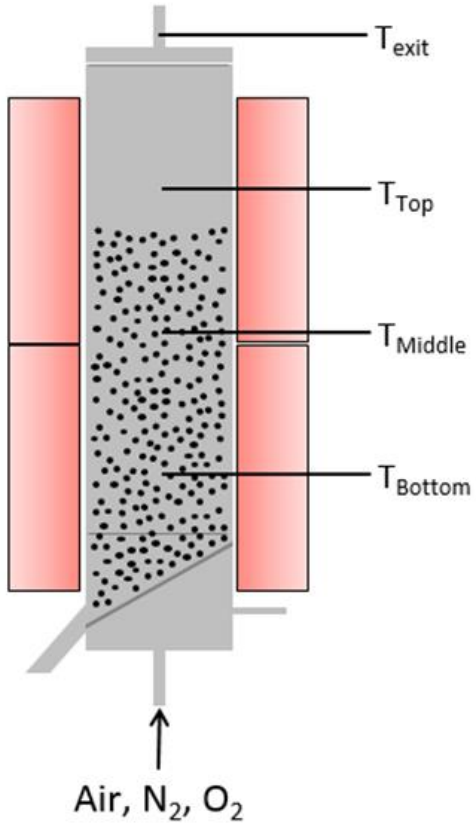

Figure 19: Schematic of regenerator with heater, sweep gas and thermocouple locations.

Following the regenerator, a cyclone was used to remove any entrained solids during trials. A condenser and desiccant filter was used to cool the flue gas and remove any water prior to gas analysis. Previous work used a Varian® CP-4900 micro-Gas Chromatograph (micro-GC) that gathered data at 5-minute intervals to measure gas composition. However, in this study the regeneration times were expected to be relatively short. Therefore, the use of the micro-GC to measure the exhaust gas composition from the regenerator was expected to be insufficient due to limited temporal resolution. Alternatively, a DeJaye Electronics Gas and Emissions Analyzer was used for continuous measurements of carbon monoxide (CO) and carbon dioxide (CO_2). The DeJaye gas analyzer was calibrated and successfully verified in series with the micro-GC during shakedown trials.

The experimental procedure for all trials in this study was as follows. The regenerator was loaded with a mixture of 0.1 kg of char and 10.0 kg of sand. These amounts are representation of the char yield and heat carrier ratios from pyrolysis trials in previous work using an auger reactor [111]. The regeneration system was then heated to a desired temperature with nitrogen as an inert sweep gas at its desired sweep gas velocity. Once the regenerator reached a steady-state temperature, a desired amount of oxygen was introduced to start the combustion and hence regeneration process. The reaction temperatures and exiting gas composition were monitored continuously throughout the process. The regeneration was considered complete when the CO_2 measurements of the exiting gas stream fell below the detection limits on a volume basis (approximately 0 vol.%). Following cooldown of the regenerator, the sand was sieved to the original desired particle size (425-500 µm) to remove any fine particles to determine the attrition of sand. Furthermore, the carbon data recovered from the gas collection system was used to normalize for a char mass in order to complete a carbon balance for each trial.

This study investigated the impact of regeneration temperature, superficial sweep gas velocity, and oxygen concentration on the burnout time of char and heat carrier from pyrolysis trials. Trials were conducted covering a temperature range of 450-750 °C, superficial fluidization velocities of 100-250% minimum fluidization, and oxygen concentrations of 13.6-28.5 vol.% of the sweep gas. The theoretical minimum fluidization velocity (u_{mf}) of the regenerator was calculated at each temperature using methods outlined in Abrahamsen et al. [126] and Kunii and Levenspiel [127]. These theoretical calculations were then experimentally verified by conducting fluidization tests with the experimental minimum fluidization velocity serving as the base velocity to

calculate the superficial fluidizing velocity for each respective trial. The minimum fluidization velocity for each regenerator temperature is shown in Table 11.

Table 11: Experimentally determined minimum fluidization velocities for all regenerator temperatures conduced in this study.

Temperature (°C)	Sand Particle Size (μm)	Minimum Fluidization Velocity, u_{mf} (m/s)
450	425-500	0.088
550	425-500	0.080
650	425-500	0.078
750	425-500	0.075

Results and Discussion

One regeneration was completed for each operating condition when comparing regenerator temperatures, superficial fluidization velocities, and oxygen sweep gas concentrations. Triplicate regenerations were conducted at a regeneration temperature of 550°C with a fluidization velocity of $1.5u_{mf}$ to ensure consistency between trials. An example of the data obtained from one regeneration is shown Figure 20 with a description of the regeneration process as follows. The regenerator was heated to its desired temperature (550°C) at a desired superficial fluidization velocity ($u_o \approx 1.5u_{mf}$) of nitrogen. Once the internal reaction temperatures reached steady state, a desired concentration of oxygen (21 vol.%) was introduced to the sweep gas to initiate the burn-off (Run Duration=0 min). As the regeneration occurred, the reaction temperatures from the internal thermocouples and the gas composition from the DeJaye Gas Analyzer were recorded. The presence of carbon dioxide and carbon monoxide verify the combustion of the char. Once the composition of both the carbon dioxide and carbon monoxide in the

gas stream was depleted, the regeneration was complete and the total carbon burn-off time was obtained (Run Duration=18 min). This procedure was used for all regenerations in this study.

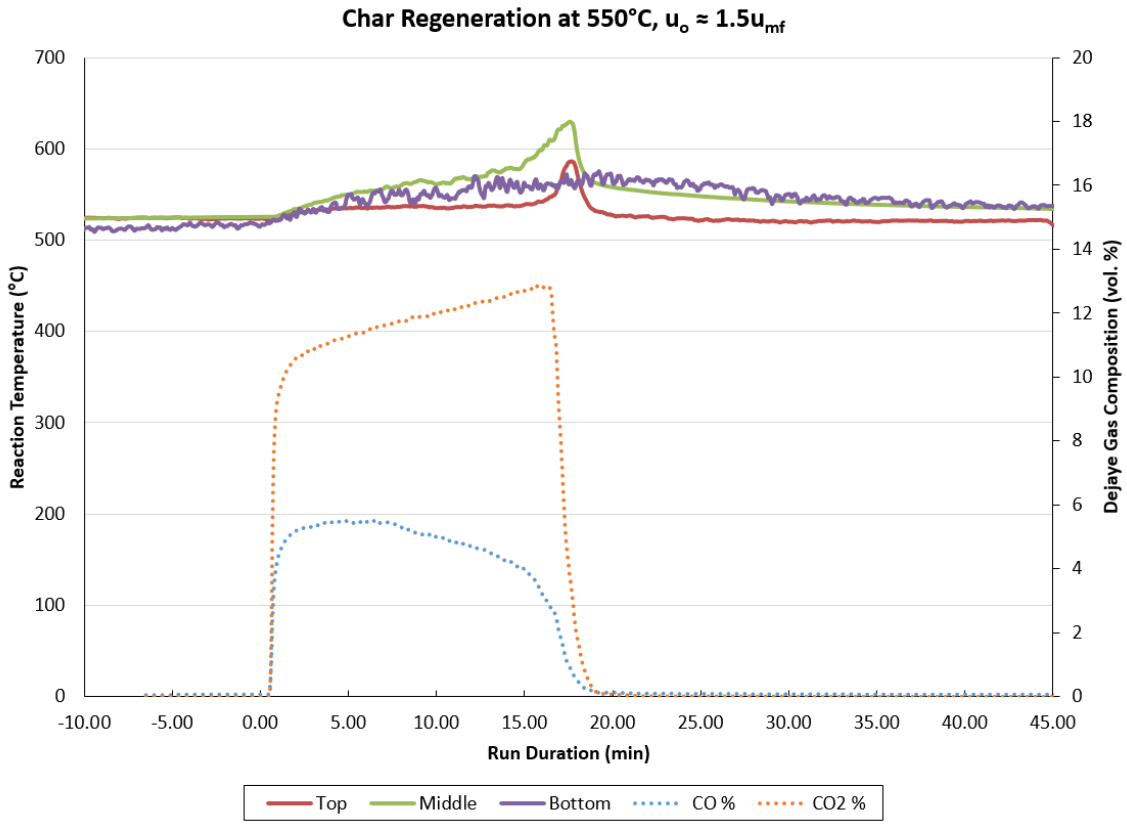

Figure 20: Example of data from the regeneration of char and sand.

It is evident from the figure that the temperature profile increased for each reaction temperature. The thermocouple denoted as "Middle" represents the thermocouple most accurately inside the bed of fluidizing sand and char material. The temperature profile also exhibited a rapid increase to its maximum temperature right before the completion of the regeneration. This is likely attributed to the fact that char particles would fluidize and segregate towards the top of the bed as a result of their density difference. The maximum temperature exotherm for each regeneration was

evaluated as the difference between the maximum temperature achieved and the steady state temperature.

Varying regenerator temperature

To test the effect of regeneration temperature on the total carbon-off, regenerations were conducted at varying regenerator temperatures of 450-750°C. These moderate combustion temperatures were chosen to represent likely operating conditions of a continuous regeneration of solids material from a biomass pyrolysis process, which typically occurring around 500°C [111]. The regenerations were conducted in air at the same fluidization regime having a superficial fluidization velocity equal to that of 1.5 times the minimum fluidization velocity at each respective temperature. The results from regenerations conducted at 450, 550, 650, and 750°C are shown in Figure 21-Figure 24.

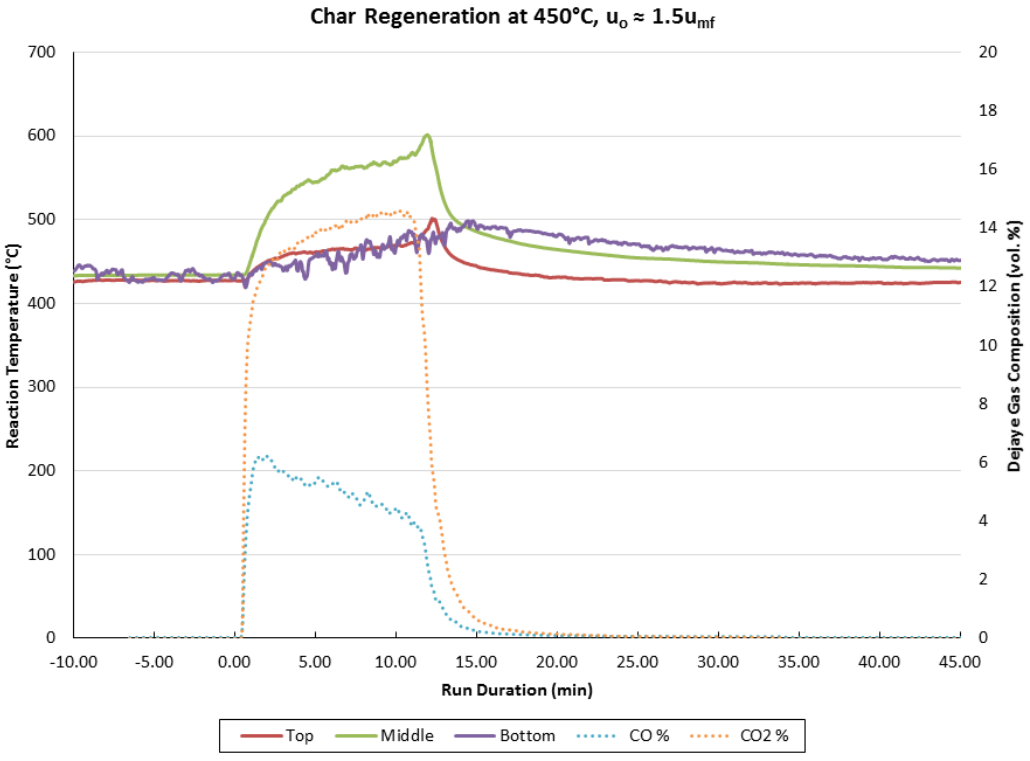

Figure 21: Regeneration conducted in air at 450°C and $1.5u_{mf}$.

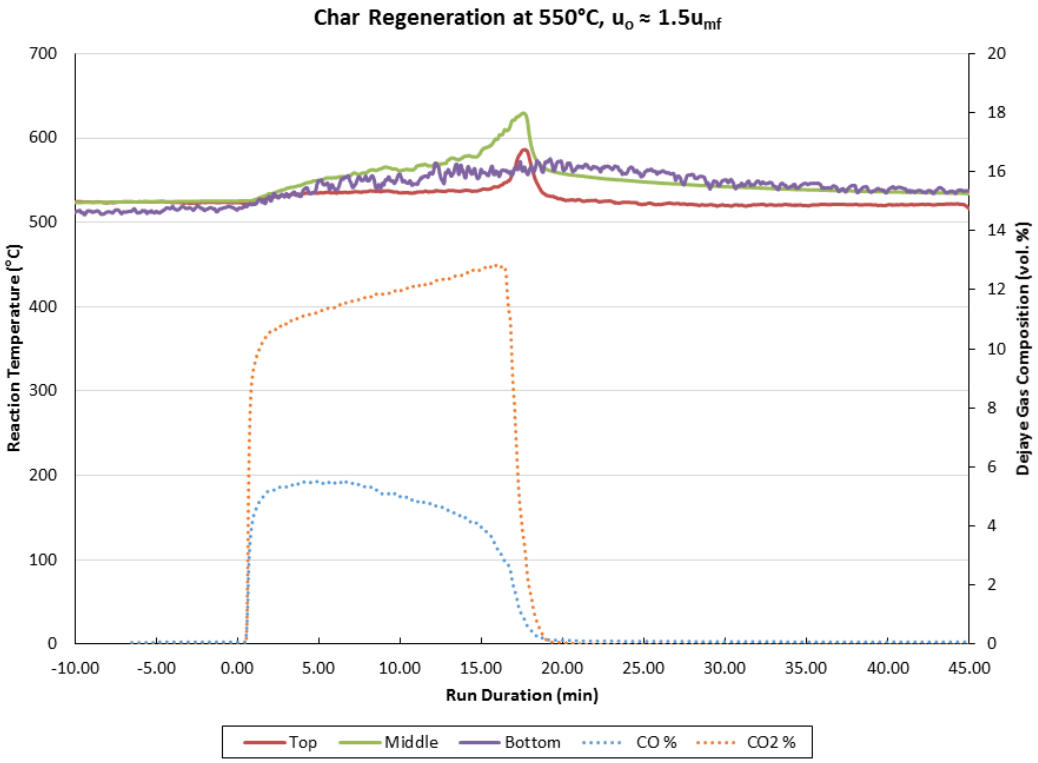

Figure 22: Regeneration conducted in air at 550°C and $1.5u_{mf}$.

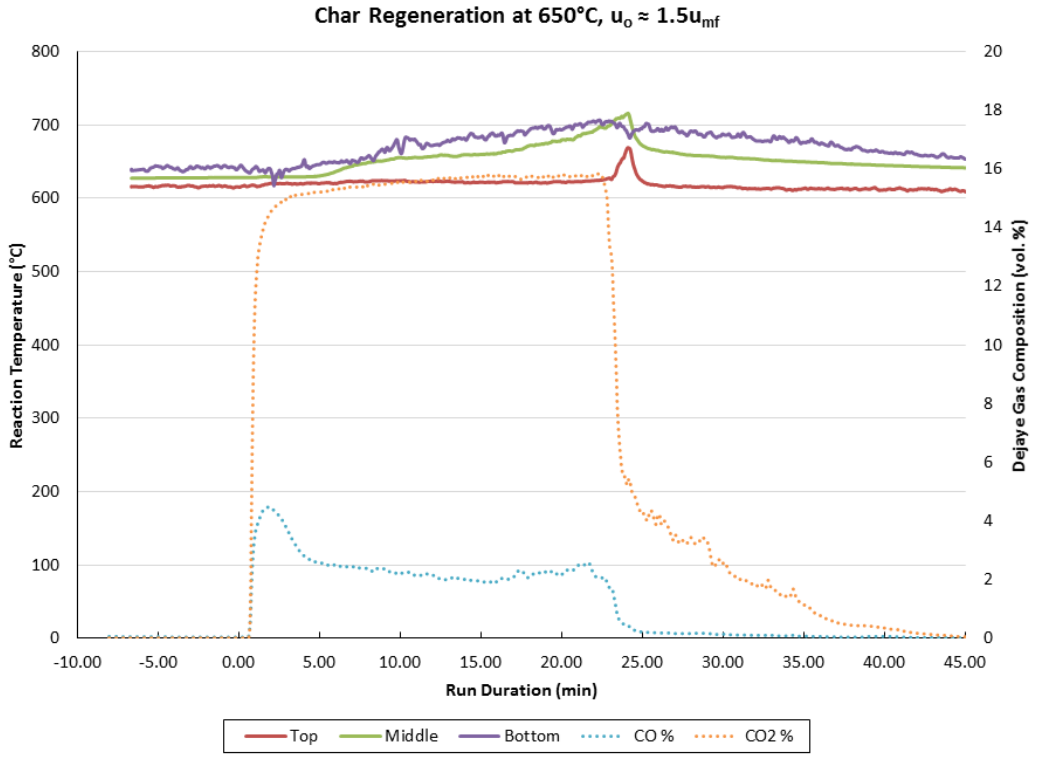

Figure 23: Regeneration conducted in air at 650°C and $1.5u_{mf}$.

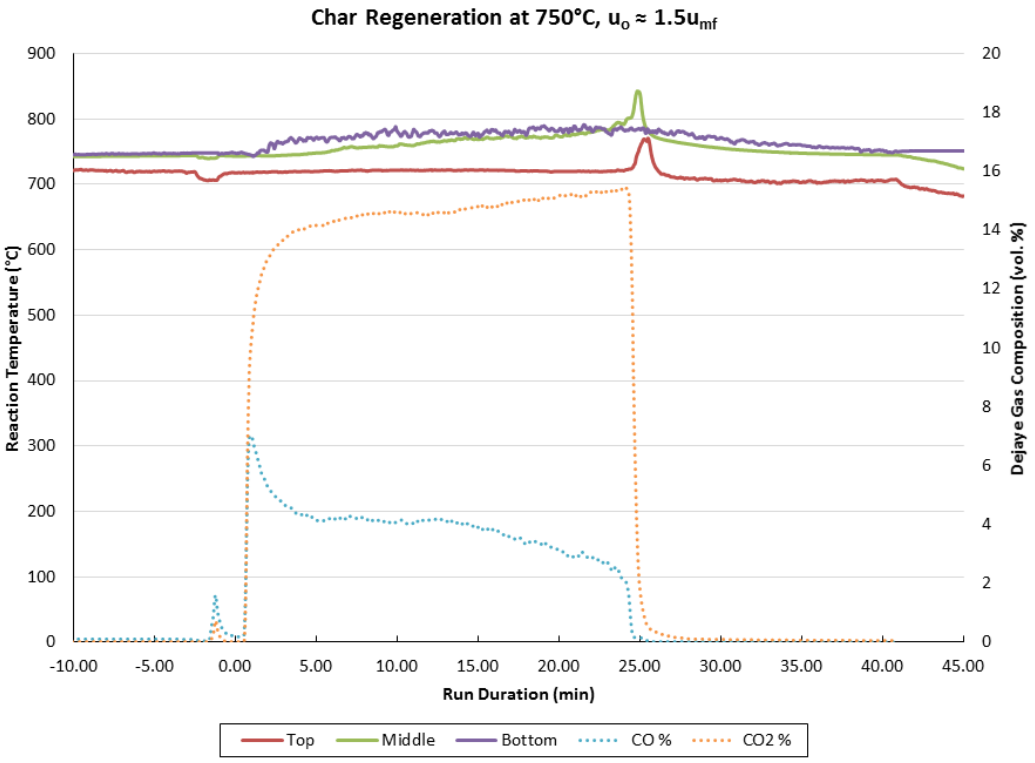

Figure 24: Regeneration conducted in air at 750°C and 1.5u_{mf}.

A comparison of figures shows that when varying the regenerator temperatures, and consequently the regeneration reaction temperatures, the carbon burn-off time increased with increasing temperature. This is attributed to the fact that each regeneration was conducted at the same state of fluidization (1.5u_{mf}) and thus each respective superficial fluidization velocity varied. A lower regeneration temperature results in a higher superficial fluidization velocity. The resulting superficial fluidization velocities and carbon burn-off times at each operating temperature are shown in Table 12.

Table 12: Summary of regeneration results with varying regenerator temperature.

Regenerator Temperature (°C)	Superficial Fluidization Velocity, $u=1.5u_{mf}$ (m/s)	Total Carbon Burn-off Time (min)	Maximum Temperature Difference, Exotherm (°C)
450	0.132	14	167
550	0.120	18	106
650	0.118	24	88
750	0.112	26	99

As shown in Table 12, the carbon burn-off time at 450°C was significantly lower than at 750°C. This is not expected as increasing temperature should increase the rate of reaction and result in a lower carbon burn-off time. These results suggest that the varying superficial fluidization velocities play a dominant role in the burn-off times at these conditions. This role was further investigated by varying the superficial fluidization velocities at the same regenerator temperature.

Another general trend observed was an increasing carbon dioxide composition with increasing reaction temperature at each respective trial. The volume percent of carbon dioxide in the exiting gas stream steadily increased for each trial as the regeneration occurred. This correlated with a steady increase of the reaction temperature profile. The carbon monoxide concentration in the gas stream decreased as the carbon dioxide increased. The increase in reaction temperature results in increased reaction kinetics and thus would favor the production of carbon dioxide as expected in complete combustion.

Varying superficial fluidization velocity

The effect of fluidization velocity on the total carbon burn-off was investigated by conducting regenerations at varying superficial fluidization velocities of 100-250% minimum fluidization. These regenerations were all conducted in air at a regenerator temperature of 550°C, which has a minimum fluidization velocity of approximately 0.080 m/s. The results for the regeneration conducted at minimum fluidization is shown in Figure 25 with the 150% minimum fluidization trial shown previously in Figure 22. The results from the regeneration trials for superficial fluidization velocities of 200% and 250% minimum fluidization are shown in Figure 26 and Figure 27, respectively.

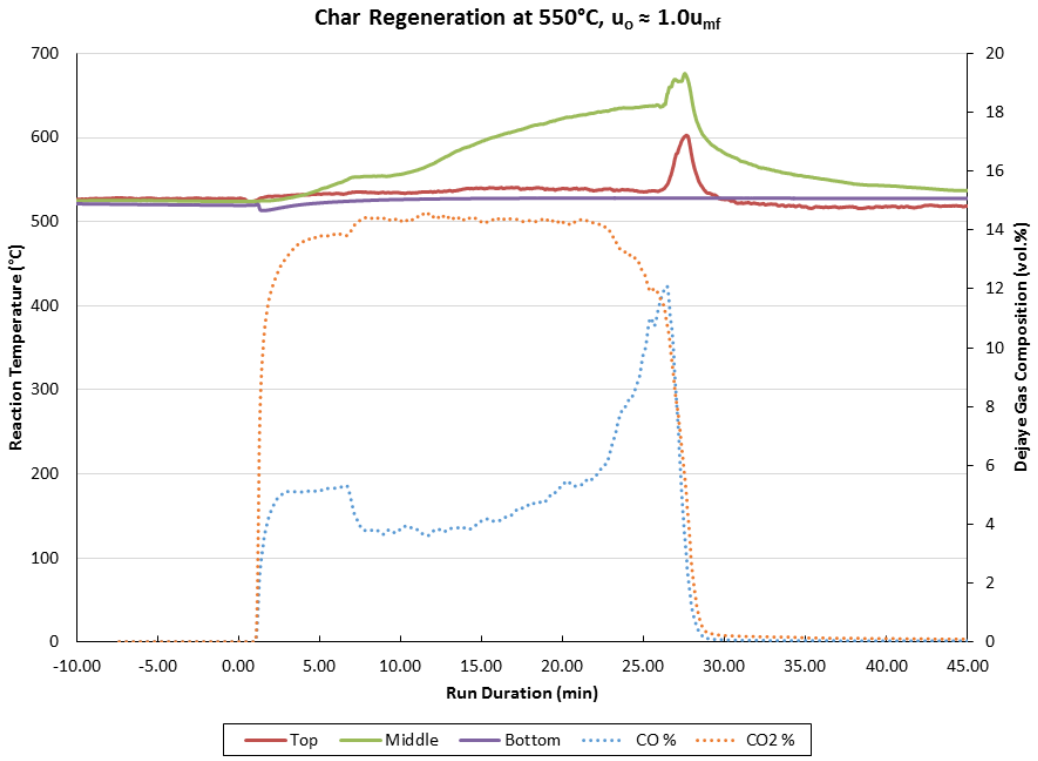

Figure 25: Regeneration conducted in air at 100% u_{mf} and 550°C.

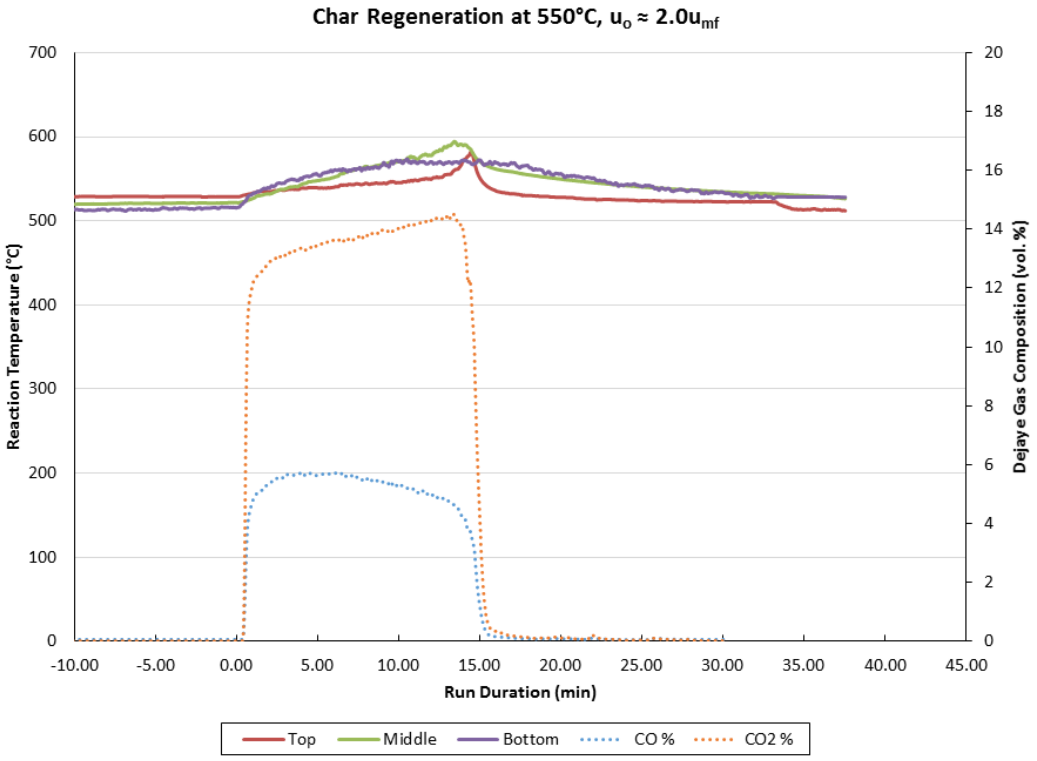

Figure 26: Regeneration conducted in air at 200% u_{mf} and 550°C.

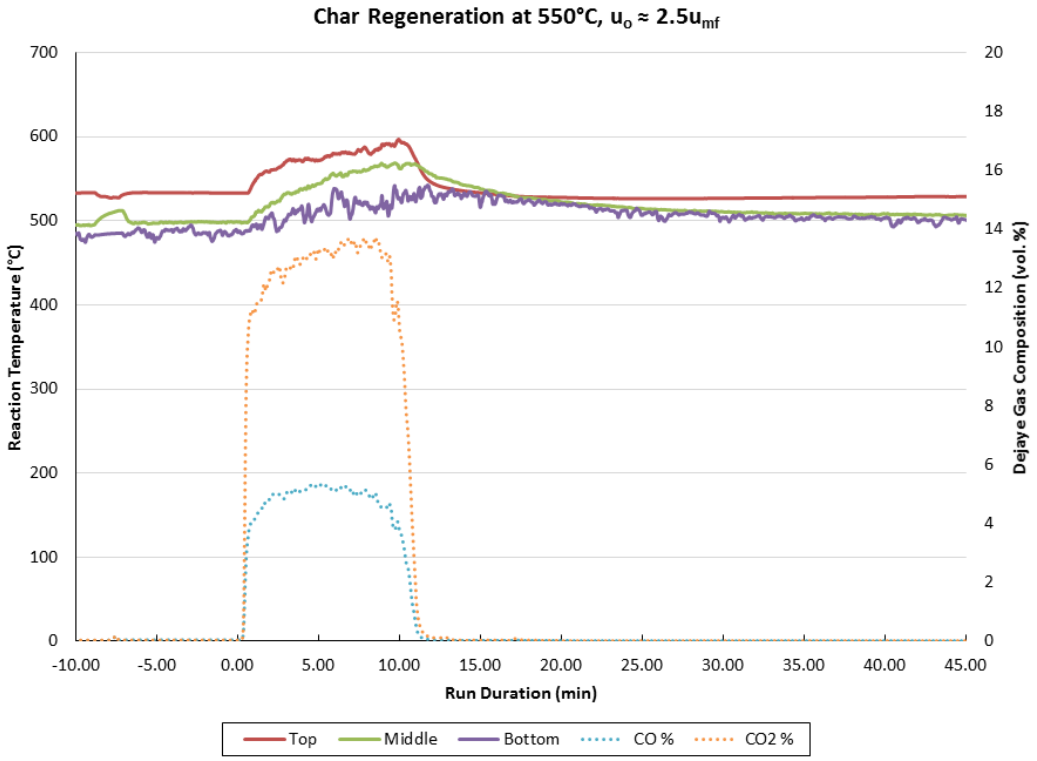

Figure 27: Regeneration conducted in air at 250% u_{mf} and 550°C.

A comparison of the results from varying the superficial fluidization velocity from 100% to 250% minimum fluidization shows the effect velocity has on carbon burn-off time. The total carbon burn-off time decreased with increasing superficial fluidization velocity. The carbon burn-off times for 200 and 250% minimum fluidization were nearly half of that for the trial conducted at minimum fluidization. The superficial fluidization velocities and resulting carbon burn-off times for each trial are shown in Table 13.

Table 13: Summary of regeneration results with varying superficial fluidization velocities.

Fluidization State	Superficial Fluidization Velocity, u (m/s)	Total Carbon Burn-off Time (min)	Maximum Temperature Difference, Exotherm (°C)
$1.0u_{mf}$	0.08	28	152
$1.5u_{mf}$	0.12	18	106
$2.0u_{mf}$	0.16	15	73
$2.5u_{mf}$	0.20	12	70

It was also observed that as the reaction temperature profile increased during each regeneration, the concentration of carbon dioxide of the exiting gas also increased. These results are consistent with the trials conducted for varying regenerator temperature. Additionally, it was also observed that the difference between the maximum reaction temperature and the steady state temperature prior to regeneration decreased with increasing superficial fluidization velocity. One probable explanation is that at higher superficial fluidization velocities, the regeneration unit sees more sweep gas for a given time interval. Therefore, more energy from the heat release during combustion is used to bring the reactor to a steady regeneration temperature and in-turn results in a lower exotherm.

Varying oxygen sweep gas concentration

To test the effect of oxygen concentration on the total burn-off time of char and heat carrier, regenerations were conducted with varying oxygen sweep gas concentrations. Regenerations in air (21.0 vol.% oxygen) served as a baseline with additional regenerations covering the range of $\pm$ 7.5% oxygen on a volume basis. The regeneration temperature and superficial fluidization velocity were held constant across all trials for accurate comparison. The regenerations were conducted at 550°C and 200% minimum fluidization (0.16 m/s). The results for the regenerations conducted with an oxygen sweep gas concentration of 13.6 and 17.3 vol.% are shown in Figure 28 and Figure 29, respectively. The results for the trial with pure air (21.0 vol.% oxygen) was shown previously in Figure 26. The regenerations with oxygen sweep gas concentrations more than air at 24.7 and 28.5 vol.% are shown in Figure 30 and Figure 31, respectively. It should be noted that the temperature profile for the regeneration trial at 17.3 vol.% oxygen, shown in Figure 29, was lost due to a software malfunction on the computer processing unit. The total carbon burn-off time was still calculated using the gas compositional analysis from the DeJaye Gas Analyzer.

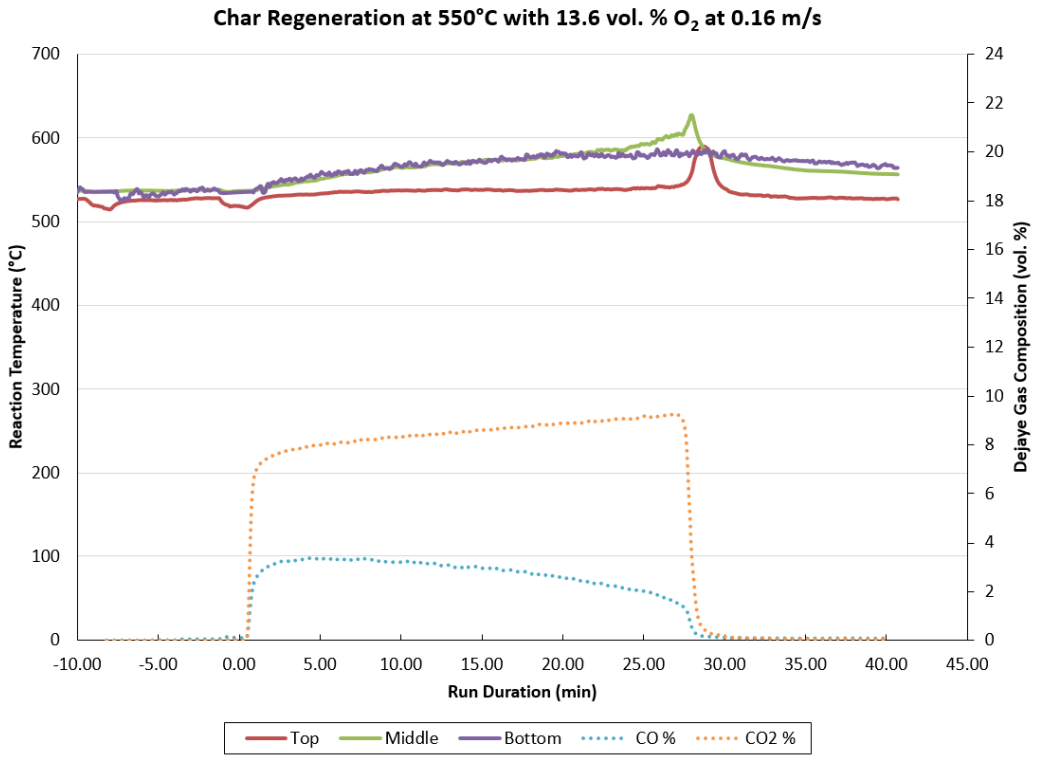

Figure 28: Regeneration conducted with 13.6 vol.% of oxygen at 550°C at 0.16 m/s of sweep gas.

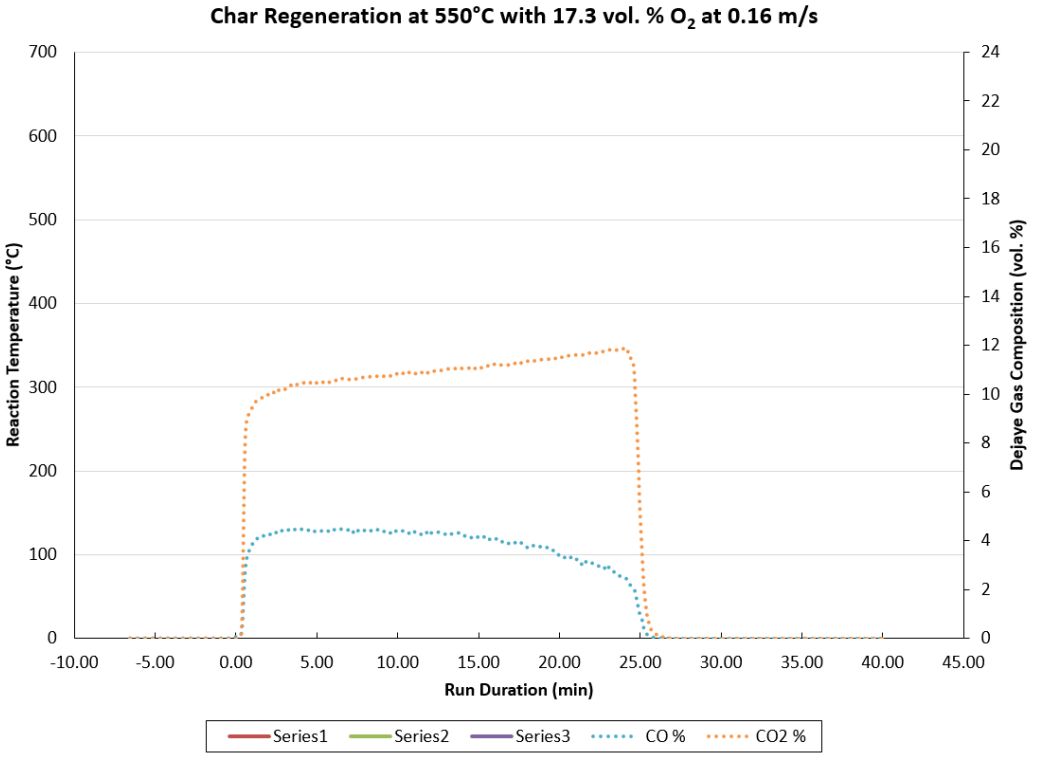

Figure 29: Regeneration conducted with 17.3 vol.% of oxygen at 550°C at 0.16 m/s of sweep gas.

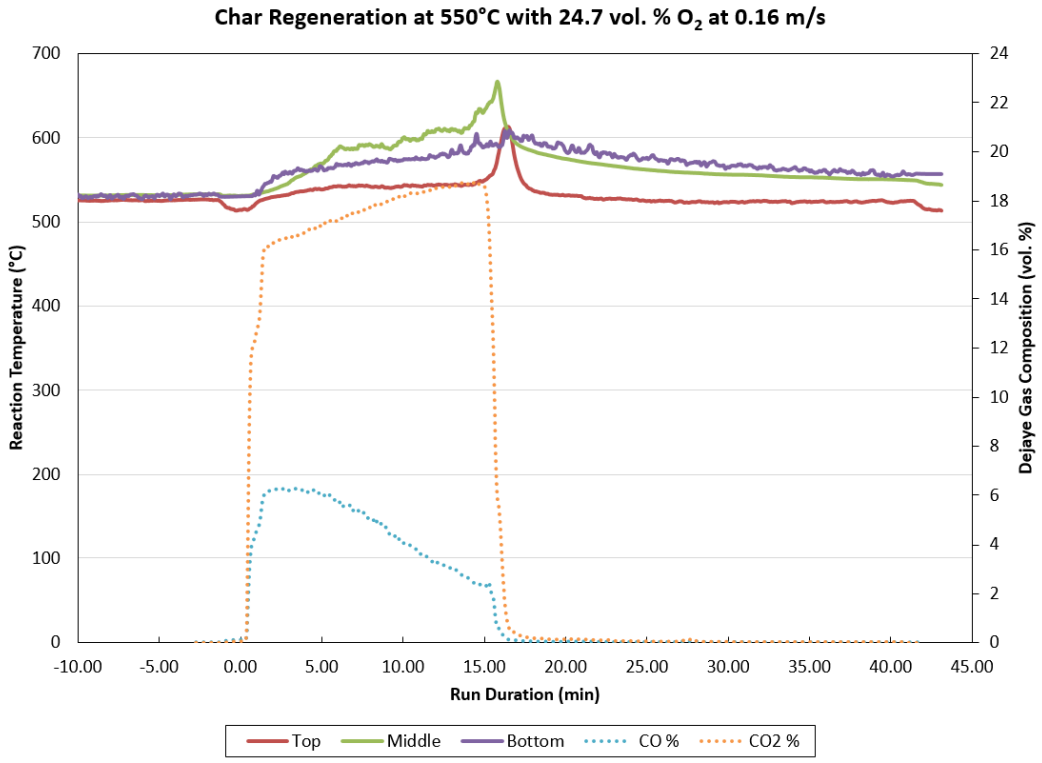

Figure 30: Regeneration conducted with 24.7 vol.% of oxygen at 550°C at 0.16 m/s of sweep gas.

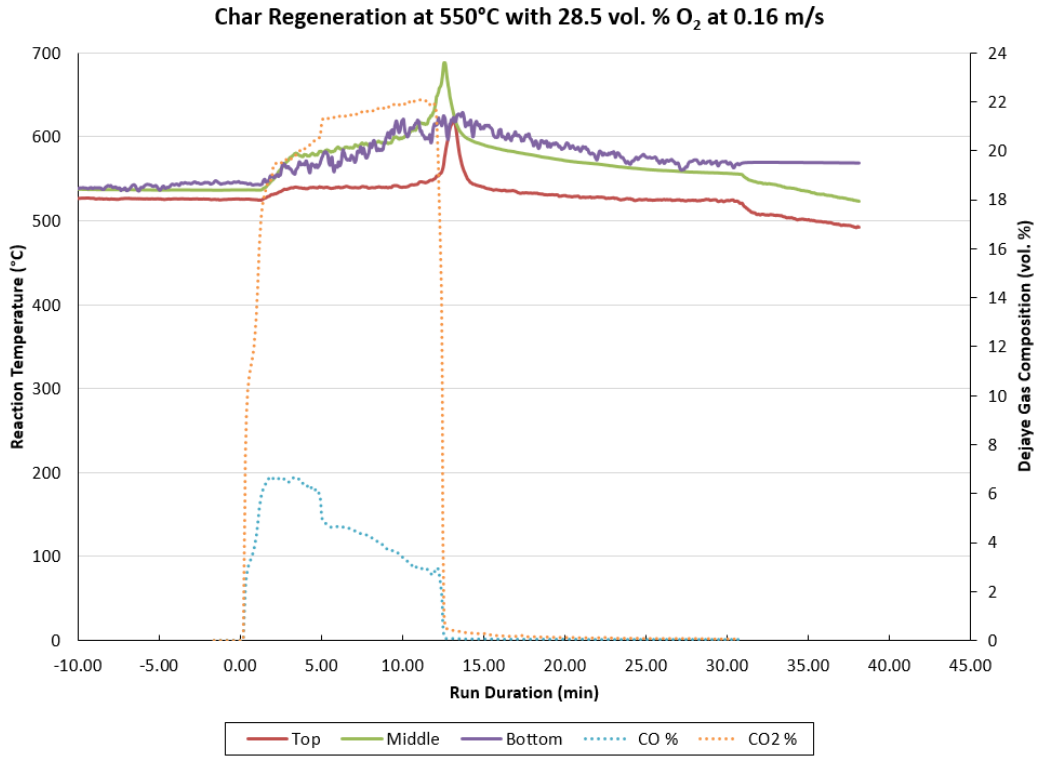

Figure 31: Regeneration conducted with 28.5 vol.% of oxygen at 550°C at 0.16 m/s of sweep gas.

Comparing the results from varying oxygen sweep gas concentrations yields a couple of conclusions. The carbon burn-off time decreased with increasing initial oxygen concentration in the sweep gas. Additionally, both the maximum reaction temperature and the concentration of carbon dioxide increased across trials with increasing oxygen sweep gas concentration. These results are summarized in Table 14.

Table 14: Summary of regeneration results with varying oxygen sweep gas concentrations.

Initial Oxygen Sweep Gas Concentration (vol.%, O_2)	Total Carbon Burn-off Time (min)	Maximum Carbon Dioxide Concentration in Exhaust Stream (vol.%)
13.6	27	8.8
17.3	25	11.8
21.0 (air)	17	14.0
24.7	16	18.3
28.5	13	22.0

The carbon burn-off time for an oxygen sweep gas concentration of 13.6 vol.% was approximately double that of the regeneration with an oxygen sweep gas concentration of 28.5 vol.%. Furthermore, the maximum carbon dioxide concentration during regeneration was significantly lower at 8.8% on a volume basis compared to 22.0% for the same oxygen sweep gas concentrations of 13.6 and 28.5 vol.%, respectively. This increase in maximum carbon dioxide concentration suggests that the regeneration process approaches complete combustion condition at increased initial oxygen sweep gas concentrations. This is further supported by the longer carbon burn-off times at lower concentrations which suggest potential operation in oxygen-starved conditions.

Conclusions

The results from this study suggest operating conditions of a fluidized bed regeneration unit will have implications on the total burn-off time of solids material from the pyrolysis of biomass. When varying the regenerator operating temperature at the same state of fluidization, it was found that the carbon burn-off times increased with increasing regenerator temperature. This was due to a decrease in the actual superficial fluidization velocities over the same temperature range due to minimum fluidization phenomena. A comparison of varying the superficial fluidization velocities at the same regenerator temperature yielded a decrease in total carbon burn-off time with increasing superficial fluidization velocity from 100% to 250% minimum fluidization. When increasing the initial oxygen sweep gas concentration at a constant temperature and superficial fluidization velocity, it was found that the carbon burn-off time decreased and the maximum amount of operating carbon dioxide production increased. Decreased burn-off times and increased carbon dioxide production would be desirable for commercial applications.

Additionally, this study provided insight to optimal operating conditions for a regeneration unit desired in continuous operation of some biomass pyrolysis processes, e.g. auger reactors. Optimal conditions determined from this work would include a regeneration temperature (approximately 550°C) similar to that of pyrolysis operating temperatures to minimalize heat loss or addition during the regeneration and recycling phase of the heat transfer media. Increased superficial fluidization velocities (at up to 250% minimum fluidization) drastically decrease the total carbon burn-off time, thus minimalizing the risk of being the bottleneck in a continuous process. Furthermore,

increasing the oxygen concentration decreases the run time and increases the amount of carbon dioxide produced from the regeneration process. Tradeoffs may exist, however, as increasing the superficial fluidization velocity decreases the maximum temperature in the bed and thus the maximum energy able to be recovered from the regeneration unit. Further optimization and implementation into a continuous pyrolysis system is needed.

Acknowledgments

The authors would like to acknowledge Phillips 66 for funding. We would also like to thank Patrick Johnston for assistance with the gas analysis techniques. The authors would also like to acknowledge Ryan Spellerburg, Eric McPeak, Zachary Paskach and Angela Wagner in their assistance with sample preparation and experimental procedures.

CHAPTER 5. LEARNING RATES AND THEIR IMPACTS ON THE OPTIMAL CAPACITES AND PRODUCTION COSTS OF BIOREFINERIES

Modified from a paper published in *Biofuels, Bioproducts, and Biorefining.*

Tannon J. Daugaard[ab], Lucas A. Mutti[a], Mark Mba Wright[abc], Robert C. Brown[ab], Paul Componation[d]

Abstract

Industry statistics indicate that technology-learning rates can dramatically reduce both feedstock and biofuel production costs. Both the Brazilian sugarcane ethanol and United States corn ethanol industries exhibit drastic historical cost reductions that can be attributed to learning factors. Thus, the purpose of this paper is to estimate the potential impact of industry learning rates on the emerging advanced biofuel industry in the United States.

Results from this study indicate that increasing biorefinery capital and feedstock learning rates could significantly reduce the optimal size and production costs of biorefineries. This analysis compares predictions of learning-based economies of scale, S-Curve, and Stanford-B models. The Stanford-B model predicts biofuel cost reductions of 55 to 73% compared to base case estimates. For example, optimal costs for Fischer-Tropsch diesel decrease from $4.42/gallon to $2.00/gallon. The optimal capacities range from small-scale (grain ethanol and fast pyrolysis) producing 16 million gallons per year

[a] Department of Mechanical Engineering, Iowa State University, Ames, IA 50010
[b] Bioeconomy Institute, Iowa State University, Ames, IA 50010
[c] Corresponding Author: markmw@iastate.edu, 515-294-0913, 2078 Black Engineering, Ames IA, 50011
[d] Department of Industrial and Manufacturing Systems Engineering, Ames, IA 50010

to large-scale gasification facilities with 210 million gallons per year capacity. Sensitivity analysis shows that improving capital and feedstock delivery learning rates has a stronger impact on reducing costs than increasing industry experience suggesting that there is an economic incentive to invest in strategies that increase the learning rate for advanced biofuel production.

Introduction

Energy security and environmental concerns have driven several countries to enact binding policies to encourage the domestic production of clean and renewable fuels. In particular, the United States enacted the Energy Independence and Security Act [110] in 2007, which included a provision for the Renewable Fuels Standard (RFS2) regulated by the Environmental Protection Agency (EPA). The RFS2 requires the production of up to 16 billion gallons of transportation fuels from lignocellulosic biomass by 2022 in addition to a mandated 15 billion gallons of conventional ethanol. These policies have led to a rapid growth of the biofuel industry both globally and in the U.S. in particular.

Cost reductions in both biomass and biofuel (first and second generation) production are some of the consequences of this rapid growth. Brazilian sugarcane ethanol and U.S. corn ethanol have showed dramatic cost reductions of 60 and 88%, respectively, since the 1980's [128, 129]. Several researchers have shown strong correlations between industry capacity growth and biofuel cost reductions [130-133]. These correlations are in agreement with well-established technology learning curve formulations [134]. In fact, technological learning relationships have been observed in a

wide range of industries [135-142]. Therefore, it seems clear that factors that improve learning rates can lead to lower production costs.

Most of the biofuel industry growth has been driven by first generation biofuel technologies. In the span of 10 years, global biofuel production increased from 238 thousand barrels per day of oil equivalent (BPDOE) to 1206 thousand BPDOE in 2012 [143]. Ethanol production accounted for 78.7% of 2011 global biofuel production [144], and biodiesel accounted for almost all of the remaining fuel. First generation biorefineries from either corn grain or sugarcane produce virtually all the commercially available transportation ethanol.

The continued growth of the U.S. biofuel industry will substantially depend on the commercialization of advanced biofuel technologies, which face significant techno-economic challenges [145]. Advanced biofuel technologies are those capable of converting a wide range of lignocellulosic feedstock into a variety of conventional transportation fuels such as ethanol, gasoline, diesel, dimethyl-ether [146] as well as emerging drop-in fuels. There has been significant investment in research and development of these technologies. However, biofuel production from advanced biorefineries has yet to meet the goals established by U.S. government policies. This lack of advanced biofuel production has prompted the U.S. EPA to reduce the annual advanced biofuel targets by more than 90% from the original mandates due to a lack of eligible supply [147]. Recent industry developments suggest that companies may be able to increase production of advanced biofuels albeit at quantities far below the mandated targets [146]. Two of the main constraints limiting advanced biorefinery adoption are high capital and feedstock costs [145].

Innovative and energy efficient technologies could overcome the high costs of pioneer facilities with sufficient commercial experience [148]. These technologies require significant initial investments that are difficult to justify without knowledge of their earning potential. Increasing their earning potential will depend on cost reductions enabled by the deployment of facilities at their optimal scale and cost reductions from technological learning. A possibility exists where a revolutionary technology could provide dramatic cost reductions but should be seen as an anomaly to the current technologies used in this study. Despite the significant literature contributions on biorefinery optimal facility sizes and learning rates [23, 141, 148, 149], there is scarce information on the impact learning rates have on optimal capacities of plant sizes in the biofuels industry. This study could lead to coordinated strategies that would result in significant economic savings and rapid technological growth.

Current infrastructure suggests that scaling up in size is more cost effective. That is capital costs per unit of capacity decrease with increasing unit size. Some recent work by Dahlgren et al. suggest the notion that "bigger isn't always better" [25]. They show small modular units can compete with large scaled-up facilities due to cost reductions by learning with the mass production of smaller units accounting for the same overall capacity. This study analyzes different advanced biofuel technologies which provide a comparison for both small scale and large scale biorefineries.

The purpose of this study is to formulate a new method to quantify the impact of economies of scale and learning rates on the production costs and optimal plant capacities of advanced biofuels technologies. For this purpose, we expand existing learning curve methods to account for economies of scale relationships that predict optimal sizes for

biorefineries. The outcome of this study is a new relationship to ease the comparison of future biorefineries sized at their optimal capacity based on their current costs and predicted learning rates.

The current paper is structured as follows: 1) we describe well-established plant scaling and learning curve methods; 2) we develop novel formulations that combine scaling relationships with learning curve calculations; 3) we present base case data for a variety of advanced biofuel technologies; 4) we calculate production costs at different plant scales and their capacities; 5) we study the sensitivity of key learning rate variables on the calculated optimal plant capacity.

Background

In a previous study, Wright and Brown investigated the optimal size of advanced biorefineries based on economies of scale (EOS) calculations [23]. In that study, they determined that the optimal plant size was primarily dependent on the capital and feedstock cost scale factors. They proposed a new factor (R_{opt}), the ratio of the capital cost (C_P) and delivery cost (C_D) scaling factors, as shown in Equation 1:

$$R_{opt} = \left(\frac{C_D}{C_P}\right)_{opt} = (1-n)/(m-1) \quad (1)$$

where m and n are power law exponents. R_{opt} allows for the rapid comparison of the optimal plant capacities for biorefineries based on different conversion technologies. Recent studies have since expanded on this analysis [149-151]. Calculation of optimal plant capacities and their respective production costs with R_{opt} yields valuable information when deciding to invest in specific biorefinery capacities.

Equation 2 shows the general formula for calculating the total production cost (C_T) of a biorefinery with capacity M based on known base case capacity (M_o), capital

(C_{Po}), delivery (C_{Do}), and feedstock (C_{Fo}) costs. This equation employs exponents representing scaling factors for processing (n) and delivery (m) of feedstock that describe the relationship between costs and capacities as a power law function:

$$C_T(M) = C_{Po}\left(\frac{M}{M_o}\right)^n + C_{Do}\left(\frac{M}{M_o}\right)^m + C_{Fo}\left(\frac{M}{M_o}\right) \quad (2)$$

In the case of capital costs (C_{Po}), the chemical industry has shown statistical evidence for cost reductions with increased capacity dating back to the 1950s [152]. In recent years, biorefineries have exhibited capital cost scaling factors of between 0.63 and 0.72 [130-133, 153, 154]. These scaling factors suggest that capital costs per unit capacity decrease by between 0.63 and 0.72 for each unit increase in capacity. On the other hand, delivery costs follow a dis-economies of scale relationship, increasing with increasing plant capacity. Nguyen and Prince suggested that values for m range between 1.5 and 2.0 depending on land availability factors [155]. The choice of these factors impacts the scaling strategies adopted by biorefineries by changing their production cost-capacity relationship [151]. In this study, we adopt a capital cost scaling factor of 0.7 and delivery cost scaling factor of 1.8. Figure 32 illustrates how these costs scale with biorefinery capacity in terms of unit products per year. Note that while total unit costs decrease rapidly at small capacities, rising delivery costs dominate beyond the optimal (minimum total cost) capacity.

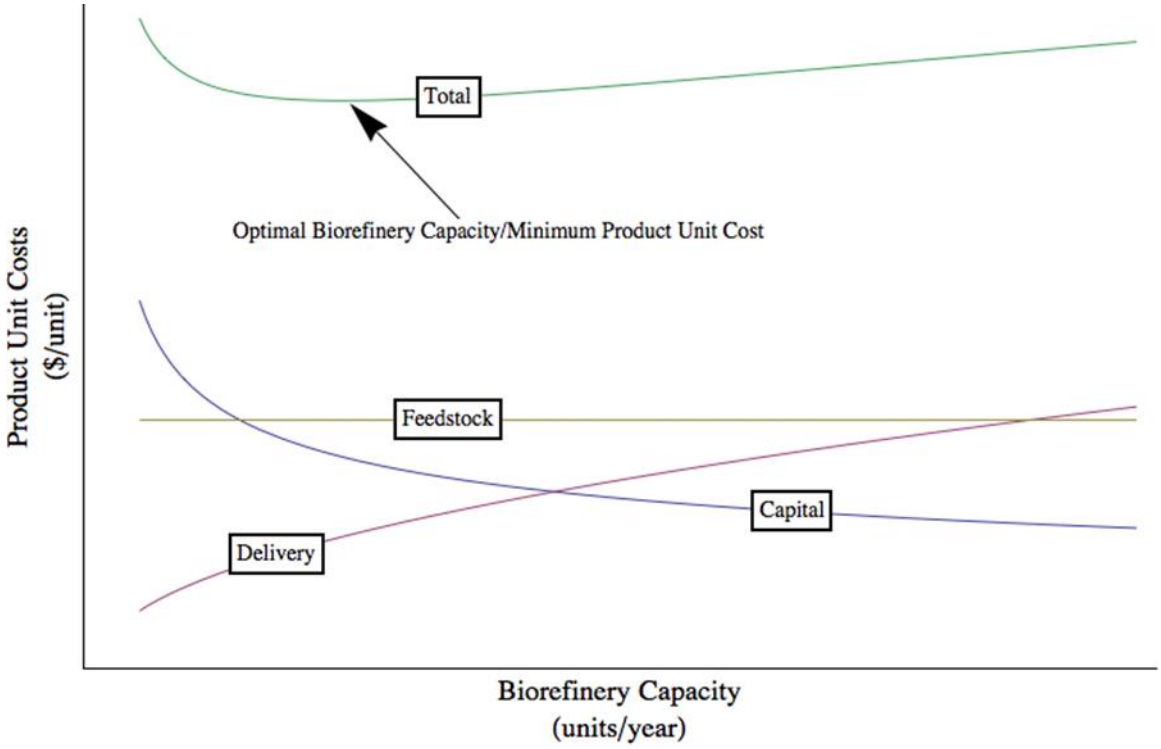

Figure 32: Scaling behavior of biorefinery product unit cost components (capital, feedstock, and delivery) based on annual production capacity.

Economies of scale models provide only a snapshot of production and capital costs for a current technology but over time the relationships of these costs will change due to learning. The effect of learning behavior was first observed in airframe manufacturing. Wright derived the log-linear model in 1936 to describe the effects of learning on production costs for airframe manufacturing [135-142]. The model is interchangeably referred as the log-linear model because it shows a linear curve in a log-log plot. It was shown that as cumulative production doubles, production costs tend to decline at a fixed rate. The graphical representation of Wright's discovery is referred to as a learning curve, which describes the effect of learning-by-doing [145, 148]. This graphical representation is derived from a power-law function between production costs and cumulative production (See Equation 3).

$$C_t(M_t) = C_o M_t^{\log_2(1-LR)} \quad (3)$$

In Equation 3, the projected cost of unit *t* (C_t) is a function of the initial unit cost (C_0), the cumulative industry capacity (M_t), and the technology-specific learning rate (LR).

McDonald and Schrattenholzer have shown a strong correlation between energy product unit costs and industry cumulative capacity [138]. These correlations suggest exponential decay relationships between costs and cumulative industry capacity. The scale factor is commonly known as the learning rate (LR). In their review, they documented learning rates for a wide range of energy technologies including integrated gasification combined cycles (IGCC), coal power plants, wind turbines, and solar panels. These learning rates varied from about 4% to over 20%. Figure 33 shows how different learning rates affect cost reductions in the single facility investment costs as the industrial cumulative capacity increases.

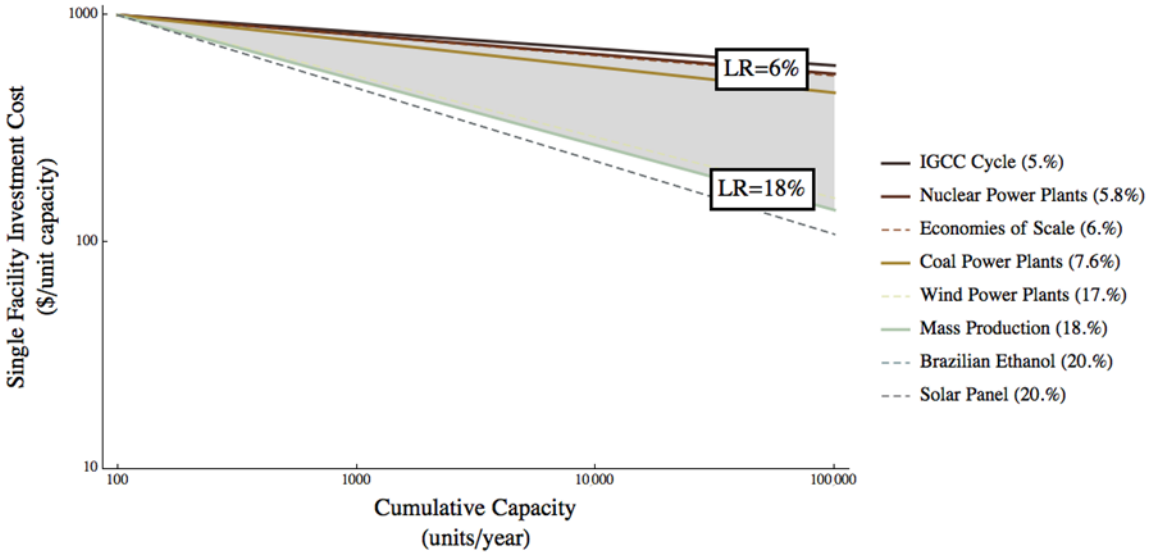

Figure 33: Log-Log plot of single facility investment costs vs. cumulative capacity for different energy systems. Data adapted from McDonald and Schrattenholzer [138, 147].

Learning rates are a function of numerous factors and can change over the lifetime of a technology. Yelle proposed that at the macroscopic level there are two

categories of learning: labor and organization learning [142]. Hirschmann suggested that learning rates in the petroleum industry were due to organizational rather than labor learning because direct labor is a negligible portion of refinery operations [156]. In general, learning rates are greater during the early industry growth stages [135] and periods of rapid growth. Lack of investment, regulatory changes, and technology shifts can reduce learning rates and even lead to periods of negative learning (i.e. unit production costs increase with industry capacity growth) [157]. The coal industry exhibited an initial period of rapid cost reductions followed by slow and steady learning rates. The wind industry on the other hand has swung between periods of high learning rate volatility. Although industry-learning rates are often reported with a fixed value, these rates can be subject to wide volatility and uncertainty. For these reasons, it is often difficult to predict future learning rates. In this study, we follow the common analysis approach of employing a fixed learning rate over the industry growth period.

Hettinga et al. and Van Den Wall Bake et al. have quantified learning rates in the U.S. corn ethanol and Brazil sugarcane ethanol industries [128, 129, 148]. In the U.S., corn production costs declined 62% between 1980 and 2005 while its production has doubled since 1975. Since 1983, corn ethanol biorefinery costs have decreased from $\$360/m^3$ to $\$45/m^3$ in 2005 – a 88% reduction [23, 128]. Brazil experienced a similar phenomenon. Their sugarcane costs decreased by more than 60% over a similar timespan, and sugarcane ethanol costs went from $\$980/m^3$ to less than $\$305/m^3$ [129, 149-151]. Crago et al. investigated in 2010 recent fluctuations of Brazilian sugarcane and US corn ethanol costs and their contributing factors [158].

Feedstock production costs for a variety of biomass types have decreased. Weiss et al. determined that biomass production learning rates for a wide range of feedstock (corn, sugarcane, rapeseed, and forest wood chips) had a range of 24±14% [148]. This compares to quoted values for the Brazilian sugarcane industry of 32% [129], and 45% for US corn production [128]. These learning rates reflect cost reductions in biomass growth, collection, and delivery among other factors.

Cost reductions in the U.S. and Brazilian biofuel industries can be attributed to various factors: increases in plant scale, efficiency improvements, increased automation, and improved feedstock yields and logistics among others [128, 129]. A retrospective view can explain how each of these factors led to lower product costs. Although it is difficult to predict which factors will continue to drive long-term cost reductions, it is of interest to estimate industry learning rate factors in order to forecast production costs. Hettinga et al. and others have done so in previous studies and shown that mid-term projections can yield costs that appear low compared to national averages but realistic when compared to the state-of-the-art technology [128].

Figure 34 shows the various factors that affect learning rates in the manufacturing industry as presented by Weiss [159]. These factors include exogenous learning such as general technological progress; endogenous learning in the form of increased tooling and automation among others; and organizational learning that includes knowledge transfer. Multilevel interactions among these factors and changes in the price of production will impact market competition, profit margins, and taxation levels in ways that typically lead to lower production, producer, and market prices.

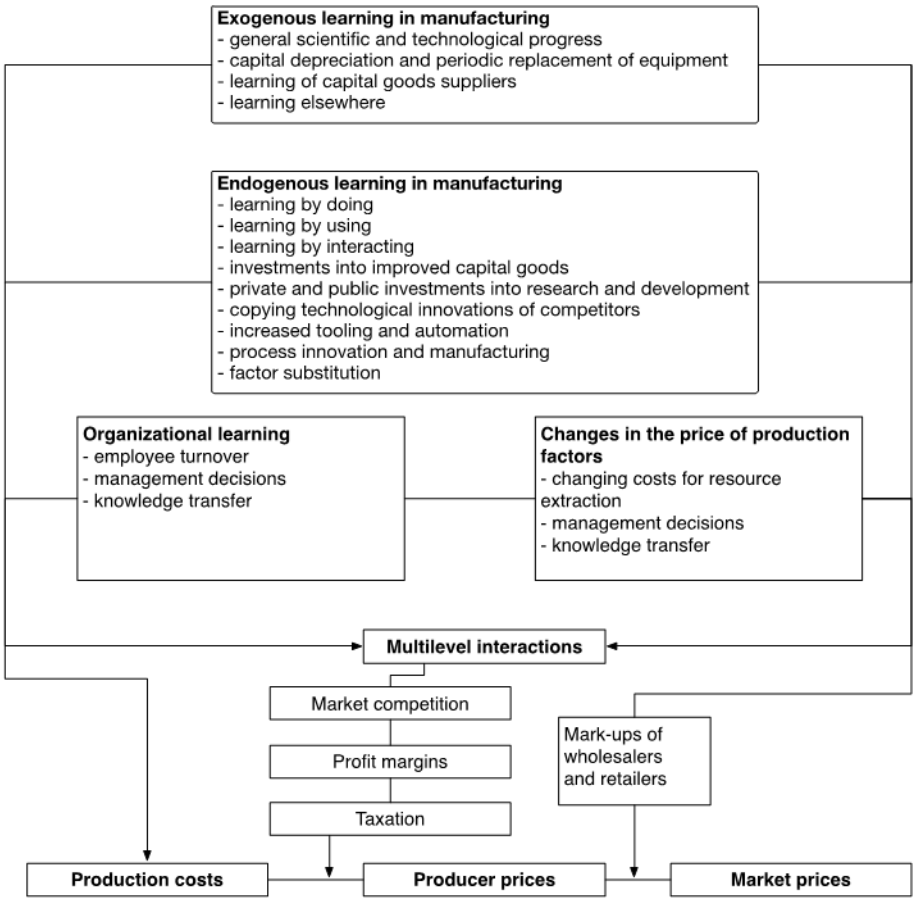

Figure 34: Exogenous and endogenous factors that affect learning rates in the manufacturing industry [159].

The purpose of this study is to formulate a new method to quantify the impact of economies of scale and learning rates on the production costs and optimal plant capacities of advanced biofuel technologies. To the authors' knowledge, integrated formulations for how economies of scale and learning rates affect the price of biofuel and the optimum size of a biorefinery plant have not been previously published.

Methodology

The scope of this investigation is to extend our previous study [23] by evaluating how learning rates contribute to the overall reduction of biofuel costs and impact the optimal sizes of different kinds of biorefineries. For this purpose, we integrate the

economies of scale equation with experience curve formulations. A key assumption in this study is that learning rates parameters are independent from scaling factors. Further investigation into their relationship may be needed in order to account for potential feedback effects, but this consideration is beyond the scope of this study. The analyzed experience curve formulations are the Stanford-B and the S-curve models [160]. These simplified models account for prior knowledge and learning experience which are then incorporated into the economies of scale equation (see Equation 3), in this study, for a more sophisticated experience curve formulation.

There are several review papers that compare the strengths and weaknesses of different learning curve methodologies [136, 137, 148]. Learning curve methodologies are applied in multiple industries, however each application is unique. The Stanford-B and S-curve methodologies were found to be applicable to our research and thus were used as the basis for developing new models. Following is a cursory review of these methodologies.

Stanford-B model

The Stanford-B Model, also known as the prior-learning model, was developed in 1949 by Stanford Research Institute (SRI) under contract by the U.S. Air Force. The model anticipates that overall costs can be reduced if workers have prior knowledge on the considered matter [160]. Stanford researchers discovered that predictions based on the Wright log-linear model could be improved by including a prior knowledge factor (B):

$$C(M) = C_o(M_t + B)^{\log_2 \varepsilon} \qquad (12)$$

where ε is defined as 1-LR. As an example, experiments conducted by the Boeing Company have showed that the Stanford-B model provided the most accurate prediction

when design differences are incorporated in similar industries [161]. However, the major drawback of the Stanford-B model is that it does not consider the fact that labor or organization learning may be forgotten [161].

In this study, we develop an overall cost equation that integrates the Stanford-B model with the economies of scale equation, Equation 2, as shown in Equation 14. We estimate the costs and optimal capacities of a biorefinery after a certain quantity of accumulated learning by taking the derivative of Equation 14 and solving for M. The resulting equation (Equation 15) can be represented by the ratio of delivery to capital costs or R_{opt}.

$$\frac{C_t}{M} = \frac{C_{po}}{M}\left(\frac{M}{M_o}\right)^n \left(\frac{M_t+B_o}{M_o+B_o}\right)^{\log_2(1-LR_p)} + \frac{C_{fo}}{M}\left(\frac{M}{M_o}\right)\left(\frac{M_t+B_o}{M_o+B_o}\right)^{\log_2(1-LR_f)} + \frac{C_{do}}{M}\left(\frac{M}{M_o}\right)^m \left(\frac{M_t+B_o}{M_o+B_o}\right)^{\log_2(1-LR_d)} \quad (14)$$

$$R_{opt} = \frac{C_d}{C_p} = \frac{\left(\frac{M_t+B_o}{M_o+B_o}\right)^{\log_2(1-LR_p)}}{\left(\frac{M_t+B_o}{M_o+B_o}\right)^{\log_2(1-LR_d)}} \frac{(1-n)}{(m-1)} \quad (15)$$

The S-Curve

Gardner Carr first described the S-Curve, also known as the Sigmoid-Curve, in 1946 as the incorporation of man-machine relationship and prior-learning experience. The Sigmoid-Curve is described as a combination of three phases that reflect the start-up effect, carryover, and flatness of the plateau [160]. During the start-up phase of the curve there is minimum learning due to the development of initial organizational and labor structures. Costs per unit can even increase during this phase. During the second phase, carryover, both organization and workers become better acquainted with the project, and

diminishing errors and forming work patterns contribute to project learning and lower production costs. During the third phase, plateau, most of the learning has already been established and hence the overall costs tend to approach a limit until an emerging technology becomes economically feasible in the market.

Based on Carr's research, Carlson attempted to describe the behavior of the S-Curve and learning rates influence by correlating DeJong's learning formula [162] with the Stanford-B model [160]. DeJong's formula introduced the incompressibility factor (ρ) to account for direct labor learning. The incompressibility factor ranges from zero to one, with zero representing a completely manual situation and unity as a completely automated situation. These extreme cases may not take into consideration other forms of learning (see Figure 3), such as organizational and structural learning. Teplitz suggests that the incompressibility factor varies for each activity [160]. For instance, he attributes a value of 0.33 to major assembly, 0.43 to aircraft subassembly, 0.50 to plating and heat treating, 0.67 to metal stamping, and 0.77 to machine shop. Equation 16 shows Carlson's S-Curve equation.

$$C(M) = C_o\left[\rho + (1-\rho)(M_t + B)^{\log_2 \varepsilon}\right] \tag{16}$$

We apply the same approach as Equation 14 by integrating the economies of scale equation and Carlson's S-Curve equation to derive the following two relationships (Equations 18 and 19) for plant unit costs and R_{opt} based on the S-Curve formulation.

$$\frac{C_t}{M} = \frac{C_{po}}{M}\left(\frac{M}{M_o}\right)^n \left[\frac{\rho_p + (1-\rho_p)(M_t+B_o)^{\log_2(1-LR_p)}}{\rho_p + (1-\rho_p)(M_o+B_o)^{\log_2(1-LR_p)}}\right] +$$

$$\frac{C_{fo}}{M}\left(\frac{M}{M_o}\right)\left[\frac{\rho_f + (1-\rho_f)(M_t+B_o)^{\log_2(1-LR_f)}}{\rho_f + (1-\rho_f)(M_o+B_o)^{\log_2(1-LR_f)}}\right] + \frac{C_{do}}{M}\left(\frac{M}{M_o}\right)^m \left[\frac{\rho_d + (1-\rho_d)(M_t+B_o)^{\log_2(1-LR_d)}}{\rho_d + (1-\rho_d)(M_o+B_o)^{\log_2(1-LR_d)}}\right]$$

(18)

$$R_{opt} = \frac{C_d}{C_p} = \frac{\left[\rho_p - (M_t+B_o)^{log_2(1-LR_p)}(\rho_p-1)\right](n-1)\left[(M_o+B_o)^{log_2(1-LR_d)}(\rho_d-1)-\rho_d\right]}{\left[\rho_d-(M_t+B_o)^{log_2(1-LR_d)}(\rho_d-1)\right](m-1)\left[(M_o+B_o)^{log_2(1-LR_p)}(\rho_p-1)-\rho_p\right]} \quad (19)$$

Table 15 shows a summary of the optimal plant size with learning rates formulations derived in this study. This table also includes derivations based on Wright's law and DeJong's Learning Curve for comparison purposes. Readers are directed to their respective studies for details [142]. The supporting information includes the step-by-step derivations of these formulas.

Table 15: Summary of combined optimal plant size and learning curve formulations.

Learning Approach	Learning Rate-based Optimal Plant Size Ratio (R_{opt})	Ref.
Economies of Scale (w/o learning)	$R_{opt} = \frac{C_d}{C_p} = \frac{1-n}{m-1}$	23
Wright's Law	$R_{opt} = \frac{C_d}{C_p} = \frac{\frac{M_t}{M_o}^{log_2(1-LR_p)}(1-n)}{\frac{M_t}{M_o}^{log_2(1-LR_d)}(m-1)}$	Eqn. 6
DeJong's Learning Curve	$R_{opt} = \frac{C_d}{C_p} = \frac{\left[M_t^{log_2(1-LR_p)}(\rho_p-1)-\rho_p\right]\left[M_o^{log_2(1-LR_d)}(\rho_d-1)-\rho_d\right](1-n)}{\left[M_t^{log_2(1-LR_d)}(\rho_d-1)-\rho_d\right]\left[M_o^{log_2(1-LR_p)}(\rho_p-1)-\rho_p\right](m-1)}$	Eqn. 11
Stanford-B Model	$R_{opt} = \frac{C_d}{C_p} = \frac{\left(\frac{M_t+B_o}{M_o+B_o}\right)^{\log_2(1-LR_p)}(1-n)}{\left(\frac{M_t+B_o}{M_o+B_o}\right)^{\log_2(1-LR_d)}(m-1)}$	Eqn. 15
S-Curve	$R_{opt} = \frac{C_d}{C_p} = \frac{\left[(M_o+B_o)^{log_2(1-LR_d)}(\rho_d-1)-\rho_d\right]\left[\rho_p-(M_t+B_o)^{log_2(1-LR_p)}(\rho_p-1)\right](1-n)}{\left[\rho_d-(M_t+B_o)^{log_2(1-LR_d)}(\rho_d-1)\right]\left[(M_o+B_o)^{log_2(1-LR_p)}(\rho_p-1)-\rho_p\right](m-1)}$	Eqn. 19

The formulations shown in Table 15 can be applied to any enterprise that includes both economies and dis-economies of scale effects. While this study focuses on the biofuel industry, dis-economies of scale have been reported in other energy production enterprises [163]. The optimal plant size ratio with learning rate describes how the ratio

of dis-economies of scale costs to economies of scale costs will change after a period of growth at given learning rates.

Case scenario data

We compare the optimal plant size of different bioenergy technologies based on the modified Stanford-B and S-curve learning models. The technologies selected convert biomass into transportation fuels that qualify as advanced biofuels in the United States. Table 16 shows a summary of the selected biorefinery technologies, their base case capacities, costs, and assumed learning rates.

Table 16: Biorefinery technology base case capacities (M_0) in million gallons per year, plant (CP_0), delivery (CD_0), and feedstock (CF_0) costs in million $, and learning rates.

Biorefinery	CP_0	CD_0	CF_0	M_0	Learning Rates		
					Plant	Delivery	Feedstock
Gasification to Fischer-Tropsch[31]	106.4	17.1	55.2	40.4	0.05	0.1	0.14
Fast Pyrolysis and Hydroprocessing[164]	45.2	18.1	46.1	41.7	0.2	0.14	0.1
Grain Ethanol[165]	5.9	1.2	18.9	16.7	0.2	0.14	0.1
Cellulosic Ethanol[166]	40.5	5.5	26.4	33.5	0.05	0.1	0.14
Gasification to Methanol[167]	40.4	5.0	26.8	43.4	0.05	0.1	0.14
Gasification to Hydrogen[167]	38.8	5.0	26.8	47.9	0.05	0.1	0.14
Gasification to Alcohols[168]	61.9	6.2	30.8	41.2	0.05	0.1	0.14

Currently no data exists from commercial operations that can be used to derive learning rates for advanced biorefinery technologies. We employed the following criteria to select learning rates for the different technologies and factors. Gasification and cellulosic ethanol technologies were assumed to have plant-learning rates comparable to current large scale manufacturing enterprises, such as IGCC and coal power plant technologies (5%); fast pyrolysis and grain ethanol were assumed to have learning rates comparable to current small-scale facilities, such as Brazilian sugarcane to ethanol (20%). These values are in line with learning rates for related technologies surveyed by

McDonald and Schrattenholzer [138]. The common finding that greater learning rates are typically associated with small, mass-produced systems supports these assumptions. We assumed that small-scale facilities (pyrolysis and grain ethanol) will lead to faster improvements (6% vs. 4%) in delivery costs due to improved supply logistics. On the other hand, large-scale facilities would lead to greater feedstock learning rates due to the significantly larger feedstock quantities required to supply said facilities. These values are speculative, and thus we conduct parameter sensitivity analyses to understand the implications of different values for these factors.

Table 17 includes the plant, delivery, and feedstock labor learning rate factors for the various technologies. As shown, the selected values are 0.1 for feedstock delivery, 0.3 for feedstock production, and 0.7/0.6 for plant labor. These values were selected based on assumptions regarding the prevailing type of manual activity involved in each step and their similarity to the values described by Teplitz [160]: delivery and feedstock operations are assumed to be closer to manual labor while plant operations are mostly automated. Small-scale pyrolysis and ethanol facilities would require more manual intervention per unit capacity.

Table 17: Incompressibility plant, delivery, and feedstock labor learning rate factors.

Biorefinery	ρ_{p0}	ρ_{d0}	ρ_{f0}
Gasification to Fischer-Tropsch	0.7	0.1	0.3
Fast Pyrolysis and Hydroprocessing	0.6	0.1	0.3
Grain Ethanol	0.6	0.1	0.3
Cellulosic Ethanol	0.7	0.1	0.3
Gasification to Methanol	0.7	0.1	0.3
Gasification to Hydrogen	0.7	0.1	0.3
Gasification to Alcohols	0.7	0.1	0.3

For the base case scenarios, we selected values of M_t and B to be sixteen and zero billion gallons of biofuel production capacity, respectively. The value for M_t is based on the U.S. 2022 production target for advanced biofuels, and results would reflect the average costs that could be expected by that date. The B factor could range anywhere from zero to over thirteen billion gallons depending on how much prior learning can be attributed to the existing first-generation biofuel industry. It is likely that many lessons learned from corn grain ethanol production would translate to the construction and operation of the advanced biorefinery industry. However, it can be argued that the differences between these industries are large enough that translational knowledge would be negligible. For the sensitivity analysis, we assume thirteen billion gallons of previous learning and vary this value by ±20%.

Results

Table 15 summarizes the derived optimal plant size relationships for each learning approach including economies of scale without learning. The supporting information includes detailed derivations of these equations. We found that the ratio of delivery to plant costs with learning for an optimal facility (R_{opt}) depends on the learning function, scale factors (n, m), learning rates (LR_p, LR_d, LR_f), and incompressibility factors (ρ_p, ρ_d, ρ_f). The learning functions employ a different number of factors as discussed in the methodology. It is clear from this summary that learning rates impact the optimal size predicted by the economies-of-scale law due to their power-law relation with the cumulative industry capacity (M_t). An increase in learning rates present in the numerator effectively reduce the delivery costs, while an increase in learning rates present in the denominator effectively reduce the capital cost of the facility. The

combined effect is that technological learning could lead to differently sized optimal facilities depending on the rate of learning at the facility and feedstock supply chain.

Table 18 shows the production costs for optimally sized biorefineries based on economies-of-scale alone, and the Stanford-B and S-Curve models. Both learning curve models predict lower costs than can be achieved by scaling-up alone. Economies of scale predict cost reductions of 0 to 9% with optimal biorefinery capacities of 30 to 138 million gallons per year (-6% to 234% change in base case capacity). The Stanford-B model predicts cost reductions of 55 to 73% for facilities with between 16 and 210 million gallons per year capacity, and the S-Curve model predicts reductions of 30 to 37% and capacities of 67 to 237 million gallons per year. The high cost reductions are driven primarily by the fast learning rates attributed to the small-scale scenarios. In the sensitivity analysis, we look at the implications of slower learning rates.

Table 18: Optimal biorefinery plant costs in $/gallon of gasoline equivalent energy based on different learning curve models and cumulative industry capacity of 16 billion gallons per year.

Technology	Base Case	EOS	Stanford-B	S-Curve
Gasification to FT[b]	$4.42	$4.24	$2.00	$3.08
Fast Pyrolysis and HP[c]	$2.62	$2.62	$0.71	$1.80
Grain Ethanol	$1.55	$1.54	$0.45	$0.97
Cellulosic Ethanol	$2.16	$2.05	$0.91	$1.45
Gasification to Methanol	$1.66	$1.56	$0.71	$1.12
Gasification to Hydrogen	$1.47	$1.39	$0.64	$1.01
Gasification to Alcohols	$2.40	$2.19	$1.02	$1.59

[a]EOS: Economies of Scale; [b]FT: Fischer-Tropsch; [c]HP: Hydroprocessing

Table 19 shows the calculated optimal biorefinery plant capacities after 16 billion gallons of cumulative industry capacity. For all technologies other than fast pyrolysis, economies of scale predict that their optimal capacity is 2 to 3 times larger than their base case. However, the economies of scale model predicts the optimal capacity for the fast pyrolysis scenario is less than its base case. The modified Stanford-B model predicts

optimal capacities larger than the base case (3-5 times) for all scenarios other than fast pyrolysis and grain ethanol. In the fast pyrolysis and grain ethanol scenarios, Stanford-B actually predicts that their optimal capacities are smaller than the base size. This is a case where starting small is a strategy for improving large scale. Our results indicate that the modified S-Curve model predicts larger optimal capacities than the other two methods. These results suggest that delivery feedstock learning rates play a large role in determining optimal biorefinery capacities and improving them may be important.

Table 19: Optimal biorefinery plant capacities in million gallons per year based on different learning curve models and cumulative industry capacity of 16 billion gallons per year.

Technology	Base Size	EOS	Stanford-B	S-Curve
Gasification + FT[b]	40.4	87.28	133.39	150.67
Fast Pyrolysis + HP[c]	41.7	39.22	22.3	75.16
Grain Ethanol	16.7	29.85	15.57	67.08
Cellulosic Ethanol	33.5	84.21	130.41	148.1
Gasification to Methanol	43.4	119.99	182.45	205.67
Gasification to Hydrogen	47.9	126.72	191.34	215.1
Gasification to Alcohols	41.2	137.82	210.33	237.45

[a]EOS: Economies of Scale; [b]FT: Fischer-Tropsch; [c]HP: Hydroprocessing

Sensitivity analysis

Figure 35 compares how total biofuel costs will scale for a large, centralized technology (Gasification + FT) and a small, distributed technology (Fast Pyrolysis + HP). As stated previously, economies of scale predict larger sizes for optimally sized facilities with the exception of the Stanford-B curve and Fast Pyrolysis scenario, which has a smaller optimal capacity.

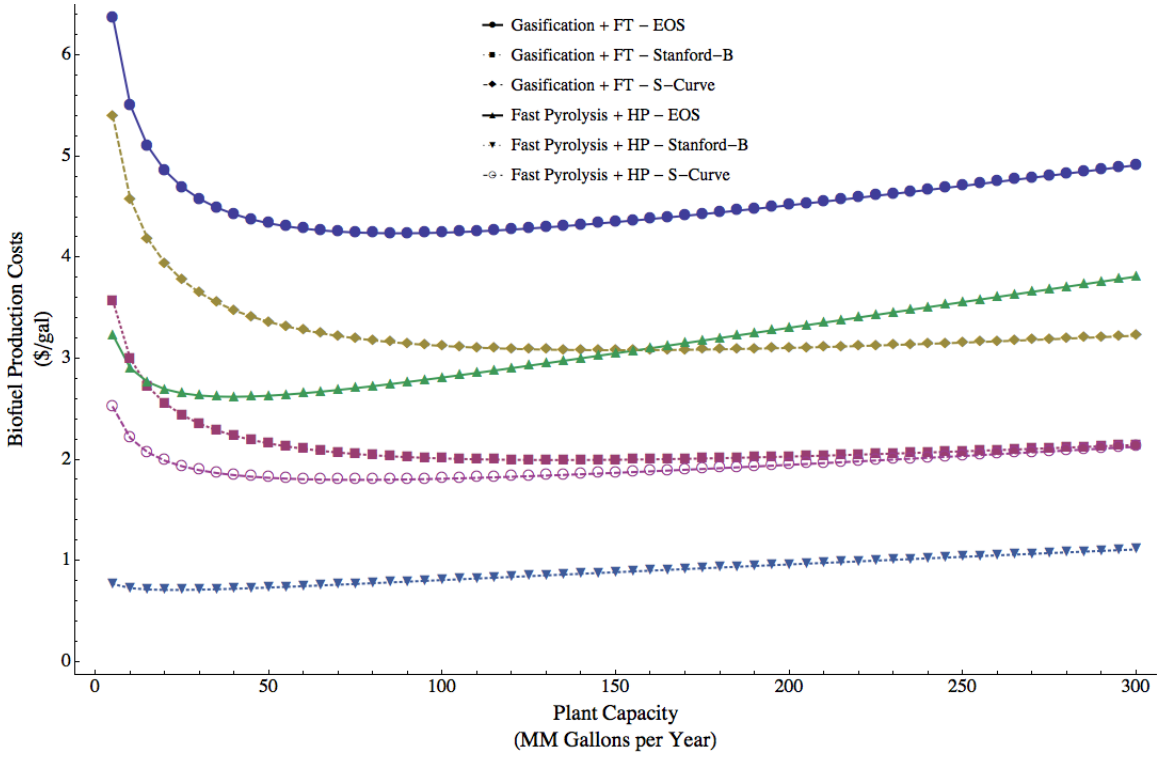

Figure 35: Gasification + Fischer-Tropsch and fast pyrolysis with hydroprocessing scenario costs ($/gal) vs. plant capacity (million gallons per year) based on economies of scale (EOS), Stanford-b, and S-curve models assuming cumulative industry capacity of 16 billion gallons per year.

Figure 36 shows the relationship between plant capital cost learning rate (LR_p) and the optimal plant size ratio (R_{opt}) for feedstock delivery learning rates of 5 to 21% based on the S-Curve and Stanford-B curve. The S-Curve shows limited sensitivity to changes in the LR_p. However, each curve indicates a minimum R_{opt} value as a function of LR_p. The Stanford curve shows a continuous decreasing value of R_{opt} with increasing learning rate. Both curves show a strong, yet opposing, sensitivity to feedstock delivery learning rate (LR_d). The impact of LR_d decreases at larger values for the S-Curve and the opposite occurs in the Stanford case. These results suggest that while capital cost learning rates could lead to lower optimal plant sizes, reductions in delivery costs might be a more significant factor in determining the optimal size of future biorefineries.

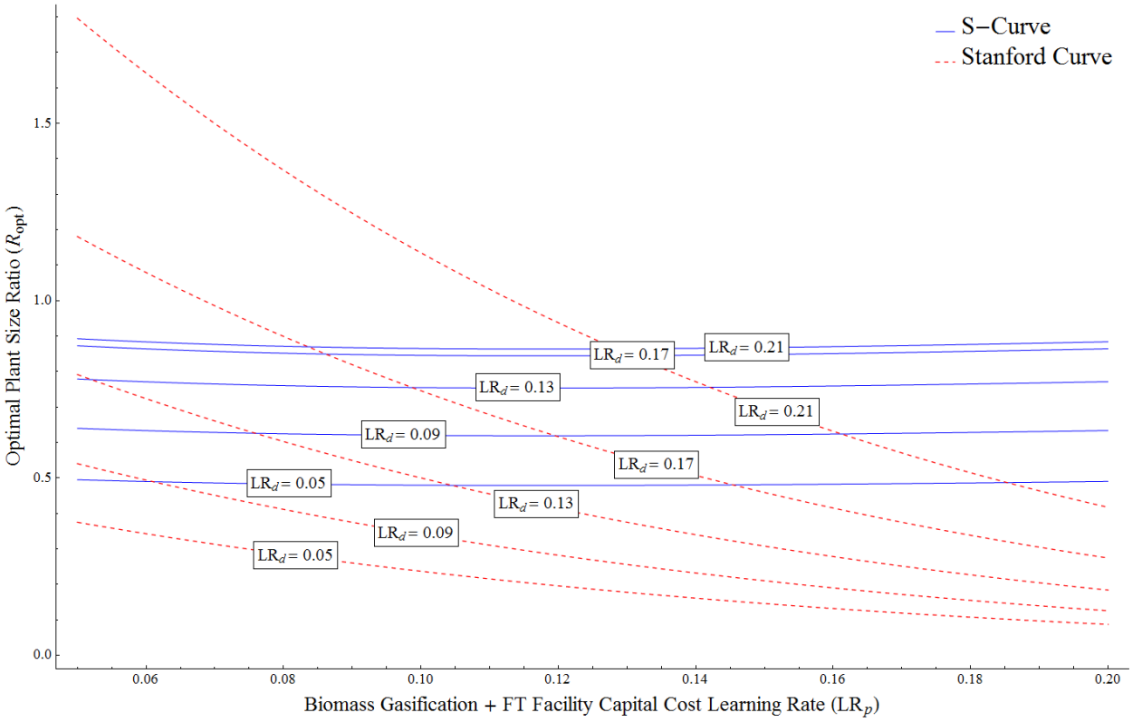

Figure 36: Biomass Gasification to Fischer-Tropsch optimal plant size vs. plant capital cost learning rate for different delivery learning rates based on S-curve and Stanford-curve models with 16 billion gallons of advanced biofuel industry capacity.

Figure 37 shows the sensitivity of R_{opt} (top) and optimal plant capacity (bottom) to various learning rate factors. Analyzed factors include plant and feedstock learning and incompressibility, prior learning, and cumulative industrial capacity. Each value was varied by ±20%. Feedstock delivery learning rates had the most impact in this analysis. This is due in part to the high feedstock contribution to production costs.

The absolute impacts of industrial cumulative capacity and prior learning assumptions are similar, but the trends are in opposite directions. The greater the amount of industrial capacity, the larger the optimal plant size ratio. On the other hand, the greater the amount of previous industrial learning, the smaller the optimal plant size ratio. This behavior can be explained as shifts in the assumed starting base case size. Increases

in the previous industrial learning factor suggest that base case capacities are closer to optimally sized.

Feedstock learning and incompressibility factors have negligible effect on the optimal plant capacity. This is expected because feedstock costs scale linearly with capacity in the economies of scale equation. There are non-logistic related improvements to feedstock production that are not well captured by this simplified model (feedstock resilience, innovative cropping methods, etc.). However, many of these improvements will like result in vertical shifts of the cost-scaling curve with small impact on the optimal capacity.

Figure 37: Optimal plant size ratio (top) and capacity (bottom) learning rate factor sensitivity analysis for Gasification + Fischer-Tropsch (left) and Fast Pyrolysis with Hydroprocessing (right) scenarios. Base case values shown in labels and varied by ±20%.

Conclusions

The purpose of this study was to evaluate the impacts of learning rates on the costs of advanced biorefineries. We reviewed several learning rate methodologies and

integrated them with the economies of scale equation. The modified equations were applied to case scenarios for biofuel production. With these methods, we estimated the optimal size and costs of advanced biorefineries after a given amount of accumulated industry capacity.

The results of this study indicate that learning rates could have a significant impact on the capacities and costs of future biorefineries. The modified Stanford-B model predicts that optimal plant sizes for large facilities with higher capital costs (gasification and cellulosic ethanol scenarios) are three to five times their base case size at a 5% capital cost learning rate. However, the same model also predicts that facilities with lower capital costs and capital cost learning rates of 20% have optimal plant sizes that are smaller than their base case sizes. Delivery cost learning rates had a more significant impact based on the sensitivity analysis. This suggests that improvements in biomass logistics could have significant impact on the capacity of future biorefineries.

These results suggest that there is a strong incentive to invest in strategies to increase the learning rates of advanced biorefineries. Several strategies could lead to smaller biorefinery facilities with significantly reduced costs. The nature of these strategies was beyond the scope of this study. However, it is clear that identifying and developing these strategies would be a clear step to reducing the costs of advanced biofuels.

Acknowledgments

The authors acknowledge the support of the Bioeconomy Institute and NSF EPSCOR, Grant Number EPS-1101284.

CHAPTER 6. CONCLUSIONS AND FUTURE WORK

Conclusions

The need and desire to produce renewable and sustainable energy grows each year as fossil fuel consumption continues to reach record highs. The construction of sustainable biorefineries would help increase national security, economic security and improve environmental quality. One promising technology to aide in the production of renewable fuels and chemicals is fast pyrolysis, which is a thermochemical process that converts lignocellulosic biomass into liquid, char, and gaseous products. Auger reactors have been gaining interest as pyrolysis reactors as they offer advantages over the traditional fluidized bed reactors. Specifically, auger pyrolyzers offer minimal dependence on inert sweep gas, high heat transfer rates with heat transfer media, ability to handle difficult feedstocks, and ability to be mass produced at modular or small commercial scales. As with any new technology, there is still much fundamental work needed to understand pyrolysis of biomass in an auger reactor with heat carrier. The purpose of this work was to address some of the voids in the literature concerning auger pyrolyzers to help mitigate risk upon scale-up.

Chapter 2 focused on the effect of thermophysical properties of heat carriers on yield and composition of pyrolysis products. Heat carriers with varying degrees of thermal diffusivities were tested in a laboratory-scale, twin-screw auger pyrolyzer. Stainless steel shot, sand, and silicon carbide were heat carriers of interest. No differences were exhibited in the average yield of organic fraction and composition of the bio-oil between heat carriers. However, significant differences were observed in reaction water

(12-16 wt.%, dry basis), char (16-22 wt.%, dry basis), and non-condensable gas (14-17 wt.%, dry basis) yields across the heat carriers. Furthermore, significant residual carbon and attrition existed for some heat carrier materials after only a single pyrolysis trial. Silicon carbide had the greatest extent of residual carbon at 20 wt.% of its total char yield. Silicon carbide and sand both had high attrition at up to 7 wt.% while stainless steel was had an undetectable amount of attrition. Given the limited number of trials for each heat carrier in this work, stainless steel shot appeared to have superior performance in both low attrition and low residual carbon yield. Other heat carriers such as sand produced more char and when coupled with a higher heat capacity, may be a more desirable material for heat recovery in a continuous regeneration process. Ultimately, this study showed that careful consideration should be made when selecting a heat carrier as tradeoffs may exist between cost, physical performance, and yields from an auger pyrolyzer.

Chapter 3 investigated the effect of recycling regenerated heat carrier on the long-term performance of a laboratory-scale auger pyrolyzer. Recycled trials of regenerated sand having a particle size of 600-1000 μm were conducted at a total of five recycles. No significant difference was found between the average product yields of organic bio-oil, reaction water and non-condensable gases given the limited number of recycles. Significant evidence of attrition ranging from 4 to 8 wt.% were found after each recycle. This would lead to increased material costs and potential particle entrainment issues during a continuous operation. Furthermore, the mean particle size of the sand heat carrier decreased with each recycle motivating a comparison of two different size fractions of sand heat carrier. It was found that the smaller sand fraction (250-600 μm)

produced significantly higher char and reaction water yields at the expense of the organic bio-oil and NCG yields when compared to the larger fraction (600-1000 μm) of sand heat carrier. This study showed that recycling sand heat carrier led to high attrition and a decreasing particle size suggesting pyrolysis product yields may change over time. This suggests that selection of heat carrier material may have importation implications for continuous pyrolysis in an auger reactor with recycled heat carrier.

Chapter 4 investigated the effect operating conditions of a laboratory-scale fluidized bed regenerator have on the carbon burn-off time and heat recovery from biomass pyrolysis char. Regenerations were conducted on char in sand heat carrier at varying conditions of regenerator temperature, superficial fluidization velocity, and oxygen sweep gas concentration. It was found that carbon burn-off times increased with increasing regenerator temperature from 450-750°C at the same state of fluidization. This was attributed to a decrease in superficial fluidization velocity. A deeper investigation yielded that an increase in the superficial fluidization velocity from minimum fluidization to 250% minimum fluidization significantly decreased the total carbon burn-off time. It was also found that the carbon burn-off time decreased and the maximum amount of operating carbon dioxide production increased with increasing initial oxygen sweep gas concentration. It was concluded that regeneration temperatures similar to pyrolysis operating temperatures may be desired. Operation at increased superficial fluidization velocities and oxygen sweep gas concentration is also preferred. However, trade-offs may exist as increasing the superficial fluidization velocity decreases the maximum temperature in the bed and thus the maximum energy able to be recovered from the regeneration unit.

Chapter 5 evaluated the impact of learning rates on the costs of advanced biorefineries. Several learning rate methodologies were integrated with the economies of scale equation and were applied to case scenarios for biofuel production to estimate the optimal size and costs of advanced biorefineries after a given amount of accumulated industry capacity. The modified Stanford-B model predicted that optimal plant sizes for large facilities with higher capital costs, such as gasification and cellulosic ethanol scenarios, are three to five times their base case size due to a 5% capital cost learning rate. The Stanford-B model also predicted that facilities with lower capital costs and higher learning rates of 20% have optimal plant sizes that are smaller than their base case sizes. Learning rates attributed to delivery costs had a more significant impact from sensitivity analysis suggesting that improvements in biomass logistics could have significant impact on the capacity of future biorefineries. The results from this study suggest that there is a strong incentive to invest in strategies to increase the learning rates of advanced biorefineries. This could lead to smaller biorefinery facilities with significantly reduced capital costs.

Future Work

Work in this dissertation has provided insight into the effect heat carriers have in biomass pyrolysis in auger reactors. This work also focused on considerations needed for successful continuous operation of auger pyrolyzers. A number of opportunities and research areas still exist to further the knowledge in auger pyrolysis.

One area of focus would be optimizing the effect of heat transfer from the heat carrier in the pyrolysis process. This work investigated stainless steel shot, silicon carbide, and two different sizes of sand. However, an optimal size of heat carrier or mass

loading ratios of heat carrier to biomass was not thoroughly investigated. Preliminary results suggest that both play an important role in the production of organic bio-oil and char. Investigating the role of particle size and mass loading ratios would provide valuable insight in the optimal selection of a heat carrier to increase heat transfer and minimize mass transfer effects during biomass pyrolysis.

Another area of focus should be the continuous and long-term recyclability of the heat carrier. This work showed significant attrition of sand after only five recycles. Another heat carrier with low or negligible attrition, such as stainless steel shot, may prove to be more desirable considering long-term operating costs and ease of downstream bio-oil processing. Specific focus to the heat carrier composition and quality should also be further investigated to determine if catalytic activity may be present after long-tern recycling. The effect of residual carbon on the heat carrier during pyrolysis should be investigated to determine if/when regeneration of the heat carrier is needed.

Optimization of the heat carrier regeneration is a critical area for further investigation. While a fluidized bed reactor was used for the regenerations in this work, it may not be the most suitable reactor for a continuous auger pyrolysis process. The use of an auger reactor to regenerate the heat carrier may prove to be more economical and feasible. The ability to sufficiently remove ash following the regeneration process is of special importance to prevent secondary reactions during the pyrolysis of recycled heat carrier. The effect of char particle size on char burn-off times should also be investigated.

Scale-up of and continuous recycling of heat carrier following pyrolysis and subsequent regeneration is one area of particular interest after the individual investigations conducted this work.

REFERENCES

1. Agency, I.E., *2015 Key World Energy Statistics*. 2015: www.iea.org/statistics/.

2. Brown, R.C., Brown, T. R., *Biorenewable Resources Engineering New Products from Agriculture*. Second Edition ed. 2014: John Wiley & Sons, Inc.

3. Administration, U.S.E.I., *Annual Energy Review 2011*. 2012, U.S. Energy Information Administration.

4. Crane, K., et. al., *Imported Oil and U.S. National Security*. 2009: http://www.rand.org.

5. Jackson, J.K., *U.S. Trade Deficit and the Impact of Changing Oil Prices*. 2016: www.crs.gov.

6. Agency, U.S.E.P., *Inventory of U.S. Greenhouse Gas Emissions and Sinks: 1990-2014*. 2016: https://www3.epa.gov/climatechange/ghgemissions/usinventoryreport.html.

7. Laird, D.A., *The Charcoal Vision: A Win–Win–Win Scenario for Simultaneously Producing Bioenergy, Permanently Sequestering Carbon, while Improving Soil and Water Quality*. Agronomy Journal, 2008. **100**(1): p. 178-181.

8. Lehmann, J., Joseph, Stephen, *Biochar for Environmental Management: Science and Technology*. 2009: Routledge.

9. Energy, U.S.D.o., *U.S. Billion-Ton Update: Biomass Supply for a Bioenergy and Bioproducts Industry*. 2011, Oak Ridge National Laboratory. p. 227.

10. Sjostrom, E., *Wood chemistry: fundamentals and applications*. Second Edition ed. 1993: San Diego: Academic Press.

11. Mohan, D., Pittman Jr., Charles U., Steele, Philip H., *Pyrolysis of Wood/Biomass for Bio-oil- A critical Review*. Energy & Fuels, 2006(20): p. 848-889.

12. Lee, H.V., S.B. Hamid, and S.K. Zain, *Conversion of lignocellulosic biomass to nanocellulose: structure and chemical process.* ScientificWorldJournal, 2014. **2014**: p. 631013.

13. Heitner, C., Dimmel, Don., Schmidt, John A., *Lignin and lignans: advances in chemistry*. 2010, Boca Raton, FL: Taylor & Francis. 651.

14. Amarasekara, A.S., *Handbook of Cellulosic Ethanol*. 2013: Wiley-Scrivener. 604.

15. Brown, R.C., *Thermochemical processing of biomass: conversion into fuels, chemicals and power*. 2011, Chichester, West Sussex, United Kingdom: John Wiley & Sons, Ltd. 330.

16. Bridgwater, A.V., *Review of fast pyrolysis of biomass and product upgrading.* Biomass and Bioenergy, 2012. **38**: p. 68-94.

17. Demirbas, A., *Sustainable cofiring of biomass with coal.* Energy Conversion and Management, 2003(44): p. 1465-1479.

18. Sami, M., Annamalai, K., Wooldridge, M., *Co-firing of coal and biomass fuel blends.* Progress in Energy and Combustion Science, 2001(27): p. 171-214.

19. Bridgwater, A.V., Peacocke, G. V. C., *Fast pyrolysis processes of biomass.* Renewable and Sustainable Energy Reviews, 2000(4): p. 73.

20. Diebold, J.P., *A review of the chemical and physical mechanisms of the storage stability of fast pyrolysis bio-oil*. 2000, National Renewable Energy Laboratory: http://www.doe.gov/bridge.

21. Vamvuka, D., *Bio-oil, solid and gaseous biofuels from biomass pyrolysis processes-An overview.* International Journal of Energy Research, 2011. **35**(10): p. 835-862.

22. Hess, J.R., Kenney, K. L., Ovard, L. P., Searcy, E. M., Wright, C. T., *Commodity-Scale Production of an Infrastructure-Compatible Bulk Solid from Herbaceous Lignocellulosic Biomass*. 2009: Uniform-Format Bioenergy Feedstock Su pply System Design Report Series.

23. Wright, M. and R.C. Brown, *Establishing the optimal sizes of different kinds of biorefineries.* Biofuels, Bioproducts and Biorefining, 2007. **1**(3): p. 191-200.

24. You, F. and B. Wang, *Life Cycle Optimization of Biomass-to-Liquid Supply Chains with Distributed–Centralized Processing Networks.* Industrial & Engineering Chemistry Research, 2011. **50**(17): p. 10102-10127.

25. Dahlgren, E., et al., *Small Modular Infrastructure.* The Engineering Economist, 2013. **58**(4): p. 231-264.

26. Daugaard, T., et al., *Learning rates and their impacts on the optimal capacities and production costs of biorefineries.* Biofuels, Bioproducts and Biorefining, 2015. **9**(1): p. 82-94.

27. Anex, R.P., et al., *Techno-economic comparison of biomass-to-transportation fuels via pyrolysis, gasification, and biochemical pathways.* Fuel, 2010. **89**: p. S29-S35.

28. Brown, T.R., *A techno-economic review of thermochemical cellulosic biofuel pathways.* Bioresour Technol, 2015. **178**: p. 166-76.

29. Gnansounou, E. and A. Dauriat, *Techno-economic analysis of lignocellulosic ethanol: A review.* Bioresour Technol, 2010. **101**(13): p. 4980-91.

30. Kazi, F.K., et al., *Techno-economic comparison of process technologies for biochemical ethanol production from corn stover.* Fuel, 2010. **89**: p. S20-S28.

31. Swanson, R.M., et al., *Techno-economic analysis of biomass-to-liquids production based on gasification.* Fuel, 2010. **89**: p. S11-S19.

32. Wright, M.M., Satrio, Justinus A., Brown, Robert C., Daugaard, Daren E., Hsu, David D., *Techno-conomic analysis of biomass fast pyrolysis to transportation fuels*. 2010, National Renewable Energy Laboratory: http://www.osti.gov/bridge.

33. Bridgwater, A.V., *Fast pyrolysis of biomass: a handbook volume 2*. Vol. 2. 2002, Newbury: CPL Press Liberty House.

34. Williams, P.T., Besler, Serpil, *The influence of temperature and heating rate on the slow pyrolysis of biomass.* Renewable Energy, 1996. **7**(3): p. 233-250.

35. Brown, T.R., M.M. Wright, and R.C. Brown, *Estimating profitability of two biochar production scenarios: slow pyrolysis vs fast pyrolysis.* Biofuels, Bioproducts and Biorefining, 2011. **5**(1): p. 54-68.

36. Antal, J.M.J., Helsen, Lieve M., Kouzu, Masato., Lede, Jacques., Matsumura, Yukihiko, *Rules of Thumb (Empirical Rules) for the Biomass Utilizaion by Thermochemical Conversion.* Journal of the Japan Institute of Energy, 2014(93): p. 684-702.

37. Bridgwater, A.V., *Fast pyrolysis of biomass : a handbook Volume 1*. Vol. 1. 1999, Newbury: CPL Press Libery House.

38. Czernik, S., Bridgwater, A. V., *Overview of Applications of Biomass Fast Pyrolysis Oil.* Energy & Fuels, 2004(18): p. 590-598.

39. Alsbou, E. and B. Helleur, *Accelerated Aging of Bio-oil from Fast Pyrolysis of Hardwood.* Energy & Fuels, 2014. **28**(5): p. 3224-3235.

40. Ciolkosz, D. and R. Wallace, *A review of torrefaction for bioenergy feedstock production.* Biofuels, Bioproducts and Biorefining, 2011. **5**(3): p. 317-329.

41. van der Stelt, M.J.C., et al., *Biomass upgrading by torrefaction for the production of biofuels: A review.* Biomass and Bioenergy, 2011.

42. Boateng, A.A. and C.A. Mullen, *Fast pyrolysis of biomass thermally pretreated by torrefaction.* Journal of Analytical and Applied Pyrolysis, 2013. **100**: p. 95-102.

43. Meng, J., et al., *The effect of torrefaction on the chemistry of fast-pyrolysis bio-oil.* Bioresour Technol, 2012. **111**: p. 439-46.

44. Ren, S., et al., *The effects of torrefaction on compositions of bio-oil and syngas from biomass pyrolysis by microwave heating.* Bioresour Technol, 2013. **135**: p. 659-64.

45. Patwardhan, P.R., et al., *Product distribution from fast pyrolysis of glucose-based carbohydrates.* Journal of Analytical and Applied Pyrolysis, 2009. **86**(2): p. 323-330.

46. Patwardhan, P.R., et al., *Influence of inorganic salts on the primary pyrolysis products of cellulose.* Bioresour Technol, 2010. **101**(12): p. 4646-55.

47. Kuzhiyil, N., et al., *Pyrolytic sugars from cellulosic biomass.* ChemSusChem, 2012. **5**(11): p. 2228-36.

48. Zhou, S., et al., *Effect of sulfuric acid on the pyrolysis of Douglas fir and hybrid poplar wood: Py-GC/MS and TG studies.* Journal of Analytical and Applied Pyrolysis, 2013. **104**: p. 117-130.

49. Kim, K.H., R.C. Brown, and X. Bai, *Partial oxidative pyrolysis of acid infused red oak using a fluidized bed reactor to produce sugar rich bio-oil.* Fuel, 2014. **130**: p. 135-141.

50. Dalluge, D.L., et al., *Continuous production of sugars from pyrolysis of acid-infused lignocellulosic biomass.* Green Chemistry, 2014. **16**(9): p. 4144.

51. Kim, K.H., et al., *The effect of low-concentration oxygen in sweep gas during pyrolysis of red oak using a fluidized bed reactor.* Fuel, 2014. **124**: p. 49-56.

52. Mullen, C.A., A.A. Boateng, and N.M. Goldberg, *Production of Deoxygenated Biomass Fast Pyrolysis Oils via Product Gas Recycling.* Energy & Fuels, 2013. **27**(7): p. 3867-3874.

53. Tarves, P.C., C.A. Mullen, and A.A. Boateng, *Effects of Various Reactive Gas Atmospheres on the Properties of Bio-Oils Produced Using Microwave Pyrolysis.* ACS Sustainable Chemistry & Engineering, 2016. **4**(3): p. 930-936.

54. Dayton, D.C., et al., *Biomass Hydropyrolysis in a Pressurized Fluidized Bed Reactor.* Energy & Fuels, 2013. **27**(7): p. 3778-3785.

55. Marker, T.L., et al., *Integrated hydropyrolysis and hydroconversion (IH2) for the direct production of gasoline and diesel fuels or blending components from*

biomass, part 1: Proof of principle testing. Environmental Progress & Sustainable Energy, 2012. **31**(2): p. 191-199.

56. Aho, A., et al., *Catalytic pyrolysis of woody biomass in a fluidized bed reactor: Influence of the zeolite structure.* Fuel, 2008. **87**(12): p. 2493-2501.

57. Bridgwater, A.V., *Production of high grade fuels and chemicals from catalytic pyrolysis of biomass.* Catalysis Today, 1996(29): p. 285-295.

58. Carlson, T.R., et al., *Aromatic Production from Catalytic Fast Pyrolysis of Biomass-Derived Feedstocks.* Topics in Catalysis, 2009. **52**(3): p. 241-252.

59. Dickerson, T. and J. Soria, *Catalytic Fast Pyrolysis: A Review.* Energies, 2013. **6**(1): p. 514-538.

60. French, R. and S. Czernik, *Catalytic pyrolysis of biomass for biofuels production.* Fuel Processing Technology, 2010. **91**(1): p. 25-32.

61. Wang, K., K.H. Kim, and R.C. Brown, *Catalytic pyrolysis of individual components of lignocellulosic biomass.* Green Chem., 2014. **16**(2): p. 727-735.

62. Yildiz, G., et al., *Challenges in the design and operation of processes for catalytic fast pyrolysis of woody biomass.* Renewable and Sustainable Energy Reviews, 2016. **57**: p. 1596-1610.

63. Liu, C., et al., *Catalytic fast pyrolysis of lignocellulosic biomass.* Chem Soc Rev, 2014. **43**(22): p. 7594-623.

64. Asadieraghi, M., W.M. Ashri Wan Daud, and H.F. Abbas, *Heterogeneous catalysts for advanced bio-fuel production through catalytic biomass pyrolysis vapor upgrading: a review.* RSC Adv., 2015. **5**(28): p. 22234-22255.

65. López, A., et al., *Catalytic pyrolysis of plastic wastes with two different types of catalysts: ZSM-5 zeolite and Red Mud.* Applied Catalysis B: Environmental, 2011. **104**(3-4): p. 211-219.

66. Yathavan, B.K. and F.A. Agblevor, *Catalytic Pyrolysis of Pinyon–Juniper Using Red Mud and HZSM-5.* Energy & Fuels, 2013. **27**(11): p. 6858-6865.

67. Gamliel, D.P., et al., *Investigation of in situ and ex situ catalytic pyrolysis of miscanthus x giganteus using a PyGC-MS microsystem and comparison with a bench-scale spouted-bed reactor.* Bioresour Technol, 2015. **191**: p. 187-96.

68. Wang, K., P.A. Johnston, and R.C. Brown, *Comparison of in-situ and ex-situ catalytic pyrolysis in a micro-reactor system.* Bioresour Technol, 2014. **173**: p. 124-31.

69. Yildiz, G., et al., *Validation of a new set-up for continuous catalytic fast pyrolysis of biomass coupled with vapour phase upgrading.* Journal of Analytical and Applied Pyrolysis, 2013. **103**: p. 343-351.

70. Meier, D., Faix, O., *State of the art of applied fast pyrolysis of lignocellulosic materials-a review.* Bioresource Technology, 1999(68): p. 71-77.

71. Scott, D.S., Majerski, Piotr., Piskorz, Jan., Radlein, Desmond, *A second look at fast pyrolsis of biomass-the RTI process.* Journal of Analytical and Applied Pyrolysis, 1999(51): p. 23-37.

72. Boateng, A.A., Daugaard, Daren E., Goldberg, Neil M., Hicks, Kevin B., *Bench-Scale Fluidized-Bed Pyrolysis of Switchgrass for Bio-Oil Production.* Industrial & Engineering Chemistry Research, 2007(46): p. 1891-1897.

73. Daugaard, D.E., *The transport phase of pyrolytic oil exiting a fast fluidized bed reactor*. 2003, Iowa State University: Retrospective Theses and Dissertations.

74. Pollard, A.S., M.R. Rover, and R.C. Brown, *Characterization of bio-oil recovered as stage fractions with unique chemical and physical properties.* Journal of Analytical and Applied Pyrolysis, 2012. **93**: p. 129-138.

75. Bridgwater, A.V., *Principles and practice of biomass fast pyrolysis processes for liquids.* Journal of Analytical and Applied Pyrolysis, 1999(51): p. 3-22.

76. Ellens, C.J. and R.C. Brown, *Optimization of a free-fall reactor for the production of fast pyrolysis bio-oil.* Bioresour Technol, 2012. **103**(1): p. 374-80.

77. Onay, O. and O. Kockar, *Pyrolysis of rapeseed in a free fall reactor for production of bio-oil.* Fuel, 2006. **85**(12-13): p. 1921-1928.

78. Pattiya, A., S. Sukkasi, and V. Goodwin, *Fast pyrolysis of sugarcane and cassava residues in a free-fall reactor.* Energy, 2012. **44**(1): p. 1067-1077.

79. Wei, L., et al., *Characteristics of fast pyrolysis of biomass in a free fall reactor.* Fuel Processing Technology, 2006. **87**(10): p. 863-871.

80. Brown, J.N., *Development of a lab-scale auger reactor for biomass fast pyrolysis and process optimization using response surface methodology*. 2009, Iowa State University: Graduate Theses and Dissertations.

81. Liaw, S.-S., et al., *Effect of pyrolysis temperature on the yield and properties of bio-oils obtained from the auger pyrolysis of Douglas Fir wood.* Journal of Analytical and Applied Pyrolysis, 2012. **93**: p. 52-62.

82. Pittman, C.U., et al., *Characterization of Bio-oils Produced from Fast Pyrolysis of Corn Stalks in an Auger Reactor.* Energy & Fuels, 2012. **26**(6): p. 3816-3825.

83. Puy, N., et al., *Valorisation of forestry waste by pyrolysis in an auger reactor.* Waste Manag, 2011. **31**(6): p. 1339-49.

84. Lakshmanan, C.M., Gal-or, Benjamin., Hoelscher, H. E., *Production of levoglucosn by pyrolysis of carbohydrates.* Industrial & Engineering Chemistry Product Research and Development, 1969. **8**(3): p. 261-267.

85. Ingram, L., Mohan, Dinesh., Bricka, Mark., Steele, Phillip., Strobel, David., Crocker, David., Mitchell, Brian., Mohammad, Javeed., Cantrell, Kelly., Pittman Jr, Charles U., *Pyrolysis of wood and bark in an auger reactor- physical properties and chemical analysis of the produced bio-oils.* Energy & Fuels, 2008(22): p. 614-625.

86. Thangalazhy-Gopakumar, S., et al., *Physiochemical properties of bio-oil produced at various temperatures from pine wood using an auger reactor.* Bioresour Technol, 2010. **101**(21): p. 8389-95.

87. de Wild, P.J., et al., *Biomass valorisation by staged degasification.* Journal of Analytical and Applied Pyrolysis, 2009. **85**(1-2): p. 124-133.

88. Liaw, S.-S., et al., *Effect of pretreatment temperature on the yield and properties of bio-oils obtained from the auger pyrolysis of Douglas fir wood.* Fuel, 2013. **103**: p. 672-682.

89. Zhou, S., et al., *Effect of sulfuric acid concentration on the yield and properties of the bio-oils obtained from the auger and fast pyrolysis of Douglas Fir.* Fuel, 2013. **104**: p. 536-546.

90. Li, B., et al., *Pyrolysis and catalytic upgrading of pine wood in a combination of auger reactor and fixed bed.* Fuel, 2014. **129**: p. 61-67.

91. Brown, J.N. and R.C. Brown, *Process optimization of an auger pyrolyzer with heat carrier using response surface methodology.* Bioresource Technology, 2012. **103**(1): p. 405-14.

92. Kingston, T.A., et al., *Characterizing 3D granular flow structures in a double screw mixer using X-ray particle tracking velocimetry.* Powder Technology, 2015. **278**: p. 211-222.

93. Kingston, T.A. and T.J. Heindel, *Granular mixing optimization and the influence of operating conditions in a double screw mixer.* Powder Technology, 2014. **266**: p. 144-155.

94. Veses, A., et al., *Catalytic pyrolysis of wood biomass in an auger reactor using calcium-based catalysts.* Bioresour Technol, 2014. **162**: p. 250-8.

95. Henrich, E., et al., *Fast pyrolysis of lignocellulosics in a twin screw mixer reactor.* Fuel Processing Technology, 2016. **143**: p. 151-161.

96. Di Blasi, C., *Influences of physical properties on biomass devolatilization characteristics.* Fuel, 1997. **76**(10): p. 957-964.

97. Meng, J., et al., *The effect of torrefaction on the chemistry of fast-pyrolysis bio-oil.* Bioresource Technology, 2012. **111**: p. 439-46.

98. Gamliel, D.P., et al., *Investigation of in situ and ex situ catalytic pyrolysis of miscanthus x giganteus using a PyGC-MS microsystem and comparison with a bench-scale spouted-bed reactor.* Bioresource Technology, 2015. **191**: p. 187-96.

99. Wang, K., P.A. Johnston, and R.C. Brown, *Comparison of in-situ and ex-situ catalytic pyrolysis in a micro-reactor system.* Bioresource Technology, 2014. **173**: p. 124-31.

100. Escudero, D. and T.J. Heindel, *Bed height and material density effects on fluidized bed hydrodynamics.* Chemical Engineering Science, 2011. **66**(16): p. 3648-3655.

101. Puy, N., et al., *Valorisation of forestry waste by pyrolysis in an auger reactor.* Waste Management, 2011. **31**(6): p. 1339-49.

102. Thangalazhy-Gopakumar, S., et al., *Physiochemical properties of bio-oil produced at various temperatures from pine wood using an auger reactor.* Bioresource Technology, 2010. **101**(21): p. 8389-95.

103. Veses, A., et al., *Catalytic pyrolysis of wood biomass in an auger reactor using calcium-based catalysts.* Bioresource Technology, 2014. **162**: p. 250-8.

104. Bridgwater, A., D. Meier, and D. Radlein, *An overview of fast pyrolysis of biomass.* Organic geochemistry, 1999. **30**(12): p. 1479-1493.

105. Demirbas, A., *Calculation of higher heating values of biomass fuels.* Fuel, 1997. **76**(5): p. 431-434.

106. Incropera, F.P., *Fundamentals of heat and mass transfer*. 2007: John Wiley.

107. Choi, Y.S., et al., *Detailed characterization of red oak-derived pyrolysis oil: Integrated use of GC, HPLC, IC, GPC and Karl-Fischer.* Journal of Analytical and Applied Pyrolysis, 2014. **110**: p. 147-154.

108. Antal, M.J. and M. Grønli, *The art, science, and technology of charcoal production.* Industrial & Engineering Chemistry Research, 2003. **42**(8): p. 1619-1640.

109. Kuhn, H., D. Medlin, and A.S.M.I.H. Committee, *Mechanical testing and evaluation / prepared under the direction of the ASM International Handbook Committee ; volume editors, Howard Kuhn, Dana Medlin*. 2000, Materials Park, OH: Materials Park, OH : ASM International.

110. Sissine, F. *Energy Independence and Security Act of 2007: a summary of major provisions*. 2007. DTIC Document.

111. Daugaard, T.J., et al., *Effect of thermophysical properties of heat carriers on performance of a laboratory-scale auger pyrolyzer.* Fuel Processing Technology, 2018. **176**: p. 182-189.

112. Coda, B. and L. Tognotti, *The prediction of char combustion kinetics at high temperature.* Experimental Thermal and fluid science, 2000. **21**(1): p. 79-86.

113. He, W., et al., *Combustion rate for char with fractal pore characteristics.* Combustion Science and Technology, 2013. **185**(11): p. 1624-1643.

114. Hurt, R., J.-K. Sun, and M. Lunden, *A kinetic model of carbon burnout in pulverized coal combustion.* Combustion and flame, 1998. **113**(1): p. 181-197.

115. Murphy, J.J. and C.R. Shaddix, *Combustion kinetics of coal chars in oxygen-enriched environments.* Combustion and flame, 2006. **144**(4): p. 710-729.

116. Scala, F. and R. Chirone, *Combustion of single coal char particles under fluidized bed oxyfiring conditions.* Industrial & Engineering Chemistry Research, 2010. **49**(21): p. 11029-11036.

117. Smith, I. *The combustion rates of coal chars: a review*. in *Symposium (International) on combustion*. 1982. Elsevier.

118. Brunello, S., et al., *Kinetic study of char combustion in a fluidized bed.* Fuel, 1996. **75**(5): p. 536-544.

119. Saastamoinen, J. and A. Tourunen, *Model for char combustion, particle size distribution, and inventory in air and oxy-fuel combustion in fluidized beds.* Energy & Fuels, 2011. **26**(1): p. 407-416.

120. Siemons, R.V., *The mechanism of char ignition in fluidized bed combustors.* Combustion and flame, 1987. **70**(2): p. 191-206.

121. Turnbull, E. and J. Davidson, *Fluidized combustion of char and volatiles from coal.* AIChE journal, 1984. **30**(6): p. 881-889.

122. Bates, R.B., C. Altantzis, and A.F. Ghoniem, *Modeling of biomass char gasification, combustion, and attrition kinetics in fluidized beds.* Energy & Fuels, 2016. **30**(1): p. 360-376.

123. Di Blasi, C., *Combustion and gasification rates of lignocellulosic chars.* Progress in energy and combustion science, 2009. **35**(2): p. 121-140.

124. Henrich, E., et al., *Combustion and gasification kinetics of pyrolysis chars from waste and biomass.* Journal of Analytical and Applied Pyrolysis, 1999. **49**(1): p. 221-241.

125. Ragland, K.W. and K.M. Bryden, *Combustion Engineering, Second Edition*. 2011: CRC Press.

126. Abrahamsen, A.R. and D. Geldart, *Behaviour of gas-fluidized beds of fine powders part I. Homogeneous expansion.* Powder technology, 1980. **26**(1): p. 35-46.

127. Kunii, D., O. Levenspiel, and H. Brenner, *Fluidization Engineering*. 2013: Elsevier Science.

128. Hettinga, W., et al., *Understanding the reductions in US corn ethanol production costs: An experience curve approach.* Energy policy, 2009. **37**(1): p. 190-203.

129. Van den Wall Bake, J., et al., *Explaining the experience curve: Cost reductions of Brazilian ethanol from sugarcane.* Biomass and Bioenergy, 2009. **33**(4): p. 644-658.

130. De Wit, M., et al., *Competition between biofuels: Modeling technological learning and cost reductions over time.* Biomass and bioenergy, 2010. **34**(2): p. 203-217.

131. Junginger, M., et al., *Technological learning in bioenergy systems.* Energy Policy, 2006. **34**(18): p. 4024-4041.

132. Junginger, M., et al., *Technological learning and cost reductions in wood fuel supply chains in Sweden.* Biomass and Bioenergy, 2005. **29**(6): p. 399-418.

133. Uyterlinde, M.A., et al., *Implications of technological learning on the prospects for renewable energy technologies in Europe.* Energy Policy, 2007. **35**(8): p. 4072-4087.

134. Cabral, L.M. and M.H. Riordan, *The learning curve, market dominance, and predatory pricing.* Econometrica: Journal of the Econometric Society, 1994: p. 1115-1140.

135. Jamasb, T., *Technical change theory and learning curves: patterns of progress in electricity generation technologies.* The Energy Journal, 2007: p. 51-71.

136. Jamasb, T. and J. Kohler, *Learning curves for energy technology: a critical assessment.* 2007.

137. Klenow, P.J., *Learning curves and the cyclical behavior of manufacturing industries.* Review of Economic dynamics, 1998. **1**(2): p. 531-550.

138. McDonald, A. and L. Schrattenholzer, *Learning rates for energy technologies.* Energy policy, 2001. **29**(4): p. 255-261.

139. Neij, L., *Use of experience curves to analyse the prospects for diffusion and adoption of renewable energy technology.* Energy policy, 1997. **25**(13): p. 1099-1107.

140. Rubin, E.S., et al., *Learning curves for environmental technology and their importance for climate policy analysis.* Energy, 2004. **29**(9): p. 1551-1559.

141. Schoots, K., et al., *Learning curves for hydrogen production technology: an assessment of observed cost reductions.* International Journal of Hydrogen Energy, 2008. **33**(11): p. 2630-2645.

142. Yelle, L.E., *THE LEARNING CURVE: HISTORICAL REVIEW AND COMPREHENSIVE SURVEY.* Decision Sciences, 1979. **10**(2): p. 302-328.

143. BP, *BP Statistical Review of World Energy*. 2010. p. 1-50.

144. Anon, *Nonconventional Liquid Fuels*. 2006, US Energy Information Administration: Washington, DC.

145. Coyle, W.T., *Next-generation biofuels: Near-term challenges and implications for agriculture*. 2010: DIANE Publishing.

146. Brown, T.R. and R.C. Brown, *A review of cellulosic biofuel commercial-scale projects in the United States.* Biofuels, bioproducts and biorefining, 2013. **7**(3): p. 235-245.

147. Schnepf, R., *Renewable Fuel Standard (RFS): overview and issues*. 2011: Diane Publishing.

148. Weiss, M., et al., *A review of experience curve analyses for energy demand technologies.* Technological forecasting and social change, 2010. **77**(3): p. 411-428.

149. Leboreiro, J. and A.K. Hilaly, *Biomass transportation model and optimum plant size for the production of ethanol.* Bioresource technology, 2011. **102**(3): p. 2712-2723.

150. Jack, M.W., *Scaling laws and technology development strategies for biorefineries and bioenergy plants.* Bioresource technology, 2009. **100**(24): p. 6324-6330.

151. Pantaleo, A., B. De Gennaro, and N. Shah, *Assessment of optimal size of anaerobic co-digestion plants: an application to cattle farms in the province of Bari (Italy).* Renewable and Sustainable Energy Reviews, 2013. **20**: p. 57-70.

152. Moore, F.T., *Economies of scale: Some statistical evidence.* The Quarterly Journal of Economics, 1959. **73**(2): p. 232-245.

153. Gallagher, P.W., H. Brubaker, and H. Shapouri, *Plant size: capital cost relationships in the dry mill ethanol industry.* Biomass and Bioenergy, 2005. **28**(6): p. 565-571.

154. Jenkins, B.M., *A comment on the optimal sizing of a biomass utilization facility under constant and variable cost scaling.* Biomass and Bioenergy, 1997. **13**(1-2): p. 1-9.

155. Nguyen, M. and R. Prince, *A simple rule for bioenergy conversion plant size optimisation: bioethanol from sugar cane and sweet sorghum.* Biomass and Bioenergy, 1996. **10**(5-6): p. 361-365.

156. Hirschmann, W.B., *Profit from the learning-curve.* Harvard Business Review, 1964. **42**(1): p. 125-139.

157. Claeson Colpier, U., *Using the experience curve to analyze the cost development of the combined cycle gas turbine*. 1999, Energy Conversion, Chalmers University of Technology.

158. Crago, C.L., et al., *Competitiveness of Brazilian sugarcane ethanol compared to US corn ethanol.* Energy Policy, 2010. **38**(11): p. 7404-7415.

159. Weiss, M. *Learning in carbon accounting and energy efficiency*. in *2003 European Wind Energy Conference*. 2009.

160. Teplitz, C.J., *The learning curve deskbook: A reference guide to theory, calculations, and applications*. 1991: Quorum Books.

161. Riahi-Belkaoui, A., *The learning curve: a management accounting tool*. 1986: Quorum Books.

162. Dar-Ei, E.M., *Learning in the Plant: The Beginnings of Organizational Learning*, in *HUMAN LEARNING: From Learning Curves to Learning Organizations*. 2000, Springer. p. 159-183.

163. Zenger, T.R., *Explaining organizational diseconomies of scale in R&D: Agency problems and the allocation of engineering talent, ideas, and effort by firm size.* Management science, 1994. **40**(6): p. 708-729.

164. Brown, T.R., et al., *Techno-economic analysis of biomass to transportation fuels and electricity via fast pyrolysis and hydroprocessing.* Fuel, 2013. **106**: p. 463-469.

165. McAloon, A., et al., *Determining the cost of producing ethanol from corn starch and lignocellulosic feedstocks.* National Renewable Energy Laboratory Report, 2000.

166. Hamelinck, C.N., G. Van Hooijdonk, and A.P. Faaij, *Ethanol from lignocellulosic biomass: techno-economic performance in short-, middle-and long-term.* Biomass and bioenergy, 2005. **28**(4): p. 384-410.

167. Hamelinck, C.N. and A.P. Faaij, *Future prospects for production of methanol and hydrogen from biomass.* Journal of Power Sources, 2002. **111**(1): p. 1-22.

168. Phillips, S., et al., *Thermochemical ethanol via indirect gasification and mixed alcohol synthesis of lignocellulosic biomass.* National Renewable Energy Laboratory, Golden, CO, NREL Technical Report No. TP-510-41168, http://www. nrel. gov/docs/fy07osti/41168. pdf, 2007.

169. Qi, F., *Discrete element method modeling of biomass fast pyrolysis granular flows.* 2017.

APPENDIX. PRELIMINARY HEAT TRANSFER ANALYSIS OF A DIRECTLY HEATED AUGER PYROLYZER

Introduction and Methodology

Directly heated auger pyrolyzers rely on heat carrier to provide high heating rates to biomass particles. It is important to understand the contribution from the different modes of heat transfer and the effect of material selection on the rates of heat transfer in directly heated auger pyrolyzers. The primary modes of heat transfer in auger reactors are thought to be conduction and radiation with the dominating mode dependent on the type of auger reactor, indirectly heated or directly heated. Fluidized bed reactors, however, are thought to be dominated by conduction (90%) with a small amount of convection (10%) [75]. One advantage of auger reactors is the use of very little carrier gas, thus making the primary modes of heat transfer conduction and radiation. Solid-solid heat transfer is then more dominating in directly heated auger pyrolyzers making the selection of a heat carrier material with desirable thermal properties of specific importance.

This work provides a preliminary analysis of heat transfer in a directly heated auger pyrolyzer. The experimental work described in *Chapter 2* served as the motivation and foundation of this work. Heat carriers with varying thermophysical properties were chosen, specifically, stainless steel shot, silicon carbide, and sand. A particle size of 1.0 mm for both the heat carrier and biomass is chosen. Furthermore, a heat carrier initial temperature of 575°C is chosen to simulate the conditions from experimental work.

For this work, the temperature gradients within the biomass and heat carrier particles are considered negligible. The energy equation for particle *i*, either biomass or heat carrier, is written as:

$$m_i c_{p,i} \frac{dT_i}{dt} = \sum Q_{ij}^{cond} + Q_{fi}^{conv} + \sum Q_{ij}^{rad} - \Delta H_i \dot{\omega}_\iota$$

where, m_i is the mass of the particle, $c_{p,i}$ is the specific heat capacity of the particle, T_i is the temperature of the particle, and t is time. Q_{ij}^{cond} and Q_{ij}^{rad} are the rates of heat transfer between particle *i* and *j* for conduction and radiation, respectively. Q_{fi}^{conv} is the rate of heat transfer for convection but was not taken to account in this work. ΔH_i is the heat of reaction and $\dot{\omega}_\iota$ is the reaction rate.

The energy equation was considered for both a single particle of biomass and a single particle of heat carrier. Conduction in this work was modeled by only particle-particle. Conduction due to the walls of the reactor or auger shaft was not considered. The rate of heat transfer due to conduction is expressed as:

$$Q_{ij}^{cond} = a_{ij} \frac{k_j A_{s,i}}{L_c} (T_j - T_i)$$

where k_i is the thermal conductivity of the contacting particle, $A_{s,i}$ is the surface area of the particle, and L_c is depth of heat transfer. In this work, a_{ij} is a surface correction factor that takes into account the number of surrounding particles contacting the surface of the particle of interest. For spheres of equal diameter in three dimensions, the Newton number/contact number is 12. Assuming each contact point accounts for 1% of the particles surface, a value of 0.12 would then be the maximum for a in particle to particle conduction. The number of respective biomass and heat carrier particles in contact with each other in a well-mixed case was considered. Conduction from the

surrounding fluid (nitrogen) was considered for the remainder of the surface area not in particle to particle contact.

The rate of heat transfer due to radiation is expressed as:

$$Q_{ij}^{rad} = \varepsilon_i \sigma A_{s,i}(T_j^4 - T_i^4)$$

where ε_i is the emissivity of the particle *i* and σ is the Stephan-Boltzmann constant 5.6696 x 10^{-8} W/(m^2*K^4). Radiation from both the surrounding particles and from the reactor walls was considered. The temperature of the reactor walls was assumed to be 515°C as external heaters around the auger reactor provide only enough heat to act as an insulator and prevent heat loss to the surroundings.

MATLAB was the software used to model this work. The mechanical and thermal properties of the materials modeled are shown in Table 20.

Table 20: Mechanical and thermal properties of biomass, heat carriers and carrier gas.

Material Property	Biomass	Stainless Steel Shot	Silicon Carbide	Sand	Nitrogen
Diameter, d_p, (mm)	1.0	1.0	1.0	1.0	-
Bulk Density, ρ_{bulk}, (kg/m^3)	300	4600	1600	1500	-
True Density, ρ_{true}, (kg/m^3)	545	7700	3210	2650	-
Heat Capacity, c_p, (J/kg*K)	2385	468	675	800	-
Thermal Conductivity, k, (W/m*K)	0.19	13.4	490	0.27	0.055
Emissivity, ϵ	0.9	0.6	0.87	0.9	-
Initial Temperature, T_o, (°C)	25	575	575	575	-
Surface correction factor, *a*	0.06	0.06	0.06	0.06	0.88

Results and Discussion

A heat transfer model between biomass and stainless steel shot heat carrier was used as the control case. The operating conditions, such as temperature and mass flow ratios, were selected to best represent the conditions for the stainless steel shot trials conducted in *Chapter 2*. A total time of 12 seconds was analyzed to represent the actual solids residence time of the laboratory-scale, twin-screw auger reactor. The temperature profile for the stainless steel case having particle diameters of 1.0 mm for both the biomass and heat carrier is shown in Figure 38.

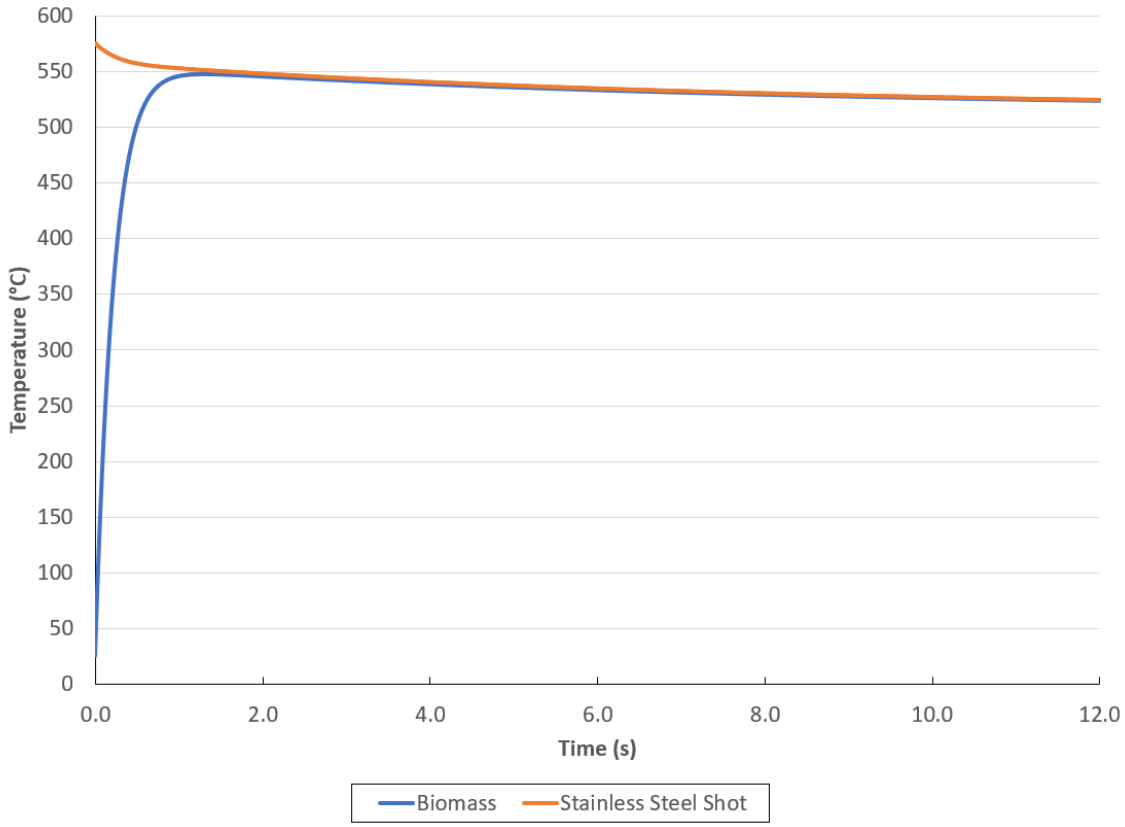

Figure 38: Temperature profile of biomass and stainless steel heat carrier particles.

The figure shows the starting particle temperatures of the biomass (25°C) and the stainless steel shot (575°C) quickly converge to a temperature of around 545°C at a time of 2 seconds. From there the particle temperatures steadily decrease due to the fact the

wall temperature of the reactor was held constant at 515°C. This suggests the majority of the heat flux to the biomass is attributed to both conduction and radiation of the heat carrier particles as opposed to the reactor walls/external heaters. Additional analysis revealed that the heat flux from conduction to the biomass particle by the heat carrier particle accounted for about 66% of the total heat flux. Furthermore, the heat flux from the radiation of the heat carrier accounted for approximately 20%.

To validate the assumption of a homogenous particle temperature, the Biot number was calculated. The Biot number is defined as:

$$Bi = \frac{hL_c}{k}$$

where L_c is the ratio of the particles volume to surface area, *k* is the thermal conductivity of the particle, and *h* is the effective heat transfer coefficient. A Biot number of <0.1 satisfies having a small error associated with the lumped capacitance method. The effective heat transfer coefficient, *h*, in this work is defined as:

$$h = \frac{Q_{total}/A_s}{T_{HC} - T_B}$$

where Q_{total} is the total rate of heat transfer to the particle, A_s is the surface are of the particle, and T_{HC} and T_B is the temperature of the heat carrier and biomass particles, respectively.

The heat transfer coefficient to biomass particle from the stainless steel shot was calculated to be around 205 W/m^2*K. Work by Qi found effective heat transfer coefficients of around 70 W/m^2*K use a more in-depth model and with particle sizes of 2.0 mm for the biomass and stainless steel heat carrier [169]. The calculated Biot number from the stainless steel shot model is approximately 0.18. While this is slightly higher

than the lumped capacitance assumption of 0.1, it is deemed within reason and thus a constant temperature profile within the biomass particle is verified.

Additional cases for the heat carriers of silicon carbide and sand used in previous work was also analyzed. Both the silicon carbide and sand particles' diameter (1.0 mm), initial temperature (575°C), and operating conditions were held constant to that of the stainless steel shot. The thermophysical properties such as the material density, heat capacity, and thermal conductivity varied due to the respective material. The preliminary results for the comparison of the biomass particle temperature as a function of time between the tested heat carriers are shown in Figure 39.

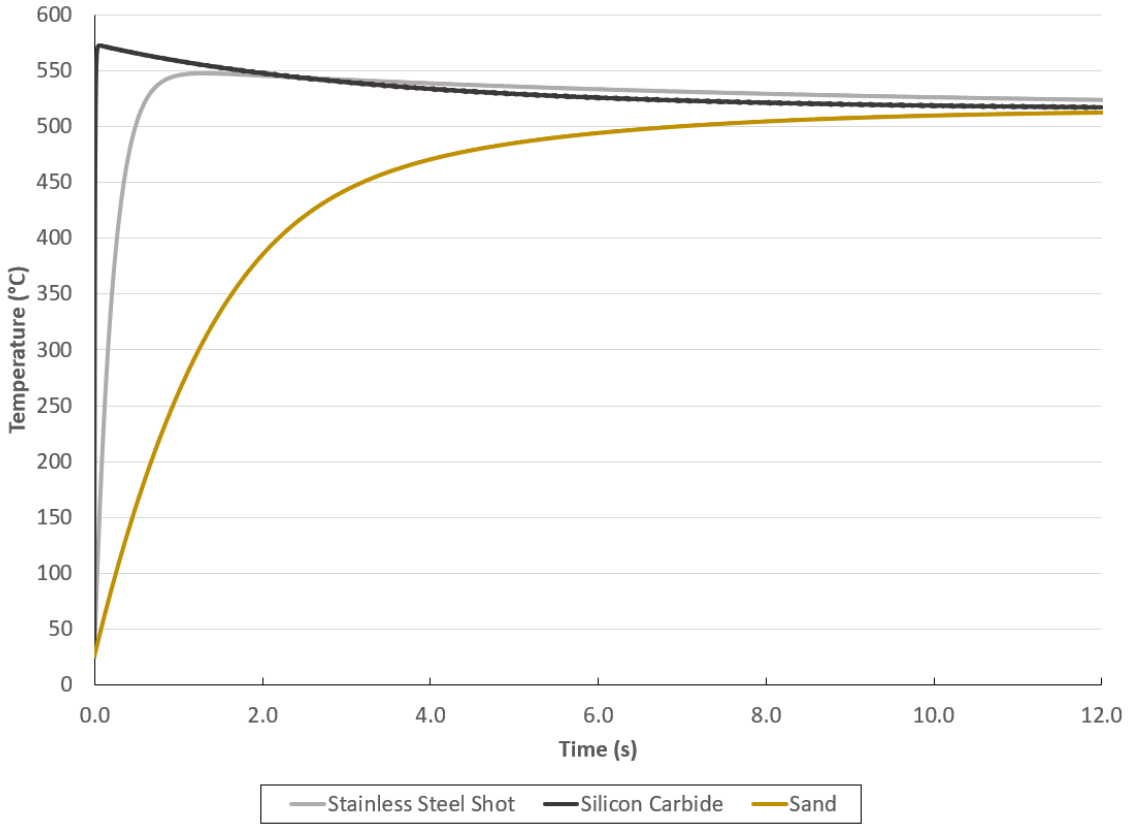

Figure 39: Biomass particle temperature from stainless steel shot, silicon carbide, and sand heat carriers.

It is clear from the figure that the high thermal conductivity of silicon carbide (490 W/m*K) dominates the rate of heat transfer. All three heat carriers have a specific heat capacity on the same order of magnitude ranging from 468-800 J/kg*K, however the thermal conductivity of the sand (0.27 W/m*K) is significantly less than that of stainless steel (13.4 W/m*K) and the silicon carbide. Radiation from the heat carrier particles have more of a contributive role for the sand case due to its lower thermal conductive.

It is clear from this work that the selection of the heat carrier material plays an important role in the rate of heat transfer to the biomass particle in a directly heated auger pyrolyzer. A heat carrier with a higher thermal conductivity will have a higher rate of heat transfer and thus promote the production of primary pyrolysis vapors. Additionally, a heat carrier with high thermal conductivity can allow for a lower initial temperature while still maintaining a desirable pyrolysis reaction temperature having implications on operating costs. Further analysis can be expanded to varying heat carrier and biomass particle sizes, as well as mass flow/volumetric flow ratios.